

A STUDY OF ALPHA-PARTICLE DECAY FROM
CERTAIN EXCITED LEVELS IN C^{12} , O^{16} , AND
 Ne^{20} FOLLOWING POPULATION OF THE LEVELS
BY BETA-DECAY

Thesis by
John Richard Stevens

In Partial Fulfillment of the Requirements
For the Degree of
Doctor of Philosophy

California Institute of Technology
Pasadena, California

1962

ACKNOWLEDGMENTS

The author takes pleasure in expressing his gratitude to the staff of the Kellogg Radiation Laboratory for the opportunity to conduct this research. In particular, the many helpful criticisms of Dr. T. Lauritsen and Dr. R. W. Kavanagh are greatly appreciated. The untiring assistance of David Groce and Peter Parker in collecting the experimental data and Barbara Zimmerman in compiling the computer program is gratefully acknowledged.

This work was supported by the Office of Naval Research and the Atomic Energy Commission.

ABSTRACT

Beta-decay to, followed by alpha-particle deexcitation of, the following levels has been investigated: the 7.656-Mev and 10.1-Mev levels in C^{12} , the 8.88-Mev, 9.59-Mev, and 9.85-Mev levels in O^{16} , and the 5.63-Mev and 5.80-Mev levels in Ne^{20} . Groups of delayed alpha particles were observed only from the first, second and fourth of these levels. The beta-unstable parent nuclei were formed through (d,p) reactions on B^{11} , N^{15} , and F^{19} , after which the delayed alpha particles were observed for a period of time comparable to the half-life of the beta-decay process. The beta-decay branching ratio to the 9.59-Mev level in O^{16} was measured and is equal to $(1.4 \pm 0.2) \cdot 10^{-5}$ corresponding to a $\log ft$ (9.59) = 6.5 ± 0.2 . The beta-decay branching ratio to the 9.85-Mev level was found to be less than $2.7 \cdot 10^{-7}$ which corresponds to a $\log ft$ (9.85) $\geq 7.2 \pm 0.2$. The ratio of the decay probability for alpha-particle emission to the total decay probability for the 8.88-Mev level was found to be $\frac{\Gamma_{\alpha}}{\Gamma_T} \leq 6.6 \cdot 10^{-5}$. This results in a lower limit for the amplitude of the parity nonconserving term in the nuclear potential of $F \leq 1.5 \cdot 10^{-5}$, where the following quantities were used: $\theta_{\alpha 2}^2 = 0.007$ and $\Gamma_{\gamma} = 10^{-3}$ ev.

Alpha-particle emission was not observed from the 5.63-Mev level or the 5.80-Mev level in Ne^{20} . Limits on the $\log ft$ value to these levels were obtained: $\log ft$ (5.63) $\geq 8.0 \pm 0.5$; $\log ft$ (5.80) $\geq 8.0 \pm 0.3$. These large values for the $\log ft$ are consistent with the assigned spin and parity of the levels involved in the beta-decay process.

TABLE OF CONTENTS

PART	TITLE	PAGE
I	INTRODUCTION	
	A. General Type of Reaction	1
	B. Incentives	2
	C. Results	7
II	DELAYED ALPHA PARTICLES FROM B ¹²	
	A. Observations Using the Alternating Gradient Spectrometer	11
	B. Observations Using a Solid-State Counter	13
III	DELAYED ALPHA PARTICLES FROM N ¹⁶	
	A. Introduction	16
	B. Experimental Arrangement	16
	C. Experimental Timing	18
	D. Target Construction	19
	E. Target Thickness	20
	F. Energy Determination of the Peak	21
	G. Identification of the Observed Spectrum	21
	H. Efficiency of the Gamma-Ray Monitor	23
	I. Experimental Effects on the Spectrum Shape	25
	J. Accumulation of the Experimental Data	34

TABLE OF CONTENTS (cont'd.)

PART	TITLE	PAGE
IV	THEORETICAL ANALYSIS	
	A. Dependence of the Spectrum Shape on the Beta-Decay Probability	36
	B. Nuclear Effects on the Alpha-Particle Spectrum	37
	C. Quantitative Results	44
	D. Comparison with Other Authors . . .	49
V	DELAYED ALPHA PARTICLES FROM F^{20}	
	A. Experimental Procedure	52
	B. Results	57
	APPENDIX I	
	Alpha-Particle Half-Life Determination .	62
	APPENDIX II	
	Calculation of the Target Response Function	65
	FIGURES	71
	REFERENCES	99

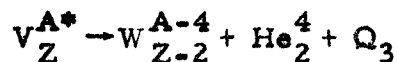
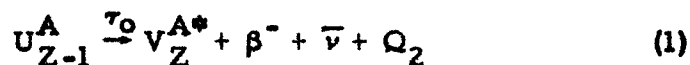
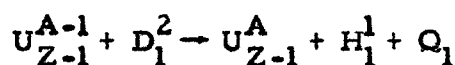
TABLES

TABLE	TITLE	PAGE
I	Properties of the Reactions	2
II	Solid-State Counter Solid Angle Measurement and Gamma-Monitor Efficiency	25
III	Parameters Varied in the Breit Wigner Single Level Formula	39
IV	Values of the Coulomb Function	39
V	Tabulation of the Results from the Separate Experiments	45
VI	Reduced Widths of O^{16}	47
VII	Results of the N^{16} Experiments	50
VIII	Gate Times for Half-Life Measurement	63
IX	Range and Straggling of N^{14} in Al^{27} and Range of N^{16} in Ni^{58}	66
X	Density of N^{16} Nuclei Along the Beam Axis	68
XI	Density of N^{16} Nuclei as a Function of the Distance to the Target Surface in the Direction of the Solid-State Counter	70

I. INTRODUCTION

A. General Type of Reaction

The reactions investigated in this series of research studies were the alpha-particle decay of selfconjugate nuclei, following formation of the nuclei by beta-decay. Excited states in C^{12} , O^{16} , and Ne^{20} were investigated for alpha-particle decay. The excited states were formed through beta-decay of a beta-unstable nucleus and the counting apparatus was activated for a period of time comparable with the half-life for the beta-decay. In order to minimize the background during the experiment, the accelerated deuteron beam was turned off during the counting cycle. Thus the experimental observations were cyclical with a period given by a few half-lives, τ_0 , of the parent nucleus. The parent beta-unstable nuclei were formed through (d,p) reactions where the production and decay scheme is illustrated below.



The target nuclei, U_{Z-1}^{A-1} , were B^{11} , N^{15} and F^{19} ; the remainder of the pertinent data is shown in Table I.

Table I

V_Z^A	Q_1	τ_0	$E(V_Z^{A*})$	J^π	Q_2	Q_3
C^{12}	1.138	20.34 msec	7.656	0^+	5.713	0.278^\dagger
O^{16}	0.275	7.35 sec	10.1	(0^+)	3.3	2.7
			8.88	2^-	1.53	1.72
			9.59	1^-	0.82	2.43
			9.85	2^+	0.56	2.69
Ne^{20}	4.374	11.4 sec	5.634	3^-	1.397	0.901
			5.80	1^-	1.23	1.1

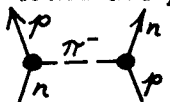
B. Incentives


Incentive for investigating these reactions stemmed from the desire to know the relative importance of different alpha-particle reactions during the process of alpha-particle burning in stellar evolution. The energy developed from the helium-burning process is largely produced during that part of the star's life when it is a red giant. The lifetime of this process is very short on the stellar time scale and the mean conversion time for the helium-burning process has been estimated as about 10^5 years (Salpeter 1957a, b). During this time roughly 10% of the star's luminosity is assumed to be due to the helium-burning process. In addition to the problem of energy generation in stellar systems, there exists also the problem of nucleosynthesis, that is, the creation of the various nuclei in their proper relative abundances. In order to determine the relative abundances of nuclei it is necessary

$^\dagger Q_3$ has been measured as 0.278 ± 0.004 Mev by (Cook 1957b).

to know in addition to the simple nuclear cross-sections the history of the material under consideration, e.g. terrestrial material, solar material, meteorite material, etc. One should know from what types of stars the material originated and through what type of environments the material has subsequently passed. In general, one attempts to determine an abundance by averaging over the material of a fairly large system such as the solar system, the Galaxy, or the universe. By postulating certain physical mechanisms and by using experimentally measured properties of nuclear reactions, an attempt is made to fit the observed abundance with a model for the history of the material in question that is consistent with the postulates. A large amount of work has been done in this field by E. M. Burbidge, G. R. Burbidge, W. A. Fowler and F. Hoyle and has been described in two review articles (Burbidge 1957) and (Fowler 1961).

Additional incentive for part of this work came from the possibility of determining an upper limit for the parity nonconserving term in internucleon interactions (Blin-Stoyle 1960) (Tanner 1957) (Wilkinson 1958). The regular strong interaction, which is parity conserving, is assumed to have a pseudo-scalar coupling, of the form $(\vec{\sigma} \cdot \vec{k})$ where \vec{k} is the momentum transferred, and where $\vec{\sigma}$ is the nuclear spin vector. A pseudo-scalar coupling by itself would not be parity conserving. However, for internucleon interactions the pseudo-scalar coupling enters once for each vertex

 in the Feynman diagram and thus appears squared in the total internucleon interaction. The strong interaction is therefore

parity conserving. Now it is conceivable that an internucleon interaction can proceed by the (V-A) type of weak coupling that has been observed in beta-decay. This interaction may be illustrated in Feynman notation as  where the coupling at each vertex is characterized by (V-A). This coupling gives rise, through the cross product $V \cdot A$ term, to a parity nonconserving term in the internucleon interaction. It will be assumed throughout that the total nuclear spin is a good quantum number and that the matrix elements between states of different spin vanish. Consider now the case of the 8.88-Mev (2^-) level in O^{16} . This level is strictly forbidden by spin and parity to decay by alpha-particle emission to the ground state of C^{12} . However, if there exists a weak internucleon interaction of the (V-A) type one would expect nearby 2^+ levels to mix with the 2^- level giving a positive parity admixture to the 8.88-Mev level. Since we have considered J as a good quantum number, there will be no mixing with states for which $J \neq 2$. The 8.88-Mev level would then be capable of deexciting to the ground state of C^{12} through alpha-particle emission with two units of relative angular momentum between the C^{12} and the alpha particle. This decay should be observable as a particle group superimposed on a slowly varying background of alpha-particle decays from nearby levels.

One can obtain an approximate wave function for the O^{16} system by using perturbation theory. The Hamiltonian for the system can be written as the sum of the strong interaction part, H_0 , and the parity mixing potential V .

$$H = H_0 + V \quad (2)$$

The perturbed wave function is then given to first order by:

$$\psi = \psi_{\text{reg}} + \sum_{\text{irreg}} \frac{H_{\text{reg, irreg}} \psi_{\text{irreg}}}{E_{\text{reg}} - E_{\text{irreg}}} \quad (3)$$

where ψ_{irreg} are the wave functions of spin two levels with positive parity, ψ_{reg} represents the unperturbed wave function for the 8.88-Mev level, and $H_{\text{reg, irreg}}$ is the matrix element of the Hamiltonian computed between the 8.88-Mev level and the spin two levels with positive parity. As a further approximation one may consider only the nearest 2^+ level because of the effect of the energy denominator. This gives one the following form for the wave function, equation 4, where ψ_{irreg} represents the wave function of the

$$\psi = \psi_{\text{reg}} + \frac{\langle \psi_{\text{reg}} | V | \psi_{\text{irreg}} \rangle}{E_{\text{reg}} - E_{\text{irreg}}} \psi_{\text{irreg}} \quad (4)$$

nearest 2^+ level. In order to compute the spectrum shape, one must compute the matrix element between this wave function, ψ , for the initial state and the $C^{12} + \text{He}^4$ wave function, hereafter denoted as the 0^+ state, for the final state. The interaction operator that describes the alpha-particle emission can be expressed as a scalar operator $(\nu T)^{\frac{1}{2}}$ where ν is the frequency with which the alpha-particle strikes the nuclear surface, and T is the probability of penetration. The matrix element for the transition between these

$$M = \langle 0^+ | (\nu T)^{\frac{1}{2}} | \psi \rangle \quad (5)$$

initial and final states, is given by equation 5. This matrix element has two parts (one from the positive admixture to the 2^- level in O^{16} and the other from a negative admixture to the ground state of C^{12}), and can be written as follows:

$$M = \left[F(0^+) \langle 0_{\text{irreg}}^+ | \psi_{\text{reg}} \rangle + F(\psi) \langle 0_{\text{reg}}^+ | \psi_{\text{irreg}} \rangle \right] (\nu T)^{\frac{1}{2}} \quad (6)$$

where

$$F(\psi) = \frac{\langle \psi_{\text{reg}} | V | \psi_{\text{irreg}} \rangle}{E_{\text{reg}} - E_{\text{irreg}}} \quad (7)$$

and

$$\Delta E = E_{\text{reg}} - E_{\text{irreg}}$$

The first term will be neglected because ΔE in $F(0^+)$ is an order of magnitude larger than ΔE in $F(\psi)$. The transition probability can be obtained from the "Golden Rule" and is proportional to the square of the above matrix element. By substituting equation 6 into the "Golden Rule", one obtains the following relationship for the decay probability from the 8.88-Mev state,

$$\Gamma_{\alpha} = F^2 \theta_{\alpha}^2 \Gamma_{\alpha W} \quad (8)$$

where θ_{α}^2 is the dimensionless reduced width determined from Table VI, Γ_{α} is the observed decay probability for alpha particle emission, and $\Gamma_{\alpha W}$ is the Wigner limit assuming uniform particle distribution in the nucleus, equations 13 and 20. For an educated guess of the magnitude of F^2 one may start with the coupling constant for (V-A) coupling as computed for beta-decay $G = 1.01 \times 10^{-5} \left(\frac{m}{m_p}\right)^2$ (Feynman 1959) where m_p is the proton mass and m is a mass involved in the coupling. For lack of a better assumption the pion mass was used for m . In this case the intensity of the parity nonconserving term is given by

$$\Gamma^2 \sim 10^{-10} \left(\frac{m_\pi}{m_p} \right)^4 = 4 \cdot 10^{-14} \quad (9)$$

The experimental measurements do not yield Γ_α but rather an upper limit on $\frac{\Gamma_\alpha}{\Gamma_T}$ where Γ_T is the total decay probability. Γ_T can be computed theoretically from the single particle model since this model has been very successful in predicting other properties of the 8.88-Mev level (Freeman 1957) (Wilkinson 1957). In particular the model has predicted successfully both the gamma-ray branching ratios and the M1, E2 admixtures in the gamma-decay to the 6.14-Mev level. There is therefore a fair degree of reliability in the calculation. Since the probability of gamma-decay is many orders of magnitude greater than the probability of alpha-particle emission, the width for gamma-decay is a good approximation to the total width.

C. Results

The first of the three reactions investigated in this work was a qualitative repeat of work done previously by Cook *et al.* (Cook 1958) on the cross-section for formation of C^{12} from three alpha particles, $B^{12}(\beta) C^{12*} \rightarrow Be^8 + He^4$. The present results were consistent with the previously published results, and the reaction was subsequently used as a check to insure that the experimental apparatus used later was working properly. In particular it was used to determine that the lack of alpha particles from Ne^{20} was real rather than the result of apparatus or operator failure. The results obtained were consistent with the existence of levels at 10.1 Mev and at 7.656 Mev in C^{12} with the proper spin and parity to decay to an alpha particle and a Be^8 nucleus. The existence of

the 7.656-Mev level could not be shown using a solid-state counter because the low energy alpha particles were obscured by the beta-particle pile-up in the counter.

The $N^{16}(\beta) O^{16*} \rightarrow C^{12} + He^4$ experiment yielded the results previously known, namely that the spin and parity of the 8.88-Mev (2^-) level were such that alpha-particle deexcitation was not allowed, and that the 9.59-Mev (1^-) level had the proper spin and parity for alpha-particle emission. Additional information has been obtained since this level was observed to be populated by beta-decay from the ground state of N^{16} for the first time, with a branching ratio equal to $(1.4 \pm 0.2) \cdot 10^{-5}$ of the total beta-decays. The lack of alpha particles from the 8.88-Mev level indicates that the positive parity admixture to the level due to a parity nonconserving term in the Hamiltonian is less than $2.4 \cdot 10^{-10}$. This value was determined by summing the weighted difference between the observed spectrum, and the theoretical spectrum representing the poorest fit to the low energy semiempirical points, equations 26, 27, and 28. This corresponds to a limit on $F^2 \leq 2.4 \cdot 10^{-10}$. Other authors obtain values for $F^2 \leq 2 \cdot 10^{-12}$ where different values of the width for alpha-particle emission have been used (Kaufmann 1961) (Alburger 1961) (Segel 1961). This limit for F^2 was obtained for an experimental value of $\frac{Y_{\alpha}(8.88)}{Y_{\alpha T}} \leq 0.052$ where $Y_{\alpha}(8.88)$ represents the yield of alpha particles from the 8.88-Mev level as determined above, and $Y_{\alpha T}$ represents the total observed alpha-particle yield. The smallest value attainable for this ratio in this experiment (with arbitrarily good resolution and a $30 \mu g \cdot cm^{-2}$ thick self supporting target) would be 7×10^{-4} for fifty hours of running time. This limit is statistical and would vary inversely with the square root of the

time.

The alpha-particle spectrum was fitted accurately using the parameters of R. W. Hill (Hill 1953) and thus confirmed the spin and parity assignments for the 9.59-Mev level, producing no changes in the cross-section factors used by Salpeter (Salpeter 1957a). A discrepancy between the theoretical and experimental spectra was observed at the high energy end of the spectrum. This discrepancy may be due to alpha particles from the 9.85-Mev (2^+) level following population by beta-decay with a branching ratio of $2.7 \cdot 10^{-7}$ corresponding to a $\log ft = 7.2$. A more conservative statement is that 7.2 is a lower limit for the $\log ft$ value to the 9.85-Mev level. The errors in this measurement are mainly due to difficulties in determining the exact shape of the corrections applied to the spectrum. These corrections are due to finite energy loss of the alpha particles in the target and to the resolution of the counting device. The counts used to obtain the $\log ft$ value were in the proper energy region, had the proper half width and had the proper spectrum shape. It is not possible to definitely rule out the chance that the difference between the two spectra was caused by an improper fit of the experimental data. A definite value for the $\log ft$ can only be claimed when structure corresponding to this level can be seen superimposed on the background from the 1^- level.

In the $F^{20}(\beta)Ne^{20*} \rightarrow O^{16} + He^4$ reaction, an attempt was made to observe alpha-particle decay from the 5.63-Mev and 5.80-Mev levels in Ne^{20} after populating the levels by beta-decay from F^{20} .

Since no alpha particles were observed it was particularly important to determine that the analyzing magnet and the gain of the electronics were properly set, and that the timing was working properly. The first two points were checked by scattering alpha particles of known energy through the magnet and observing them with a pulse-height analyzer. The N^{15} target was substituted for the F^{19} target to check that the timing was operating properly. The absence of alpha particles in the part of the experiment that used the alternating gradient spectrometer as a particle detector, gave rise to a lower limit for the log ft for beta-decay followed by alpha-particle deexcitation of the 5.63-Mev level, of $\log ft(5.63) \geq 8.0$. The experiment was also carried out with a solid-state counter yielding $\log ft(5.63) \geq 7.0 \pm 0.7$. However, the state may decay by gamma-ray emission instead of by alpha-particle emission. R. W. Kavanagh (Kavanagh 1958) has looked for gamma-rays using a γ - γ coincidence technique, assuming that the level cascades through the 1.6-Mev level. From the absence of gamma-rays and the background statistics one can obtain a lower limit for the $\log ft(5.63) \geq 6.5 \pm 0.2$. Limits on the $\log ft(5.8)$ for beta-decay to the 5.8-Mev (1^-) level were obtained similarly: $\log ft(5.8) \geq 7.4 \pm 0.2$ for alpha-particle deexcitation, and $\log ft(5.8) \geq 6.6 \pm 0.2$ for gamma-ray deexcitation. These limits for the log ft are consistent with the spin and parity assignments for the levels given by the Chalk River Tandem Accelerator Group (Chalk River 1961).

II. DELAYED ALPHA PARTICLES FROM B^{12}

A. Observations Using the Alternating Gradient Spectrometer

The investigation of the $B^{11}(d,p)$ reaction was carried out using a 1.8-Mev deuteron beam from the Kellogg Laboratory 2-Mev electrostatic accelerator. The beam was analyzed by a 90° magnetic analyzer and then focused on the B^{11} target which was a thin layer of B^{11} deposited on a thick tantalum backing. The target was obtained from the Atomic Energy Research Establishment, Harwell, England. In order to reduce the background due to prompt reactions, the delayed alpha particles from the 7.656-Mev and 10.1-Mev levels in C^{12} were counted, figure 1. The particles were delayed by the 20.2 millisecond beta-decay half-life of B^{12} . Two rotating shutters were incorporated in the beam tube in order to pulse the beam, and to admit the alpha particles to the alternating gradient spectrometer. The experimental layout is shown in figure 2 of references (Cook 1957a) or (Cook 1957b), and a similar arrangement is shown in figure 5 of this report. When the beam was intercepted on the tantalum shutter above the magnetic analyzer, the bias for the counter at the focus of the spectrometer was turned on and the output was recorded in a ten-channel pulse-height analyzer. A monitor counter, which counted beta- and gamma-pulses was also turned on at this time, and its output was recorded in a biased scaler. The pulse-height analyzer was biased so that the singly-charged alpha-particle peak was displayed and the doubly-charged group (the group of higher energy at a given momentum setting) was stored in Surplus. A series of observations at different magnet settings was taken corresponding to the following energy

regions:

$$0.106 \text{ Mev} \leq E(\text{He}^+) \leq 1.148 \text{ Mev}$$

$$0.424 \text{ Mev} \leq E(\text{He}^{++}) \leq 4.59 \text{ Mev}$$

The counts at each magnet setting were then normalized according to the number of counts in the monitor scaler and the counts per unit solid angle at equal energies for different charge states were then combined. The contribution due to neutral helium atoms was taken into account by estimating the fraction of neutral atoms from the charge exchange curves in figure 2. This method yields the results illustrated in figure 3, where the ordinates have been normalized at the arbitrary value of $B\rho = 300$ kilogauss-cm. Perhaps a more realistic normalization would have been to normalize the area under the present curve to the area under C. Cook's curve. This was not done because of the difficulty in estimating the area under the solid-state spectrum and the desire to compare the magnetic spectrometer spectrum with the spectrum from the solid-state counter. There are two other ways of computing what the total alpha-particle spectrum from the two levels in C^{12} should be. One can take just the doubly-charged alpha-particle yield and correct this using the charge-exchange fraction of figure 2, to give the total spectrum. This gives a spectrum that agrees well with the one in figure 3 above $B\rho = 300$ kilogauss-cm, but one which increases more rapidly than the illustrated one for low values of $B\rho$. One can also compute the alpha-particle spectrum by taking the singly charged alpha particles and correcting their spectrum for the charge-exchange effect. This gives good agreement with figure 3 below $B\rho = 150$

kilogauss-cm but a lower value of the yield above this setting. This inconsistency was also observed by C. Cook and can be attributed to one of the following three causes. First: if the solid angle of the magnet varied by as much as 10% between settings of $\frac{1}{3} (B\rho)_{\max}$ and $\frac{2}{3} (B\rho)_{\max}$, and if the variation were such that the settings for low magnetic rigidity had a larger solid angle than the settings for high magnetic rigidity, one could account for the observed discrepancies. Second: the effective charge-exchange fraction for the spectrometer may not be the true charge-exchange fraction. The alteration would be due to collisions with residual gas molecules in the vacuum chamber. Third: the charge-exchange coefficients given in figure 2 may be in error. The magnitude of the necessary error is indicated by the circles in figure 2. It seems most reasonable that the charge-exchange fraction is inaccurate, or that the vacuum in the spectrometer was poor enough to alter the average charge. The agreement between figure 3 and the previous results of C. Cook was considered adequate to insure that the experimental apparatus was working properly. Since the charge-exchange fraction is not needed to better accuracy than it is known, for the following experiments, it was not remeasured.

B. Observations Using a Solid-State Counter

The alpha-particle spectrum from B^{12} was also observed with the aid of a solid-state counter (Nordberg 1961). The experimental arrangement was identical to that used with the alternating gradient spectrometer, except that a solid-state counter was placed at 90° to the incident beam to detect the alpha particles. Its

position is illustrated in figure 5. The solid angle of the counter was 0.10 steradians. The advantages of the solid-state detector over the magnetic spectrometer are that the solid-state counter is not affected by charge exchange in the sense that the magnet is, that the entire alpha-particle spectrum can be recorded simultaneously, thereby removing the error introduced by having to normalize yields at different momentum settings, and that the solid angle is larger than the magnet's solid angle. The solid-state counter removes the error introduced by the charge-exchange fraction because neutral atoms of helium assume a charged state after passing into the counter, and thus can create ion pairs while decelerating. There is, however, one serious disadvantage. This is the presence of background at low energies due to the piling-up of the beta-particle counts. This background occurs at an alpha-particle energy of about 800 kev, and obscures the alpha-spectrum below this energy, as shown in figure 3. No attempt was made to subtract the background from the spectrum, because no appreciable change would occur in the spectrum above $E_{\alpha} = 1.2$ Mev while below this energy the error bars would soon become comparable with the scale of the graph.

The energy calibration for the counter was determined by placing the counter at the image point of the alternating gradient spectrometer, and by scattering alpha particles from a thick copper target. The spectrometer constant for the alternating gradient spectrometer was obtained by locating the profile of scattered alpha particles of known energy from the thick copper target.

The alpha particles of known energy were in turn obtained from the electrostatic accelerator regulated by a magnetic analyzer whose constant was obtained from the $B^{10}(\alpha, p\gamma)C^{13}$ reaction using the 12.70-Mev level in N^{14} . This determined the scale for the abscissa. The ordinate was obtained by normalizing to the yield at $B\rho = 300$ kilogauss-cm.

The agreement with the previous experiment indicated that the solid-state apparatus was working properly.

III. DELAYED ALPHA PARTICLES FROM N^{16}

A. Introduction

The states investigated in O^{16} are shown in figure 4 and are the 9.85-Mev, 9.59-Mev, and 8.88-Mev levels. The 8.88-Mev level was previously known to be populated by beta-decay from N^{16} with a branching ratio of 1.1% (Wilkinson 1956), while beta-decay to the first two levels had not been observed. The 8.88-Mev (2^-) level has been observed to deexcite by gamma-emission where the branching ratios and the multipole mixtures have been experimentally measured (Kuehner 1959). The spin and parity of this level are such that alpha-particle decay to the ground state of C^{12} is forbidden. The levels at 9.85 Mev and 9.59 Mev are known to have the proper spin and parity to emit alpha particles if populated by beta-decay. Thus one would expect to observe alpha particles from the 9.59-Mev level, since the beta transition is allowed. Alpha particles from the 9.85-Mev level may or may not be seen depending on the sensitivity of the experiment, because the beta-decay would be a first forbidden transition. By measuring the alpha-particle yield and by monitoring the yield with the number of beta particles to, or gamma-rays from the excited states in O^{16} , one can determine the branching ratio for beta-decay to the excited levels.

B. Experimental Arrangement

In order to investigate these two levels, an experimental arrangement was used similar to that of the B^{12} experiment. The main difference between the two experiments was caused by the increased beta-decay lifetime of N^{16} compared to that of B^{12} . The half-life of

N^{16} is 7.37 seconds (Bleuler 1947) (Martin 1954). With this long half-life one is not only able to pulse the beam in the vacuum tube but, since the time constant for the electrostatic accelerator is about two seconds, one is able to pulse the voltage on the accelerating tube. The experimental layout is illustrated in figure 5, the target chamber in figure 6, and the timing cycle in figure 7. The bombarding beam was a magnetically-analyzed 1.8-Mev deuteron beam, figure 5. The tantalum beam chopper, located above the analyzer, was solenoid-operated with a period of about twenty-five seconds. The purpose of this shutter was to intercept the beam and to define accurately the time when the beam was removed from the target. As the energy of the high voltage terminal dropped, an accelerating voltage was reached such that the mass separator magnet would transmit the lower mass beam. If this beam were not intercepted on the beam chopper it would pass through the analyzing magnet and strike the target during the counting cycle. Therefore it was necessary to intercept the beam, and desirable to intercept it as far as possible from the counters. In case this chopper failed, an event never observed during the experiment, there was an additional shutter in the target chamber which would intercept the beam at the entrance to the target chamber, figure 6. The target chamber shutter served a dual purpose in that it shielded both the magnet and the solid-state counter from the target during the bombarding part of the cycle, eliminating saturation and deterioration of the counters. This shutter system was fail safe because if the target chamber shutter failed to operate it would block the incident beam. In addition to these mechanical shutters,

electrical gates prevented counts from entering the monitor scaler and the pulse-height analyzer during the bombardment of the target and during the time when apparatus was switching from the bombarding part of the cycle to the counting part of the cycle. On certain runs, two additional gates were added, which operated two scalars recording the alpha-particle spectrum during different parts of the counting period. The ratio of counts in these two scalars was used to determine the lifetime of the alpha particles, Appendix I.

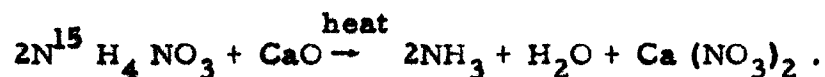
C. Experimental Timing

A typical operating cycle proceeded as illustrated in figure 7. The spray to the belt was turned on and the voltage on the accelerator tube increased to its final value in three seconds. The mechanical shutters above the magnetic analyzer and in the target chamber opened before the accelerator reached the operating energy. When the accelerator reached the proper energy, the regulating slits in front of the target chamber held the deuteron beam on the target. The shutter in the target chamber removed the tantalum shield from the beam entrance and placed a cylindrical shield around the target in order to shield the magnetic spectrometer and the solid-state counter from the prompt particles. The beam was allowed to bombard the target for approximately eight seconds. During this time the voltages on the photomultiplier and the solid-state counter were turned off. Target bombardment was terminated by turning off the spray and deactivating both shutters. The counter voltages were turned on, and after 1.5 seconds, sufficient time for the voltages to stabilize, the gates on the scalars were opened and

delayed activity was observed in the gamma- and alpha-counters for about nine seconds. The process was then repeated.

D. Target Construction

The target requirements were that the target should be capable of withstanding several microamps of beam current, and that it should be thin enough that the alpha-spectrum would not be appreciably affected by energy losses in the target. In order to satisfy the first requirement a refractory material TiN was used. A successful method of making TiN targets is to heat titanium in an ammonia atmosphere. This process nitrides the titanium with a density of nitrogen nuclei in proportion to the diffusion of nitrogen into the titanium. This process gives rise to a poorly defined target layer, which contradicts the requirement for a thin target. In order to overcome this difficulty, a thin layer of titanium was evaporated on a thick nickel backing. This was then nitrided in the above manner to give a well defined target layer $1.8 \cdot 10^{17}$ target nuclei $\cdot \text{cm}^{-2}$ thick. The N^{15} was obtained in the form of ammonium nitrate from the Eastman Kodak Company, and was enriched so that 67% of the nitrogen in the ammonium radical was N^{15} . The reaction used to liberate the ammonia was:



The reaction was carried out in an evacuated chamber and the gaseous products, NH_3 and H_2O , were removed from the system by liquid nitrogen trapping as soon as they were formed. The gas was then dried by passing the mixture over KOH and the remaining

dry ammonia was then passed over a target blank which was heated in an induction furnace. The temperature of the blank was chosen high enough to nitride the titanium yet low enough to minimize diffusion of the titanium into the nickel backing. Targets of TiN^{15} and TiN^{14} were made in this manner by D. Hebbard (Hebbard 1960). The TiN^{14} target was used to ascertain that the results of the experiment were really due to N^{15} , and not due to a contaminant introduced in the target making process.

E. Target Thickness

The thickness of the N^{15} target was determined by observing the yield of 4.43-Mev gamma rays from C^{12} , following the $\text{N}^{15}(\text{p}, \alpha\gamma)$ reaction, through the 12.52-Mev level in the compound nucleus O^{16} . The resonance occurs at an incident proton energy of 429 kev. The target was found to be 7 kev thick to 429-kev protons, figure 8. Assuming that the chemical composition is TiN , that the titanium at the surface is completely nitrated, and that 67% of the nitrogen is N^{15} , a surface density of $1.8 \cdot 10^{17}$ target nuclei $\cdot \text{cm}^{-2}$ is obtained. This corresponds to a thickness of 28 kev for 1.7-Mev alpha particles.

The N^{14} target was made from ammonium nitrate where the nitrogen in the ammonium radical represented the natural abundance of nitrogen isotopes. In order to determine the approximate thickness of the N^{14} target, it was irradiated with the same beam current, and the same total charge as the N^{15} enriched target. The yield of the 6&7-Mev gamma-radiation from O^{16} was compared with the yield obtained from the TiN^{15} target. Using the natural abundance and the quoted enrichment of the TiN^{15} target, the measurement resulted

in a thickness of $2.2 \cdot 10^{17}$ atoms of nitrogen $\cdot \text{cm}^{-2}$ for the natural nitrogen target as opposed to $2.7 \cdot 10^{17}$ atoms of nitrogen $\cdot \text{cm}^{-2}$ in the N^{15} enriched target. The accuracy of the thickness measurement for the natural nitrogen target is $\pm 20\%$. The TiN^{14} target was considered similar enough to the TiN^{15} target to serve as a background target.

F. Energy Determination of the Peak

The energy calibration of the solid-state counter proceeded as follows. The counter was placed at the exit aperture of the alternating gradient spectrometer and a thick gold target was bombarded with 1.82-Mev alpha particles. The spectrometer field was varied and the alpha-particle pulse-height was plotted versus the energy of the alpha particles. This measurement resulted in the crosses of figure 9. The points at $E_{\alpha} = 2.65$ Mev were obtained from a $\text{Po}(\alpha)$ source, $E_{\alpha} = 5.3$ Mev, after doubling the amplifier gain, and were later used to determine the change in the calibration of the electronics so that data accumulated at different times could be combined. The points at $E_{\alpha} = 1.75$ Mev came from the scattering of alpha particles through a thin piece of gold leaf. The spread in the points at $E_{\alpha} = 1.75$ Mev and $E_{\alpha} = 2.65$ Mev indicates the magnitude of the corrections applied to the energy scale of the different spectra in order to combine them. The energy spectra obtained from the magnetic analyzer and from the gold leaf, for calibration purposes, are illustrated in figure 12b, curves (3) and (1) respectively.

G. Identification of the Observed Spectrum

After the group of particles had been observed it remained

to be proved that they were alpha particles and that they originated from the states of interest in O^{16} . The first check was to see that the energy of the group was consistent with the energy available for decay of the excited states in O^{16} . The solid-state counter was calibrated as previously indicated and the peak of the group was found shifted 130 kev lower in energy than would have been expected from simple consideration of the reaction dynamics. When the effects on the energy of the spectrum peak due to penetrability, to beta-decay phase-space, and to target geometry were considered, the shift in peak energy appeared reasonable. This is illustrated by the agreement between the theoretical and the semiempirical spectra in figure 21.

The origin of the particles was checked by measuring their lifetime. This was accomplished by recording the alpha-particle spectrum in two scalers which were gated as shown in figure 7. The ratio of counts between the two scalers was computed. The method used to convert this ratio to half-life is described in Appendix I. The ratio, R , of counts in the fast scaler to those in the slow scaler was found to be $R = 1.83 \pm 0.12$. This value of R results in an experimental half-life of 7.3 ± 0.7 seconds which is in excellent agreement with the value of 7.37 ± 0.05 seconds printed in the literature (Ajzenberg-Selove 1959). This agreement indicates that the decay products are associated with a reaction involving the beta-decay of N^{16} .

The particles were identified as alpha particles by placing a 0.0064 mm aluminum foil in front of the counter. This foil was

sufficiently thick to stop alpha particles of 1.8 Mev. With the foil in place the group was no longer observed. The group was also observed through the alternating gradient spectrometer at a setting that corresponded to $E_{\alpha} = 1.7$ Mev for He^{++} . The particles observed in the spectrometer could have been either protons or alpha particles of 1.7 Mev, however protons should have been observed in the spectrum with the foil in front of the solid-state counter. The group definitely consists of alpha particles.

The target of natural-abundance nitrogen described previously was irradiated in order to determine how much of the spectrum was due to N^{15} and how much of the spectrum was due to impurities in the target. This target was prepared, to within the accuracy of the target making technique, in the same manner as the N^{15} target, and should have contained any impurities that were introduced in the target making process. The yield from this target was reduced by the ratio of the abundance of N^{15} between the two targets and thus lacked most of the low energy tail due to the beta-decays. The noise from the electronics and the counter increased exponentially below channel 10. This evidence completed the identification of the group as alpha particles from states around 9.59 Mev in O^{16} .

H. Efficiency of the Gamma-Ray Monitor

The efficiency of the gamma-ray monitor was computed in two different ways. The spectrum of gamma-radiation is displayed in figure 10. The first method was to determine the efficiency from the theoretical tables of NaI crystal efficiencies taking into account details of the present geometry. Using the National Bureau of Standards' tables compiled by E. A. Wolicki et al. (Wolicki 1956),

one obtains a value for the total efficiency of the gamma-monitor of 0.27% where the absorption of the gamma rays due to the material between the crystal and the target chamber has been taken into account.

The second method was experimental, using the $F^{19}(p, \alpha\gamma)$ reaction. This reaction proceeds through an s-wave interaction at a resonance $E_p = 340.5$ kev, and yields an alpha-particle angular distribution that is nearly isotropic. The experimental measurements (Van Allen 1941) show that the angular distribution of alpha particles is isotropic to within 2%. The angular distribution of the gamma rays has been measured by Van Allen (Van Allen 1941) and was found isotropic to within 5%. Due to the isotropy of the alpha- and gamma-distributions, a coincidence experiment is not necessary to determine the efficiency, rather one needs only to compare the yield of alpha particles in a known solid angle to the yield of gamma-rays in the monitor scaler. In order to determine the solid angle of the solid-state counter accurately, the target was assumed to be a point source which gave an inverse-square yield of alpha particles. The ratio of alpha particles to total charge striking the target was computed for three different positions of the solid-state counter, and the distance between positions was measured accurately. The solid angle was determined using readings from two of the positions and then checked for consistency with the yield at the third position. This procedure was necessary because of the inaccuracies involved in making a direct measurement of the distance from the target surface to the solid angle defining aperture of the solid-state counter. The values of the solid angles obtained at the three different positions and the

efficiencies computed for the gamma-ray monitor are given in Table II.

Table II

<u>Position (inches)</u>	<u>Ω (steradians)</u>	<u>Efficiency %</u>
$\delta (=0.345 \pm 0.004)$	0.218	0.24
$0.262 + \delta$	0.070	0.25
$0.537 + \delta$	0.033	0.24

The efficiency computed was the total efficiency considering as gamma rays only those counts above the monitor bias. In order to compute the efficiency from the tables of E. A. Wolicki et al., one must estimate the number of counts that are represented in the low energy tail of the spectrum. The gamma-ray spectrum was extrapolated to zero pulse height by using a straight line parallel to the abscissa drawn from the point of minimum yield below the peak. This resulted in a correction factor of 1.5 for the efficiency computed from the tables. The experimentally determined efficiencies agree well with the value of 0.27% computed from the tables of E. A. Wolicki et al. (Wolicki 1956).

I. Experimental Effects on the Spectrum Shape

Two possible effects of the target geometry on the results of the experiment are a change in the alpha-particle : gamma-ray ratio and an alteration in the shape of the alpha-particle spectrum. The ratio of alpha-particle yield to gamma-ray yield can be affected if one of the decays is not observed. Since it is possible for recoiling N^{16} nuclei to escape from the face of the target at target angles $\omega < 48^\circ$, one must investigate the distribution of the recoil N^{16} in

the target chamber. If they are distributed with a geometry such that one type of radiation is observed preferentially over the other, the alpha : gamma ratio would vary with target angle. If, for example, the N^{16} could recoil to a region where the gamma rays were counted but the alpha particles were not, the alpha : gamma ratio would decrease giving a smaller branching ratio to the state considered than was correct. The recoiling N^{16} should have been caught by the tantalum beam catcher and removed from the target chamber while data were being recorded. Since this effect becomes more pronounced as the target angle is decreased and N^{16} nuclei escape from the target in increasing numbers, the ratio of alpha-particle to gamma-ray counts was plotted as a function of target angle for target angles between 7° and 45° . No change in the ratio was observed for the angles considered, to within an accuracy of 5%, figure 11a. In order to determine whether or not the assumption (that the number of N^{16} recoils escaping from the target increased with decreasing angle) was correct, the O^{16} gamma-ray yield, multiplied by the sine of the target angle ω to correct for target thickness variation, was plotted as a function of the target angle for the same range of angles. The expected results were observed and are shown in figure 11b. As the target angle decreased, the fraction of escaping N^{16} nuclei increased, and the gamma-ray activity per bombarding particle per target nucleus decreased. The remaining effect is due to the increasing size of the beam spot on the target. This decreases the effective alpha-counter solid angle. If appreciable this solid angle effect should have appeared in figure 11a as a decrease in the alpha : gamma ratio. The change in solid angle was calculated from the geometry and found less than 2%. Thus the recoil of the

nucleus out of the target seems to be the most important effect discussed, and apparently has no significant effect on the alpha-particle : gamma-ray ratio. Figure 11b illustrates the decrease in the number of N^{16} nuclei that decay in the target backing as a function of the target angle. The points have been normalized to 100% at $\omega = 48^\circ$ where all of the N^{16} nuclei will remain in the target backing. This percentage is expected to decrease to 50% at $\omega = 0^\circ$, and the results appear consistent with this expectation.

The shape of the alpha-particle spectrum can be altered by various effects. Since the N^{16} nuclei recoil into the target backing, there will be a depth distribution of decaying O^{16} in the target and the spectrum will be shifted and broadened by the corresponding energy loss of the alpha particles. The spectrum will also be altered by the response function of the particle detector, by multiple scattering in the target backing and target chamber, and by surface irregularities.

First let us consider the recoil process. The N^{16} nucleus is recoiling due to the center-of-mass motion and due to the Q-value of the (d,p) reaction. It will come to rest at a depth $L \cdot \cos \omega$ in the target where this depth is a function of the laboratory angle θ for the heavy particle recoil from the reaction, figure 12b and (Marion 1960), and the target angle ω , figure 11a. The distribution of N^{16} nuclei will lie on a surface of revolution in the laboratory frame of reference where the density of N^{16} nuclei on the surface can be obtained from stripping differential cross-sections measured by Zimmermann (Zimmermann 1958). To complicate matters further, there are three excited states in addition to the ground state

of N^{16} that are involved in the (d,p) reaction. The four reactions, with their respective differential cross-sections, have to be taken into account. This gives four surfaces of revolution as the locus of stopped N^{16} nuclei in the target backing. This distribution is spread out by the fact that the recoiling nuclei suffer a certain amount of straggling which for the energies considered amounts to approximately $50 \mu\text{g}\cdot\text{cm}^{-2}$ (Powers 1962). This spreads the four surfaces together. Additional mixing of the reaction products might occur through the recoil mechanism from the beta-decay of N^{16} to O^{16} . This recoil may distort the spectrum if the depth of the origin of the alpha particles were varied or if the energy of the alpha particle were varied due to the recoil from the beta-decay. The two effects are correlated in that when the dynamics of the decay are such that the alpha particle loses energy due to the recoil, the change in position of the recoiling nucleus increases the path of escape from the target. Therefore the two effects add. The final correction takes into account the increase in path length for the escaping alpha particles due to the 15° rotation of the target normal from the axis of the solid-state counter.

The position of the N^{16} nuclei was determined as follows. For a given reaction, the energy as a function of recoil angle was determined, and the range at the corresponding angle was read off of a range energy curve for nitrogen in nickel (Powers 1962). The differential cross-section for N^{16} recoils in the laboratory system was obtained from the differential cross-section measurements of Zimmermann. Zimmermann's work gives the differential cross-section for protons from the stripping reaction in the

center-of-mass system but this can be converted to the heavy particle differential cross-section in the laboratory system by using the relationships of Appendix II. Upon integration of this differential cross-section over the surface at a constant distance along the beam direction one obtained the number of N^{16} nuclei in a differential interval at a given distance along the beam axis. What one really wanted was the number of N^{16} nuclei giving rise to observed alpha particles that had traversed a distance L while escaping from the target. This was obtained by taking the density of particles on the surface of rotation and projecting it onto the plane defined by the beam direction and the direction to the alpha-particle counter. The number of N^{16} nuclei at a given distance from the surface was then given by the integral of the projected density along a strip at a distance $L \cdot \cos \omega$ from the target surface. The integration was performed over the region where the density of N^{16} nuclei was essentially nonzero. This integration was then carried out for different values of L yielding the density of recoil nuclei as a function of the distance from the target surface in the direction of the alpha-particle counter. Before integrating over the density at a constant value of L , and in order to facilitate computation, the densities of recoil nuclei along the beam axis from the four interactions were combined and an average value of the positions of the nuclei in the target backing was determined. This approximation seemed justified since the locus of the recoil nuclei was spread out due to the effect of straggling. The distribution thus computed corresponded to N^{16} nuclei positioned on an infinitesimally thin surface of revolution. The breadth of the distribution was taken into account by folding a finite width

gaussian into the computed distribution function where the width of the gaussian was determined from the positions of the different groups and the characteristic straggling breadth. The straggling has been measured for nitrogen atoms stopping in aluminum by D. Powers and has been found to remain essentially constant over the energy region of interest. The atoms were found to stop within $25 \mu\text{g} \cdot \text{cm}^{-2}$ of the mid-point of their range, to within 10% accuracy for $50 \text{ kev} \leq E_{\text{N}^{16}} \leq 500_{\text{kev}}$. Appendix II illustrates the mathematics involved in this calculation.

After the beta-decay, the recoiling O^{16} nuclei have a velocity $(\frac{v}{c})_{\text{max}} = 1.5 \cdot 10^{-5}$. Now since the width of the 9.59-Mev level is approximately 0.6 Mev, the recoiling O^{16} nuclei will travel (using $\frac{v}{c} = 1.5 \cdot 10^{-5}$ and $\tau = \hbar/\Gamma$) $4.9 \cdot 10^{-3}$ fermi before breaking up into an alpha particle and a carbon nucleus. Clearly this recoil effect may be neglected. The recoil shift in the energy may also be neglected since the velocity of the alpha particle due to the excitation energy available in the center-of-mass system is given by $\frac{v}{c} = 3 \cdot 10^{-2}$ which is three orders of magnitude greater than recoil velocity due to the beta-decay recoil. The error in the alpha-particle energy due to the center-of-mass motion is much less than 1%.

The recoil N^{16} nuclei calculation was applied to the theoretical yield in the following manner. The density of N^{16} nuclei as a function of depth in the target was transformed to an energy distribution of alpha particles leaving the surface of the target by assuming that the stopping power for alpha particles in nickel was $0.82 \text{ kev} \cdot \text{cm}^2/\mu\text{g}$, and nearly constant for the alpha-particle energies

of interest. This spectrum was calculated for a narrow level with $E_{\alpha} = 1.65$ Mev. The energy spectrum has been broadened according to the $50 \mu\text{g}\cdot\text{cm}^{-2}$ straggling breadth. This computed energy response function, figure 12a, was then folded into the theoretical cross-section.

The next effects that should be discussed are the counter response function and the effect of multiple scattering on the spectrum shape. In order to determine the counter response function, the counter was placed at the image point of the alternating gradient spectrometer with the slits adjusted for about 1% momentum resolution. The spectrum obtained is illustrated in figure 12b curve (3), by the open circles. This spectrum is symmetrical with a width that is characteristic of the resolution of the solid-state counter. The effect of this response function on the alpha-particle spectrum would be a simple symmetrical broadening. The solid-line spectrum shown in figure 12b, curve (1), is that of alpha particles scattered through a thin piece of gold leaf mounted over a hole in a tantalum target blank. The scattered alpha particles were observed directly by the solid-state counter. The existence of the pronounced low energy plateau in this spectrum needs to be explained. One possibility is that the small angle scattering from the beam-defining slits in front of the target chamber may contribute somehow to the low energy background. This effect would not have to be considered in reducing the experimental data since no beam is present during the counting period. The forward scattering from the beam defining slits was reduced by placing a tantalum shield at the entrance to the

target chamber. This shield had a circular aperture sufficiently large that the incident beam could not strike the edges of the shield yet sufficiently small that the shield would intercept alpha particles scattered at more than two degrees from the beam axis. If the low energy background were due to small angle scattering originating at the beam defining slits, one would expect a difference in the spectrum shape when the beam passes through the foil as compared to when the beam is scattered from the surface of the foil. The difference would be caused by the scattered portion of the incident beam striking the tantalum support for the gold leaf giving a thick target yield of alpha particles from the tantalum. In the case where the beam passed through the foil ($\omega = -45^\circ$), the incident beam that was scattered through small angles would strike the tantalum support and be either absorbed or scattered away from the counter. In the case where the beam scatters from the surface of the foil ($\omega = 45^\circ$), the incident beam scattered through small angles can be scattered by the tantalum target support into the solid-state counter. In addition to the difference in the shape of the peaks, due to the effect of energy loss in the foil, the ratio of the area under the low energy plateau to the area under the peak should change in proportion to the amount of small angle scattering present from the beam defining slits. This ratio should be smaller for $\omega = -45^\circ$ than for $\omega = 45^\circ$. This ratio was smaller for the case where the beam was scattered from the surface of the target, $\omega = 45^\circ$, than for the case where the beam was scattered through the target by 5%. The ratios were the same to within the experimental accuracy indicating that

scattering from the beam defining slits was not responsible for the plateau. The low energy plateau could also be accounted for by assuming that the beam scattered from the back of the target chamber after passing through the gold foil and that the back scattered particles were counted. This explanation seems unlikely because the beam was caught in a six-inch long brass tube which was collimated so that the back scattered particles were unable to reach the counter.

The magnitude of the contribution to the low energy alpha-particle spectrum from backscattering can be estimated by integrating the Rutherford cross-section from 90° to 180° . By assuming that the average range of the alpha particles was $1 \text{ mg} \cdot \text{cm}^{-2}$ and that the integrated cross-section could be evaluated for an average alpha-particle energy of 1 Mev, a value for the peak: plateau ratio of 10^3 was obtained. This eliminates backscattering as a possible cause of the plateau. Multiple scattering may have contributed to the plateau in the gold foil spectrum but need not be considered when analyzing the delayed alpha-particle spectrum.

The most plausible explanation for the plateau is the fact that alpha particles lose energy irregularly as they leave a target through a rough surface. The surfaces of the gold foil and the TiN target were visibly rough, and could have accounted for the large energy lost by some of the alpha particles. In order to fit the experimental spectrum with a theoretical analysis using the same parameters that Hill obtained from the elastic scattering of

alpha particles from C^{12} , the counter response function illustrated in figure 12b, curve (2), and the target response function figure 12a were used. The counter response function that was needed to fit the experimental spectrum did not have quite as pronounced a low energy tail as the response function obtained by scattering from the gold foil.

J. Accumulation of the Experimental Data

Once the spectrum had been identified, the problem was to obtain statistically meaningful data. With typical counting rates of a few hundred counts each hour it was obviously necessary to maximize the experimental yield. The most effective variables were the beam energy, the beam current, the target thickness, and the target angle. The values chosen were $E_d = 1.8$ Mev, $i = 6-8 \mu$ amps, $t = 1.8 \cdot 10^{17}$ target nuclei \cdot cm $^{-2}$, and $\omega = 15$ degrees. Data were accumulated on three separate occasions with each attempt lasting from two to three days, and were analyzed separately. These attempts were then combined to give the results presented here. The untouched data of one of the attempts is shown in figure 13. The low energy background was determined by inserting a 0.0064 mm aluminum foil in front of the counter. This allowed the electrons from the beta-decay to penetrate the foil and to be recorded while the alpha particles were stopped in the foil. The background was plotted versus pulse height on log-log paper and found to be a straight line. For future runs the background was determined by plotting the low energy increase of

counts on log-log paper and by extrapolating the background linearly to the energy region of the alpha particles. This background was subsequently subtracted from each of the runs. After the yield of each of the three spectra was analyzed in this way, the abscissas were changed according to the energy calibration and the curves were normalized so that the total number of counts in each spectrum remained unchanged. The three curves were then combined to give the result illustrated in figure 14, where the dashed curve has been drawn through the experimental points. The values of this solid curve, at 100 kev intervals, represent what in future will be called the semiempirical points. The semiempirical spectrum, plotted in center of mass energy for the $C^{12} + He^4$ system, was then fitted theoretically.

IV THEORETICAL ANALYSIS

A. Dependence of the Spectrum Shape on the Beta-Decay Probability

Since the level populated in the compound nucleus O^{16} is very broad, $\Gamma_{cm} = 645$ kev, the energy dependence of the beta-decay process must be taken into account in the theoretical analysis of the alpha-particle spectrum. The total probability of beta-particle emission, $\lambda(\epsilon_0)$, is proportional to the following integral:

$$\lambda(\epsilon_0) \approx \phi(Z) \int_0^{\eta_0} (\epsilon_0 - \epsilon)^2 f(Z, \eta) d\eta. \quad (10)$$

$$\epsilon = (1 + \eta^2)^{\frac{1}{2}}$$

where η is the momentum of the electron in units of mc , ϵ is the total energy of the electron in units of mc^2 , the zero subscript indicates the maximum value obtainable, and $\phi(Z)$ is a function that depends only on Z and not η ($\phi(8) = 1.019$). The Fermi Function $f(Z, \eta)$ contains the electrostatic dependence and part of the phase-space dependence of the beta-decay probability. $f(Z, \eta)$ is tabulated by U. Fano (Fano 1952). Values of $\lambda(\epsilon_0)$ were obtained that corresponded to energies, E , in the center of mass system of the $C^{12} + He^4$ nuclei from 1.2 Mev to 3.0 Mev in 100-kev steps. The conversion from $\lambda(\epsilon_0)$ to $\lambda(E)$ was accomplished using the following relationship:

$$\epsilon_0 = \frac{1}{mc^2} (3.757 \text{ Mev} - E). \quad (11)$$

Figure 15 illustrates the variation of $\lambda(E)$ with respect to both ϵ_0 and E .

B. Nuclear Effects on the Alpha-Particle Spectrum

The spectrum shape can be described using the single level Breit-Wigner formalism (Wigner 1947) (Lane 1958), since there are no other spin-one levels within 2 Mev. Since the level is broad, one must include the energy dependence of the width and of the resonance energy. The relationship used was:

$$\sigma(E) \approx \frac{\Gamma_{\alpha l}(E)}{[E - E_{\alpha l} - \Delta_{\alpha l}(E)]^2 + \frac{\Gamma_{\alpha l}^2}{4}} \quad (12)$$

where the terms are defined as follows:

$$\Gamma_{\alpha l}(E) = 2 \gamma_{\alpha l}^2 P_l(r, E) \Big|_{r=\underline{a}} \quad (13)$$

\underline{a} is the interaction distance in fermi, a variable parameter

$\gamma_{\alpha l}^2$ is the reduced width in Mev, a variable parameter

$$P_l(r, E) = \frac{P}{A_l^2(\rho, \eta)} \quad (13a)$$

$$\rho = kr = 2 \frac{E}{B} \eta = 0.380 r E^{\frac{1}{2}} \quad (13b)$$

$$\eta = 0.158 Z_1 Z_2 \left(\frac{\mu}{E}\right)^{\frac{1}{2}} = 3.28 E^{-\frac{1}{2}} \quad (13c)$$

$$\mu = \frac{A(C^{12}) A(He^4)}{A(C^{12}) + A(He^4)} = 3 \text{ amu} \quad (13d)$$

$$B = \frac{Z_1 Z_2 e^2}{\underline{a}} = 17.3 \underline{a}^{-1} \text{ Mev} \quad (13e)$$

$$\Delta_{\alpha l} = -\gamma_{\alpha l}^2 \left(l + \frac{\rho}{2} \frac{d \ln A_l^2}{d\rho} \right)_{\eta=\text{const}} \text{ Mev} \quad (13f)$$

E_R is the resonant energy in Mev, a variable parameter

$$E_{\alpha l} = E_R - \Delta_{\alpha l} (E_R) \quad (13g)$$

$\alpha 1$ refers to the particular mode of decay of the 9.59-Mev level into $C^{12} + He^4$, and l refers to the relative orbital angular momentum, which was taken equal to unity from the elastic scattering work of R. W. Hill (Hill 1953). By combining equations 10 and 12 one obtains the theoretical spectrum of alpha particles from the 9.59-Mev level.

$$\sigma_{Th}(E) = \frac{C \lambda(E) \Gamma_{\alpha 1}(E)}{[E - E_{\alpha 1} - \Delta_{\alpha 1}(E)]^2 + \frac{\Gamma_{\alpha 1}^2}{4}} \quad (14)$$

where C is a constant. For additional information see (Griffy 1960).

The cross-section $\sigma_{Th}(E)$ can be written in the following form $\sigma_{Th}(E; \underline{a}, \gamma^2, E_R, l)$ in order to emphasize the dependence of the cross-section on the variable parameters. For the 9.59-Mev level this can be rewritten as $\sigma_{Th}(E; \underline{a}, \gamma^2, E_R, 1)$ since the relative angular momentum of the level is known. The remaining parameters were varied using a Burroughs 220 computer in order to determine which values would give a good fit to the semiempirical points. The range of parameters used is given in Table III.

Table III

Parameter	Maximum	Minimum	Increment
<u>a</u> fermi	6.23	4.63	0.20
$\gamma_{\alpha 1}^2$ Mev	3.8	0.2	irregular
E_R Mev	2.8	2.2	0.1
E Mev	3.0	1.2	0.1

The values of the natural logarithm of the coulomb function $\ln A_1^2 (\rho_j, \log \eta_j) = \ln (F_1^2 + G_1^2)$ were stored in the computer for values of $\rho_j = 1.0, 2.0, 3.0, 4.0, 5.0, 6.0$ and $\log \eta_j = 0.0, 0.1, 0.2, 0.3, 0.4, 0.5$. The subscript j indicates tabulated values of the variables (Bloch 1951). Values of $\ln A_1^2$ were stored as a six by six matrix in the computer and are given in Table IV. ρ_c and $\log \eta_c$ were calculated for the c^{th} choice of the center of mass energy E.

Table IV. Values of $\ln A_1^2$

$\log \eta$ ρ	0.0	0.1	0.2	0.3	0.4	0.5
1.0	2.668	3.407	4.451	5.911	7.919	10.64
2.0	1.165	1.583	2.233	3.239	4.773	6.982
3.0	0.6493	0.8707	1.231	1.844	2.884	4.602
4.0	0.4213	0.5560	0.7681	1.129	1.780	2.991
5.0	0.3018	0.3982	0.5346	0.7678	1.167	1.957
6.0	0.2320	0.3079	0.4083	0.5633	0.8269	1.334

The value of $\ln A_1^2$ was then determined by taking the values of $\ln A_1^2$ at constant $\log \eta_j$ and fitting a polynomial in ρ of order five to this set of points. This gave a functional relationship for $\ln A_1^2$;

$$\left. \ln A_1^2(\rho) \right|_{\log \eta_j = \text{const.}} = \sum_{n=0}^5 C_n \rho^n \quad (15)$$

which was then solved by setting $\rho = \rho_c$. This computation was carried out for all six tabulated values of $\log \eta_j$ and resulted in a set of six values of $\ln A_1^2(\rho_c, \log \eta_j)$. This set of points was then fitted with a fifth order polynomial in $\log \eta$, equation 16, and then evaluated at $\log \eta = \log \eta_c$.

$$\ln A_1^2(\rho_c, \log \eta) = \sum_{n=0}^5 B_n (\log \eta)^n \quad (16)$$

which yielded values for $\ln A_1^2$ corresponding to a given value of the center-of-mass energy and a given value of the interaction radius \underline{a} . Nineteen values of $\ln A_1^2$ were computed for the values of the center-of-mass energy given in Table III. The derivative of $\ln A_1^2$ with respect to ρ at a constant value of η_c was evaluated by a finite difference method. The interval in ρ was 0.5 and the following values of ρ_i were used to compute the derivative:

$$\rho_i = \rho_c - 1.0; \rho_c - 0.5; \rho_c; \rho_c + 0.5; \rho_c + 1.0.$$

The subscript i indicates variables associated with the interval used to compute the derivative. The quantity $\ln A_1^2(\rho_i, \log \eta_j)$ was evaluated for each of the six values of $\log \eta_j$ giving six values of $\log \eta_j$ versus $\ln A_1^2(\rho_i, \log \eta_j)$. These values were fitted with a fifth

order polynomial in $\log \eta$.

$$\ln A_1^2(\rho_i, \log \eta) = \sum_{n=0}^5 D_n (\log \eta)^n \quad (17)$$

Equation 17 was then evaluated at $\log \eta = \log \eta_c$. This process was repeated for each of the five values of ρ_i giving five values of $\ln A_1^2(\rho_i, \log \eta_c)$. The derivative was then determined by substituting these values into equation 18 (Hildebrand 1956)

$$\left. \frac{d \ln A_1^2}{d \rho} \right]_{\eta=\eta_c} = \frac{1}{6} \left[\ln A_1^2(\rho_1) - 8 \ln A_1^2(\rho_2) + 8 \ln A_1^2(\rho_4) - \ln A_1^2(\rho_5) \right]_{\eta=\eta_c} \quad (18)$$

Values of the parameters along with the computed values of A_1^2 and $\frac{d \ln A_1^2}{d \rho}$ were then substituted into the equations numbered 13 in order to obtain $\sigma_{Th}(E)$. C in equation 14 was initially chosen equal to one, and the maximum value of the cross-section, $\sigma_{max}(E)$, was determined. All the points were then normalized by taking C equal to $100/\sigma_{max}(E)$. The results of these calculations are shown in figures 16, 17, and 18, where each figure illustrates the effect of varying one of the parameters. Figure 16 shows that the peak of the spectrum moves to lower energies as the interaction radius increases, that the width of the spectrum at half maximum decreases with decreasing interaction radius, and that the curve becomes asymmetric as the interaction radius decreases. The effect of decreasing the resonance energy, E_R , on the spectrum is to shift the peak to lower energies, and to decrease the width of the spectrum at half maximum. This is illustrated in figure 17. The effect of the reduced

width $\gamma_{\alpha 1}^2$ on the spectrum shape is illustrated in figure 18. As the reduced width is increased the peak of the spectrum is shifted to lower energies and the width at half maximum is increased. The variation of the level shift as a function of the center of mass energy is plotted in the lower graph of figure 19. Values of the level shift for various values of the interaction radius used can be obtained from this family of curves.

The theoretical spectrum must be corrected for the target response function and the counter response function before a meaningful comparison between the theoretical and the semiempirical spectra can be made. As mentioned earlier in section III-I, there is some question about the exact form of the counter response function that should be used. In order to evaluate the different response functions, the theoretical spectra were compared to the semiempirical points for each of the three response functions considered. The comparison consisted of computing the deviation of the theoretical spectra from the semiempirical points for various values of the level parameters \underline{a} , E_R , and $\gamma_{\alpha 1}^2$. The deviation computed was a root square deviation as defined in equation 19,

$$\delta = \left[\sum_{E=1.2}^{3.0} (\sigma_{\text{exp}}(E) - \sigma_T(E))^2 \right]^{\frac{1}{2}} ; \Delta E = 0.1 \text{ Mev} \quad (19)$$

where σ_T is the theoretical spectrum, σ_{T_h} , after being corrected for the response functions of the target and the counter, and σ_{exp} is the semiempirical alpha-particle spectrum. The upper graph of figure 19 illustrates the sets of level parameters (\underline{a} , $\gamma_{\alpha 1}^2$) that correspond to the minimum deviation of the theoretical spectra from

the experimental spectrum. Curves (a), (b) and (c) represent the set of parameters that would be associated with the counter response functions of figure 12b, curves (1), (2) and (3) respectively. As stated in section III-1, curve (b) includes the set of parameters used by Hill in order to fit the elastic scattering data. The values of δ that correspond to these three curves vary from $11 \leq \delta \leq 20$ where the units for δ are given by the ordinate of figure 14. Any theoretical spectrum that had a value of δ less than 20 was considered a good fit to the semiempirical spectrum. The value $\delta = 20$ was used as the definition of a good fit because the difference between the semiempirical values and the limits of the error bars corresponding to each value resulted in this value of δ . The Wigner limit for uniform particle distribution

$$\gamma_{\alpha W}^2 = \frac{3}{2} \left(\frac{\hbar^2}{\mu \underline{a}} \right) \quad (20)$$

in the nucleus is given by equation 20, and is illustrated on the upper drawing of figure 19.

Figures 20 and 21 illustrate the shape of various theoretical spectra corresponding to different choices of the level parameters and the counter response functions used in figure 19. The great similarity between the fits for various sets of \underline{a} and $\gamma_{\alpha 1}^2$ is such that a unique value for the level parameters cannot be determined from this experiment alone. Given one of these parameters, the other can then be determined from the upper graph of figure 19 to within the accuracy of the experiment: i. e., to within the accuracy that the counter response function is known. The shape of the theoretical

spectra changes with the different counter response functions, but by changing the level parameters good fits to the semiempirical points could be obtained. Therefore the counter response function could not be determined uniquely from this experiment alone.

The theoretical spectrum obtained by using the level parameters determined by Hill is illustrated in figure 21. The effect of folding the different response functions into this theoretical spectrum is illustrated by the three solid curves in the same figure. Since there appears to be no preference for one set of level parameters over another, the parameters determined by Hill were used, and the counter response function that gave the best approximation to the semiempirical points was determined. It should be noted that although the counter response function and the target response function were determined separately, the experiment could not distinguish between the two, and only discrepancies between the product of the response functions and the experiment could be determined. The response function of the system was split into two parts to facilitate comparison with the known responses in the special cases already discussed.

C. Quantitative Results

The branching ratio to the 9.59-Mev and 9.85-Mev levels was determined by comparing the total yield of alpha particles to each level with the total number of gamma rays monitored. The gamma rays were monitored in a 2 x 2 NaI crystal whose efficiency for gamma-ray conversion was determined as described in section

IIH. The branching ratio was computed by averaging the results of measurements made at three different times. The results are illustrated in Table V where the numbers indicated under "Total" correspond to the yield corrected for solid angle, efficiency, and

Table V

Run	Total- $Y_{\alpha}(9.59)$	Total- $Y(N^{16})$	$Y_{\alpha}(9.59)/Y(N^{16})$
1	$6.94 \cdot 10^5$	$4.72 \cdot 10^{10}$	$1.47 \cdot 10^{-5}$
2	2.67	2.18	1.22
3	3.49	2.19	1.59
Combination	13.00	9.09	$(1.4 \pm 0.2) \cdot 10^{-5}$

gamma-ray branching ratio. The average value of the branching ratio to the 9.59-Mev level is $(1.4 \pm 0.2) \cdot 10^{-5}$. The branching ratio to the 9.84-Mev level can be obtained by comparing the area under the theoretical curve to the area between the theoretical curve and the semiempirical points in the region where $E \approx 2.6$ Mev, see figure 21. This calculation results in an upper limit for the beta-decay branching ratio to the 9.84-Mev level in O^{16} . The branching ratio is less than $2.7 \cdot 10^{-7}$.

The log ft value to the 9.59-Mev level has been computed in two different ways. In one case the f-value for the peak of the theoretical spectrum was used and in the other case a weighted average of the f-values over the energy range $1.2 \text{ Mev} \leq E \leq 2.8 \text{ Mev}$ was used. The half-life was determined from the observed half life $t_{1/2}(N^{16})$ (Ajzenberg-Selove 1959) and the decay probabilities

measured above by using equation 21.

$$t_{\frac{1}{2}}(9.59) = t_{\frac{1}{2}}(N^{16}) \frac{Y(N^{16})}{Y_{\alpha}(9.59)} = 5.25 \cdot 10^5 \text{ sec} \quad (21)$$

This gave $\log t_{\frac{1}{2}}(9.59) = 5.72 \pm 0.1$. The value of $\log f$ which corresponds to the peak of the alpha-particle spectrum is $\log f = 0.4 \pm 0.1$ (Evans 1955). This gave a value of $\log ft = 6.1 \pm 0.2$. The second method determined a weighted average for the f -value over the theoretical spectrum according to the following relationship:

$$\langle f \rangle_{av} = \frac{\sum_{E=1.2}^{2.8} f(E) \sigma_{Th}(E)}{\sum_{E=1.2}^{2.8} \sigma_{Th}(E)} ; \Delta E = 0.1 \text{ Mev} \quad (22)$$

which gave $\log \langle f \rangle_{av} = 0.82 \pm 0.1$.

After combining this with the value of $\log t_{\frac{1}{2}}$, one obtained that the $\log ft(9.59) = 6.5 \pm 0.2$. Since the theoretical spectrum of the 9.85-Mev level is narrow, $\Gamma_{\alpha 2} = 800 \text{ ev}$, the barrier penetrability and beta-decay phase space effects will not shift the peak and one can obtain a limit for the $\log ft$ value to the 9.85-Mev level by using the f -value for the peak. The half-life for the level is:

$$t_{\frac{1}{2}}(9.85) \geq t_{\frac{1}{2}}(N^{16}) \cdot \frac{Y(N^{16})}{Y_{\alpha}(9.59)} \cdot \frac{Y_{\alpha}(9.59)}{Y_{\alpha}(9.85)} = 2.7 \cdot 10^7 \text{ sec} \quad (23)$$

giving $\log t_{\frac{1}{2}}(9.85) \geq 7.43$

and $\log f = -0.2$

whence $\log ft(9.85) \geq 7.2 \pm 0.2$

A relationship for the strength of the parity nonconserving term in the internucleon potential has been given in equation 8. In order to determine the value of F^2 from equation 24, one must determine the probability for alpha-particle emission, or in this

$$F^2 = \frac{\Gamma_\alpha}{\theta_{\alpha 2}^2 \Gamma_{aw}} \quad (24)$$

case, an upper limit for the probability of alpha-particle emission from the 8.88-Mev level. One must also determine the dimensionless reduced width $\theta_{\alpha 2}^2$. The dimensionless reduced width can be estimated by comparing experimentally measured widths of isotopic spin zero levels in O^{16} with their computed Wigner limits. This comparison is presented in Table VI. In order to determine

Table VI. Reduced Widths of O^{16} (Lane 1960)

J^π	$E(O^{16})$	$\Gamma_{obs} (kev)$	θ_{α}^2	Reference
1^-	9.59	6.45	0.85	(Hill 1953)
2^+	9.85	0.75	0.0015	"
4^+	10.36	27	0.26	(Bittner 1954)
0^+	11.25	2,480	0.76	"
2^+	11.51	79.5	0.03	"
3^-	11.62	1,200	0.73	"
1^-	12.45	173	0.04	"

an average value for the reduced width one can compute the geometric mean over all the isotopic spin zero levels which gives $\theta_{\alpha}^2 = 0.11$. However both known spin 2^+ levels have lower values for the reduced

width than the other levels. Until this has been explained theoretically, and it has been shown that the width of the 8.88-Mev level will not be reduced by whatever effect diminished the widths of the 2^+ levels, it is more conservative to use the geometric mean of the 2^+ levels. This gives a value of $\theta_{\alpha 2}^2 = 0.007$. The Wigner limit $\Gamma_{\alpha W}$ is given by:

$$\Gamma_{\alpha W} = 2 \gamma_{\alpha W}^2 P_2 \quad (25)$$

where $\gamma_{\alpha W}^2$ is given by equation 20. Using the curves for penetrabilities by W. T. Sharp et al. (Sharp 1955), this gives rise to a value of $\Gamma_{\alpha W} = 40$ kev. This experiment measured the ratio of $\frac{Y_{\alpha}(8.88)}{Y_{\alpha T}}$ where $Y_{\alpha T}$ is the total alpha-particle yield. Since no structure was seen in the energy region of interest, only an upper limit can be placed on this ratio. The method used to determine this upper limit was to compute the difference between the semiempirical yield and the theoretical spectrum figure 21, curve (c), and to weight it according to the expected spectrum shape. The expected spectrum shape is shown by the dotted curve in figure 21, and represents a ratio of $\frac{Y_{\alpha}(8.88)}{Y_{\alpha T}} = 1.67 \cdot 10^{-2}$. The relationship used to determine the upper limit for the $\frac{Y_{\alpha}(8.88)}{Y_{\alpha T}}$ ratio was:

$$\frac{Y_{\alpha}(8.88)}{Y_{\alpha T}} \leq \frac{\sum_{E=1.2}^{2.1} q(E) [Y_{\alpha}(E) - \sigma_{TC}(E)]}{3.0 \sum_{E=1.2} Y_{\alpha}(E)} \quad (26)$$

where $Y_{\alpha}(E)$ is the experimental yield in the channel corresponding to the energy E and $q(E)$ is the ratio of the height of the dotted curve in figure 21 at the energy E to the peak height of the curve. This method gives a value of $5.2 \cdot 10^{-2}$ for $\frac{Y_{\alpha}(8.88)}{Y_{\alpha T}}$. This ratio of yields can be converted to the ratio of decay probabilities by the

following relationship:

$$\frac{\Gamma_{\alpha}}{\Gamma_T} = \frac{Y_{\alpha}(8.88)}{Y_{\alpha T}} \cdot \frac{Y_{\alpha}(9.59)}{Y(N^{16})} \cdot \frac{Y(N^{16})}{Y_{\gamma}(8.88)} \quad (27)$$

where $Y_{\alpha}(9.59)/Y(N^{16})$ is the beta-decay branching ratio to the 9.59-Mev level, $Y_{\gamma}(8.88)/Y(N^{16})$ is the branching ratio to the 8.88-Mev level, and $Y_{\alpha T} = Y_{\alpha}(9.59)$ has been assumed. One must now eliminate the total decay probability from equation 27, where Γ_T is the sum of the alpha-particle decay probability, Γ_{α} , and the gamma-ray decay probability Γ_{γ} . Since $\Gamma_{\alpha} \ll \Gamma_{\gamma}$, we may approximate Γ_T by Γ_{γ} , where Γ_{γ} can be computed using the independent particle model. Credence in the resulting value for Γ_{γ} is enhanced by the fact that the independent particle model has successfully predicted the gamma-ray branching ratios for gamma-decay from the 8.88-Mev level, and the position of the 8.88-Mev level, (Freeman 1957) (Wilkinson 1957). This method results in a value for $\Gamma_{\gamma} = 10^{-3}$ ev. Combining these values in equation 24, one obtains a limit for the intensity of the positive parity admixture in the 8.88-Mev level of:

$$F^2 \leq \frac{\Gamma_{\alpha}}{\Gamma_T} \cdot \frac{\Gamma_{\gamma}}{\theta_{\alpha 2}^2 \Gamma_{\alpha W}} = 2.4 \cdot 10^{-10} \quad (28)$$

Uncertainties in evaluating Γ_{γ} and $\theta_{\alpha 2}^2$ can introduce an order of magnitude error in the estimate of F^2 in either direction.

D. Comparison with Other Authors

Table VII compares the results of various authors using experiments that involved the levels of interest in O^{16} .

Table VII. Results

	Kaufmann (Kaufmann 1961)	Alburger (Alburger 1961)	Segel (Segel 1961)	Stevens (present)
<u>9.59-Mev level</u>				
Thousands of alpha-counts	50.1	75.3	11.0	8.5
beta branch $\cdot 10^5$	(1.20 \pm 0.05)	(1.24 \pm 0.2)	(0.61 \pm 0.15)	(1.4 \pm 0.2)
log ft			6.8 \pm 0.1	6.5 \pm 0.2
<u>9.85-Mev level</u>				
beta branch $\cdot 10^7$				<2.7
log ft		>7.3	>8.1	>7.2 \pm 0.2
<u>8.88-Mev level</u>				
$\theta_{\alpha 2}^2 \Gamma_{\alpha W}$ (kev)	0.6 to 6.0	6.7	3	0.28
$\Gamma_Y \cdot 10^3$ (ev)	3	2	3	1
$\Gamma_{\alpha} / \Gamma_T \cdot 10^6$	≤ 2.74	≤ 24	≤ 2.0	≤ 66
$F^2 \cdot 10^{11}$	$\leq (1.3 \text{ to } 0.13)$	≤ 0.7	≤ 0.2	≤ 24
Target	gas	Zr N foil	gas	TiN on Ni

The experiment of Kaufmann et al. appears to be the most accurate of the four experiments considered. The reasons for this preference are that the highest accuracy is claimed for the beta-decay branch to the 9.59-Mev level and that the experimental corrections to the theoretical spectrum for a gaseous target are smaller in magnitude than the corrections for a solid target. For solid targets the recent work of Alburger et al. is more accurate than the present work because of superior statistics and because no

correction was made to the abscissa of the data. In Alburger's work, the errors introduced in the present experiment by combining different spectra were non-existent. The work of Alburger et al., like the present work, suffered from the inaccuracies in the determination of the proper response function for analyzing the shape of the spectrum. Since the experiment of Alburger et al. was performed using a self-supporting foil of ZrN, approximately 120-kev thick to 1.7-Mev alpha particles, rather than the 28-kev thick target supported on a thick nickel backing as in the present experiment, the target effect correction was somewhat reduced. The value of the branching ratio quoted by Segel et al. is lower by a factor of two than that obtained by the other three authors. In the work of Segel et al., the contribution to the total gamma-spectrum due to the gamma-decays in the target chamber as distinct from the observation chamber in which the alpha particles were detected, has apparently not been measured and appears to be a possible source of the factor of two difference between their results and the results of other authors.

DELAYED ALPHA PARTICLES FROM F^{20}

A. Experimental Procedure

The alpha-particle decays from the 5.63-Mev and 5.8-Mev excited states in Ne^{20} , figure 22, were looked for in a manner similar to that used to detect alpha particles from the excited states in O^{16} . The (d, p) reaction on F^{19} yields the beta-unstable nucleus F^{20} which decays with a half-life of 11.4 seconds (Wong 1954). The nearness of this decay-time to that of N^{16} , 7.35 seconds, enables one to use the identical experimental apparatus and procedure in both cases. In this particular case, since no alpha particles were observed from Ne^{20} , one was able to check the operation of the apparatus with the N^{15} (d, p) experiment in order to ascertain whether the null result was real or the result of some instrument failure.

The alpha-particle spectrum was observed both by using the alternating gradient spectrometer and the gold-silicon barrier counter. The results obtained in both cases were consistent with each other. In order to obtain reproducible results when using the alternating gradient spectrometer, it was necessary to locate the object point very accurately. When the beam was not aligned at the object point of the spectrometer, the counting rate fluctuated by as much as 20% with variations in the position of the beam spot on the target. By positioning the incident beam at the object point of the spectrometer, the variations in counting rate were reduced because the rate of change of counting-rate with position becomes small at this point. The object point was determined in the following manner. By varying the position of the beam defining slits at the en-

trance to the target chamber in the vertical direction, a plot of counting-rate versus beam position was made, where the position of the beam was located by using a small optical telescope mounted on the spectrometer. The target angle was $\omega = -45^\circ$ for this measurement. Then the beam was returned to the position where maximum counting rate was observed, and the target angle changed to $\omega = -20^\circ$. At this target angle the beam was moved horizontally by the beam defining slits at the entrance to the target chamber. The spectrometer entrance slit was adjusted for maximum yield for each setting of the beam defining slits. This yield was then plotted as a function of target position in order to determine the location of maximum yield along the beam direction. Finally the target angle was changed to $\omega = -80^\circ$ and the counting rate was recorded as a function of distance from the face of the magnet. Typical curves of the counting-rate variations in the target chamber are shown in figure 23. It is clear from this figure that the target chamber axis needed to be moved away from the magnet.

The calibration of the incident beam was accomplished using the $B^{10}(\alpha, p\gamma)C^{13}$ reaction at $E_\alpha = 1.78$ Mev. Alpha particles were then scattered from a gold blank and the alternating gradient spectrometer was calibrated from the position of the scattered alpha-particle step. The alpha particles were detected at the image point of the spectrometer by a thin CsI crystal which was thick enough to stop 1.5-Mev protons. The thickness was approximately 0.5 mils. The CsI crystal was mounted on a quartz disc with Eastman 910 adhesive and the quartz disc was in turn mounted on a Dumont 6291 phototube with Dow Corning 200 Fluid 10⁶ cs silicone grease. The phototube was followed by a preamplifier, amplifier, and a ten-channel pulse height analyzer. This detection system was

calibrated by scattering alpha particles of known energy through the spectrometer and observing their pulse-height as a function of the photomultiplier voltage and the amplifier gain. The results are shown in figure 24. They allowed one to choose the photomultiplier voltage and the amplifier gain such that the centroid of the energy spectrum would appear in the center channel of the pulse height analyzer. Alpha particles from the 5.63-Mev (3^-) level would have 700 kev energy. They can be expected to lose on the average 80 kev while escaping from the CaF_2 target surface and the copper backing, into which the F^{20} recoiled due to the $\text{F}^{19}(\text{d}, \text{p})$ reaction. In order to observe as much of the spectrum as possible the magnet was set for 620-kev He^+ nuclei with the poorest resolution possible $\Delta p/p = 12\%$. The photomultiplier high voltage used was 1080 volts, and the fine attenuator was set at 40, according to figure 24.

Since the expected yield of alpha particles was very small, the target should be stable to large beams. The target should also be thick enough to produce a reasonable yield yet thin enough that the spectrometer, when used with the poorest resolution, would cover the major part of the energy spectrum. Since the alpha particles had to escape from the target surface, it was necessary to hold the surface contamination to a minimum during the experiment. Alpha-particle spectra are known to be severely affected by irregularities in surface structure, therefore it was necessary to have an extremely smooth target. In order to satisfy the above requirements the following target-making technique was pursued. CaF_2 was chosen as the target material. This material has the undesirable characteristic of being unstable at 1300°C and of being non-conducting. For cooling purposes, a copper sheet was used for backing.

and the sheet was lapped and buffed in order to obtain a smooth surface for the CaF_2 . The CaF_2 was then evaporated onto the polished copper backing in a vacuum system. By choosing the proper amount of material a thickness which was consistent with most of the above requirements was obtained. Because of the instability of the CaF_2 , the target could not be run at temperatures high enough to keep carbon from depositing on the surface. The rate of deposition of carbon on the surface was measured by observing the shift of the elastically scattered alpha particles from the CaF_2 surface. The rate of deposition was such that after 300 μ coulombs of charge had struck the target, the surface layer of carbon was 20-kev thick to 1.0-Mev protons. In order to circumvent this carbon build-up the obvious solution of moving from one target spot to another after bombardment by 300 μ coulombs was incorporated in the experimental procedure.

Since many targets would be used, it was necessary to provide several targets of similar thickness that were uniformly thick over the individual targets. This control was accomplished by measuring the displacement of the proton step, scattered from the backing material, due to the layer of CaF_2 on the surface. A profile of a 50-kev thick target is shown in figure 25. The normal target thickness used was 20 kev to 1-Mev protons. This corresponded to 120-kev energy loss for 0.7-Mev alpha particles at $\omega = -20^\circ$.

The experiment was conducted in a manner similar to that of the $\text{N}^{15}(\text{d}, \text{p})$ experiment. The target was bombarded; the electrostatic accelerator was turned off; the counters were activated for 11 seconds; and then the cycle was repeated. After 300 μ coulombs the counts were re-

corded and a background run (as described below) was taken for a comparable amount of charge. The target was then moved to a new spot and the procedure repeated. The pulse height spectra obtained are illustrated in figure 26 where the spectra appear to be mainly those of photomultiplier noise. There is a consistently high reading of the low energy spectrum during the runs compared to the low energy spectrum during the background checks. The background run was obtained by inserting a 0.008-mm-thick aluminum foil in front of the CsI crystal and then proceeding with the usual counting cycle. The difference in counts may be attributable to scattered light from the fluorescent target reaching the CsI crystal. The background counting rate was sensitive to the amount of light in the room and the target chamber was always enclosed in a black cloth during runs. It was also noted that the background could be decreased by about a factor of two by not forming F^{20} . This contribution to the background was probably due to scattered neutrons or electrons.

In order to obtain a limit for the log ft value for beta-decay to the 5.63-Mev and 5.80-Mev levels, assuming that they can alpha-decay, one must know the total number of F^{20} that were formed. Since approximately 100% of the F^{20} nuclei beta-decay to the 1.6-Mev level which subsequently decays by a 1.6-Mev gamma ray, it is possible to determine the F^{20} activity by monitoring the gamma-decay of the 1.6-Mev level of Ne^{20} . In order to observe the delayed gamma-radiation a plastic scintillator was used. The plastic scintillator was placed at 90° to the beam axis in the plane defined by the incident beam and the spectrometer trajectory, at a distance of fifteen inches

from the target. The plastic scintillator was a cylinder 1.7 inches in diameter, and 0.68 inches thick, mounted on a Dumont 6292 photomultiplier. Both the solid angle of the spectrometer and the solid angle of the plastic scintillator were 0.01 steradians. The efficiency for the plastic scintillator, excluding solid angle corrections, was taken equal to 10 %, and was obtained from the attenuation coefficients in the tables of G. White (White 1952) by assuming that the gamma-ray spectrum could be extrapolated horizontally to zero energy. A typical gamma-ray spectrum with monitor scaler bias is shown in figure 27, where the bias is indicated by the dashed line.

B. Results

A limit for the log ft value to the state at 5.63 Mev can be computed using the following relationship:

$$\log ft \geq \log f + \log \left[t_{\frac{1}{2}}(F^{20}) \frac{Y}{Y_{\alpha}} \right] \quad (29)$$

where $\log f$ is obtained for beta-particles with a maximum energy of 1.42 Mev from the tables of Feenberg and Trigg (Feenberg 1950); $\log f = 1.3 \pm 0.1$. Y_Y is the total yield of gamma-rays after correcting for counter efficiency and solid angle. $t_{\frac{1}{2}}(F^{20})$ is the experimentally determined half-life of F^{20} ; given by Wong (Wong 1954) as 11.4 seconds. Y_{α} is the total yield of alpha particles, after correcting for charge exchange; where the limit for the total number of alpha particles was chosen as the difference in counts between the spectrum and the background above the twenty volts bias, figure 26. By combining the histograms of the two runs, a difference of $Y = 18 \pm 11$ was obtained. Although the error is

small enough to indicate that Y represents a value rather than a limit, it is believed that the difference could be attributed to some process such as phosphorescence of the target. In determining Y_α , a value for the charge exchange ratio He^+/He of $\frac{1}{2}$ has been used, and a factor of two has been included in order to account for the fact that the momentum window of the spectrometer admits only half of the spectrum. Using $Y_\alpha = 4Y$, and $Y_\gamma = 3.1 \cdot 10^7$, one obtains a lower limit for the log ft to the 5.63-Mev level of:

$$\log ft \geq 8.0 \pm 0.5$$

The error is determined by the inaccuracies in evaluating the efficiency of the gamma-monitor and by the unknown fraction of counts that could be attributed to the 5.80-Mev level. The theoretical spectrum shown in figure 26 was obtained by using the energy calibration indicated in figure 24, the measured momentum resolution of the alternating gradient spectrometer of 12%, and the electronic and CsI counter resolution of 14%. This gives an overall energy resolution of 28% which is indicated by the breadth of the theoretical spectrum. Because the identical procedure was used successfully to discover the 1.7-Mev alpha particles from the 9.59-Mev level in O^{16} , it was felt that the value of the $\log ft \geq 8.0 \pm 0.5$ represented a reliable measurement.

The experiment was later performed by substituting a solid state detector for the magnetic spectrometer, and a two-inch cylindrical NaI crystal for the plastic gamma-ray monitor. A pronounced low energy tail was observed in the alpha-particle spectrum due to the large flux of beta-decays to the 1.6-Mev level. See figure 28. This made observation of the possible alpha particles extremely difficult, because the energy region where alpha particles were anticipated coincided with the tail of the beta-particle spectrum.

In order to obtain an estimate of the log ft for decay to the two excited states, assuming alpha-decay as the mode of deexcitation, it was necessary to compute the spectrum shape of each level. This was done using the Breit-Wigner formalism with penetration factors obtained from the Chalk River work of Sharp, Gove and Paul (Sharp 1955), and the beta-decay phase-space corrections from the graphs of Feenberg and Trigg (Feenberg 1950). The spins and parities used were those stated by Chalk River (Chalk River 1961) and a reduced width of $\gamma^2 = 100$ kev, roughly 0.2 of the Wigner limit was arbitrarily chosen. It was then assumed that the effects of the target and alpha-counter on the spectrum could be approximated by the response functions used for analysis of the alpha-particle spectrum from O^{16} . These response functions were folded into the theoretical cross-sections in order to obtain the expected spectrum. The upper limit on the number of alpha particles was defined as the sum of the square roots of the number of counts in each channel, where the summation was evaluated over the channels contained between the half-height points of the theoretical spectrum. The results of this calculation give 82 probable counts to the 5.63-Mev level and 31 probable counts to the 5.80-Mev level. These correspond to log ft values of:

$$\log ft(5.63 \text{ Mev}) \geq 7.8 \pm 0.3$$

$$\log ft(5.80 \text{ Mev}) \geq 8.0 \pm 0.3.$$

When the alternating gradient spectrometer was used, only alpha particles from the 5.63-Mev region were observed; however, the low energy tail of the 5.80-Mev level should have been observed in this region. This would have amounted to 10 % of the total spectrum from the above assumed theoretical calculations. Since a value of $\log ft \geq 8.0 \pm 0.5$

was obtained for the 5.63-Mev level, a value of $\log ft \geq 7.0 \pm 0.7$ would follow for the 5.80-Mev level. The error has been arbitrarily increased to take into account the unknown spectrum shape.

If the levels are populated by beta-decay and decay by gamma-radiation rather than particle emission, the above calculated $\log ft$ values would merely attest to the fact that the spin and parity of the states did not allow alpha-particle emission. In order to establish a value or limit for the $\log ft$ to any given state, all possible modes of decay must be investigated. Kavanagh (Kavanagh 1958) has investigated γ - γ and β - γ coincidences from the $F^{20}(\beta)Ne^{20*}$ reaction in the energy region of interest. The β - γ coincidence work could not be applied to the 5-Mev levels because the discriminator bias on the beta-counter was too high to count beta rays with energies as low as those leaving Ne^{20} in the 5-Mev levels. For the γ - γ coincidence to be applicable the 5-Mev levels must deexcite by a cascade through the 1.6-Mev level. Because of the isotopic selection rule on E1 radiation in self-conjugate nuclei, the decay of the 5.80-Mev level to the ground state will be inhibited compared to E2 decay to the first excited level. Decay of the 5.63-Mev level directly to the ground state will be inhibited by the high multipolarity of the radiation required. Assuming that these two levels cascade through the 1.63-Mev (2^+) level, one can obtain limits on the $\log ft$ from γ - γ coincidences as follows:

$$\log ft (5.63) \geq 6.5 \pm 0.2$$

$$\log ft (5.80) \geq 6.6 \pm 0.2$$

The large limits obtained for the $\log ft$ value indicate that the beta-decay is probably at least first forbidden, a conclusion which is

consistent with the spin and parity assignments of the levels concerned. Since the spin and parity of the 5.63-Mev and 5.80-Mev levels are such that alpha-particle emission is possible, the levels will decay preferentially by particle emission. The limits for beta-decay can then be obtained from the alpha-particle experiment and the best limits obtained in these experiments are given below.

$$\log ft(5.63) \geq 8.0 \pm 0.5 \text{ page 58}$$

$$\log ft(5.80) \geq 8.0 \pm 0.3 \text{ page 59}$$

APPENDIX I

Alpha-Particle Half-Life Determination

The calculation of the lifetime of the alpha particles was accomplished with the timing illustrated in the last two lines of figure 7. One assumes, for this calculation, that the beam intensity is nearly constant throughout the measurement and that it strikes the target for the same length of time during each cycle. This implies that the activity of the target is the same at the beginning of each counting period, or that the number of cycles is sufficiently large to average out any effects due to varying target activities. If the number of N^{16} formed at time $t = 0$ is given by A_j , then the number remaining after a time t will be given by $A_j e^{-t\lambda}$ where λ is the decay rate for N^{16} . The number of decays counted in the fast scaler after one cycle will be given by,

$$C_o A_j (e^{-t_1\lambda} - e^{-t_2\lambda}) + C_o B_j (e^{-(t_5-T)\lambda} - e^{-(t_6-T)\lambda}) \quad (30)$$

where B_j represents the activity at $t = T$ for the second half of the cycle, and C_o is a constant of proportionality depending on the geometry of the counter. The total number of counts in the fast scaler N_f is given by the sum of the above expression over all j cycles.

$$N_f = C_o \sum_j \left[A_j (e^{-t_1\lambda} - e^{-t_2\lambda}) + B_j (e^{-(t_5-T)\lambda} - e^{-(t_6-T)\lambda}) \right] \quad (31)$$

A similar expression results for the number of counts in the slow scaler N_s ,

$$N_s = C_o \sum_j \left[A_j (e^{-t_3 \lambda} - e^{-t_4 \lambda}) + B_j (e^{-(t_7-T)\lambda} - e^{-(t_8-T)\lambda}) \right] \quad (32)$$

By making use of the above assumption one can equate A_j to B_j , and then the ratio, R , of counts in the fast scaler to counts in the slow scaler is given by,

$$R = \frac{N_f}{N_s} = \frac{e^{-t_1 \lambda} - e^{-t_2 \lambda} + e^{-(t_5-T)\lambda} - e^{-(t_6-T)\lambda}}{e^{-t_3 \lambda} - e^{-t_4 \lambda} + e^{-(t_7-T)\lambda} - e^{-(t_8-T)\lambda}} \quad (33)$$

The values of t_i were obtained by using a 60 cycle pulser with the switching circuit. The following values resulted.

Table VIII t_i			
t_1	1.05 sec	t_5-T	1.00 sec
t_2	7.15	t_6-T	7.20
t_3	6.75	t_7-T	6.92
t_4	12.28	t_8-T	12.55

The above equation for R can be solved graphically by substituting different values of λ and obtaining corresponding values for R . A curve can then be plotted of $\log R$ versus λ which is nearly a straight line over the range of $0.0 \leq \lambda \leq 0.4$. The experimentally determined value of R is

$$R = 1.83 \pm 0.12.$$

From the graph of $\log R$ versus λ one obtains a value for λ which when converted to half-life gives $t_{\frac{1}{2}} = 7.3 \pm 0.7$ seconds, which agrees well with the values quoted by (Bleuler 1947) of $t_{\frac{1}{2}} = 7.35 \pm 0.05$ seconds, and (Martin 1954) of 7.38 ± 0.05 seconds.

APPENDIX II

Calculation of the Target Response Function

The range of N^{14} in Al^{27} has been measured by D. Powers (Powers 1962) and is presented in the second column of Table IX. In order to convert these range measurements to the case of N^{14} in Ni^{58} equation 34 was used. Equation 34 is applicable for $M_1 < M_2$.

$$\langle R \rangle_{av} = \frac{0.68}{\left[\epsilon \left(1 - \frac{2M_1}{3M_2} \right) \right]^{\frac{1}{3}}} \frac{M_2^2 (Z_1^{\frac{2}{3}} + Z_2^{\frac{2}{3}}) E_1}{Z_1 Z_2 (M_1 + M_2)} \quad (34)$$

and ϵ is given by

$$\epsilon = 1 + \frac{(M_2 - M_1)^2}{2M_2 M_1} \ln \left[\frac{M_2 - M_1}{M_2 + M_1} \right] \quad (35)$$

By substituting the proper values into equations 34 and 35, one obtains the range at a constant energy by the following relationship,

$$\frac{\langle R(Ni) \rangle}{\langle R(Al) \rangle} = 2.03 \quad \left. \vphantom{\frac{\langle R(Ni) \rangle}{\langle R(Al) \rangle}} \right\} \text{At constant energy}$$

The range was reduced by 6.2% to transform the range for N^{14} to the range for N^{16} . The factor of 6.2% was also obtained from equations 34 and 35. The corrected ranges are given in the third column of Table IX.

Table IX

N energy kev	$\langle R(\text{Al}^{27}) \rangle_{-2}$ $\mu\text{g} \cdot \text{cm}^{-2}$	$\langle R(\text{Ni}^{58}) \rangle_{-2}$ $\mu\text{g} \cdot \text{cm}^{-2}$	Straggling $\mu\text{g} \cdot \text{cm}^{-2}$
50	31 ± 10	59	41
100	75 ± 8	142	25
200	116 ± 13	221	45
300	158 ± 14	300	61
400	201 ± 15	381	46
500	221 ± 17	419	58

When the N^{16} nuclei recoil, their distribution will be symmetric about the beam axis and can be determined from the reaction dynamics and the above stated range-energy relationship. Let us define the distance along the beam axis as the z direction and the origin of the coordinate system will be the point of interaction. $\rho(z)$ then describes the distance of the N^{16} recoil from the beam axis. From the reaction dynamics one obtains the energy of the N^{16} recoil for a given value of recoil angle ξ , and by combining this energy with the range-energy relationship the position of the stopped N^{16} can be obtained where:

$$\rho(z) = \langle R \rangle \sin \xi \quad (36)$$

This determines a surface of revolution which contains all the N^{16} recoils. Of course, one will obtain four different surfaces, one for each of the different levels involved in the reaction. These four surfaces are then averaged to give one common surface. This average was a weighted

average computed for constant z , and the values of $\rho(z)$ were weighted according to the number of N^{16} recoils present on each surface.

In order to perform this average one must know the density of N^{16} nuclei along each of the surfaces, $N(s)$. The (d,p) stripping reactions to the ground state and the first three excited states of N^{16} have been studied by Zimmerman (Zimmerman 1968). The relationship used to convert from the center-of-mass system to the laboratory system is given in equation 37, where θ is the angle of the light particle in the

$$\sigma(\zeta) = \frac{\sigma(\theta)}{\cos(\theta + \zeta)} \left(\frac{\sin \theta}{\sin \zeta} \right)^2 \quad (37)$$

center-of-mass system, ζ is the angle of the heavy particle in the laboratory system, and σ represents the respective cross-sections. This is then converted to the density of particles along the beam direction, $N(z)$, according to equation 38:

$$N(z) = 2\pi \sigma(\zeta) \frac{dz}{dz} \sin \zeta \quad (38)$$

$N(z)$ is presented in Table X for the four levels involved in the interaction. The sum of $N(z)$ for the four levels is also presented. The values for the sum of the N^{16} densities and the weighted average of $\rho(z)$ were used to determine the distribution of N^{16} nuclei at a constant depth $L \cdot \cos \omega$ where L is the distance the alpha particle must travel in the target before escaping and being counted in the solid-state counter.

Table X. $N(z)$ for different levels in N^{16}

$E(N^{16})$ $z(\mu g \cdot cm^{-2})$	0.00	0.119	0.295	0.392	$\sum N(z)$ E
25	0	140	(7)	(600)	747
50	12	50	18	300	380
75	28	7	50	65	150
100	27	7	62	15	111
150	23	18	42	37	120
200	17	18	25	52	112
250	13	14	15	47	89
300	11	10	9	38	68
350	12	7	9	27	55
400	15	3	11	17	46
450	16	2	15	6	39
500	18	(0)	(19)	(0)	37

$$L = z \tan \omega + \rho(z) \cos \gamma \quad (39)$$

γ is the angle that $\rho(z)$ makes with the scattering plane, such that when $\gamma = 0^\circ$, $\rho(z)$ lies in the scattering plane and is directed away from the alpha-particle counter.

The density of N^{16} on the surface of revolution, $N(s)$, was determined by dividing $N(z)dz$ by the area of a circular strip with radius $\rho(z)$, equation 40. This surface density was then projected

$$N(s) = \frac{N(z)}{2\pi \rho(z)} \quad (40)$$

onto the scattering plane where $N(p)$ is the density in the plane. This density was integrated along the z variable for a constant value of L

$$N(p) = \frac{2 N(s)}{\sin \gamma} \quad (41)$$

where the constraint on z is given by equation 39. By using equation 39, $\rho(z) \sin \gamma$ can be replaced, and the integral over z becomes:

$$N(L) = \int_{z_1}^{z_2} \frac{N(z) dz}{\pi [\rho^2 - (L - z \tan \omega)^2]^{\frac{1}{2}}} \quad (42)$$

where $N(L)$ is the linear density as a function of L , and z_1 and z_2 are given by the following expressions:

$$z_1 = \frac{L - \rho(z_1)}{\tan \omega} \quad z_2 = \frac{L + \rho(z_2)}{\tan \omega}$$

This integral was then evaluated using Weddle's six-point rule in order to obtain the density of N^{16} nuclei as a function of the distance traversed in the target before reaching the solid-state counter. This dependence is given in Table XI for a target angle $\omega = 15^\circ$. The straggling was taken into account by folding a gaussian function with a $50 \mu\text{g} \cdot \text{cm}^{-2}$ width at half-height into the calculated distribution. The distribution of N^{16} nuclei was converted to an energy loss spectrum for a monoenergetic alpha-particle source with $E_\alpha = 1.65 \text{ Mev}$. The values of L were

converted to alpha-particle energy lost, by assuming that the stopping power was nearly constant over the region of interest and was given by $\epsilon = 0.82 \frac{\text{cm}^2\text{-kev}}{\mu\text{g}}$. The resultant response function is shown in figure 12a.

Table XI

$L(\mu\text{g}\cdot\text{cm}^{-2})$	$N(L)$
0	276
10	256
20	263
30	252
40	206
65	150
90	126
115	99
140	98
165	96
190	81
215	74
240	61
250	62

Figure 1. Energy levels of C^{12}

The $B^{11}(d, p)$ reaction produces B^{12} nuclei at an energy $E_d = 1.8$ Mev with a cross-section of 290 millibarns (Cook 1957a) which then beta-decay to various excited states in C^{12} as indicated in figure 1. The states of interest in this experiment are the 7.656-Mev and 10.1-Mev states. Both of these states alpha-decay either by passing through Be^8 in a two body decay or by breaking up directly in a three body decay. The energy spectrum of the alpha particles from these two states is illustrated in figure 3. The spectrum varies from zero up to 1.8 Mev, and has been successfully described by Cook as a series of two body decays.

Figure 1

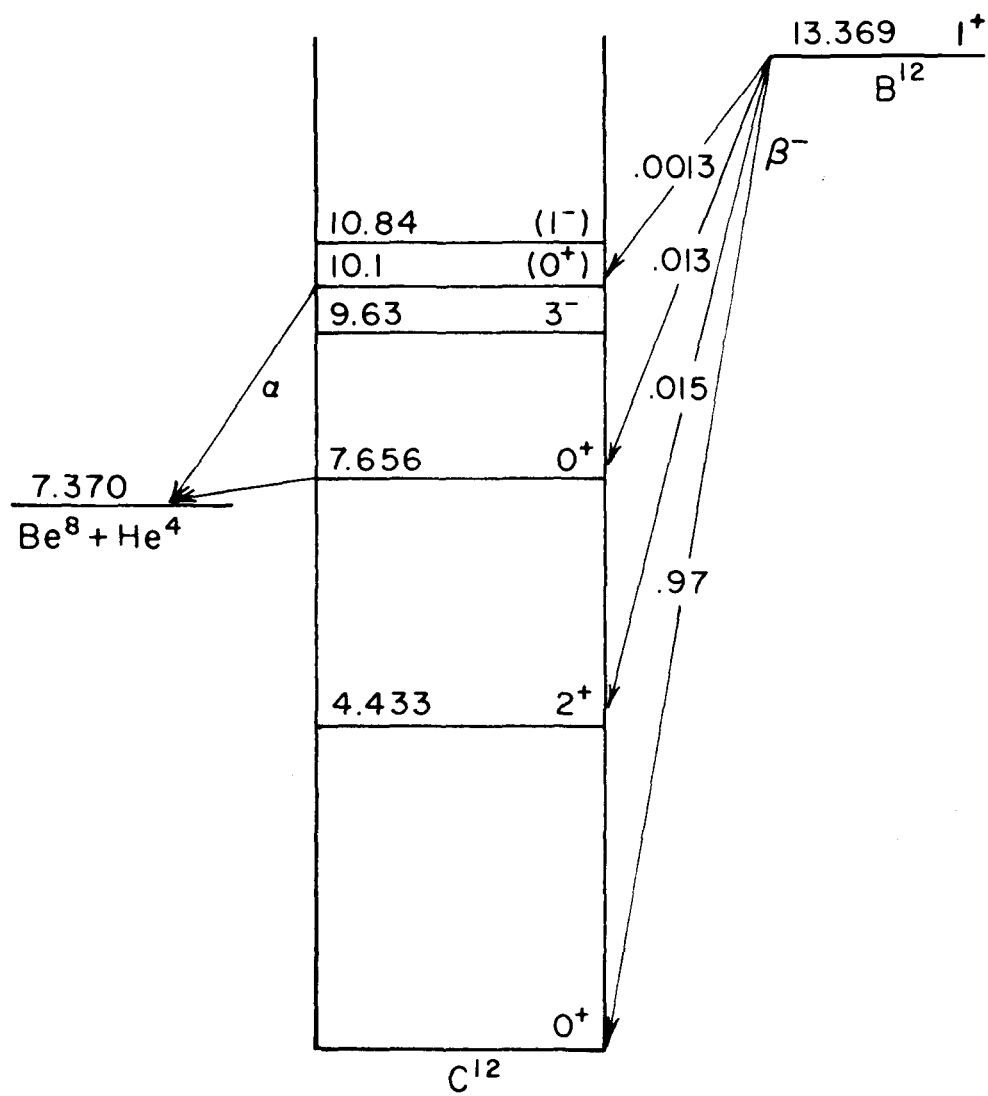


Figure 2. Charge exchange curves for He^4

When one observes reaction products through a magnetic analyzer, one must know what the charge-exchange fraction is in order to calculate the total yield. Figure 2 shows this charge-exchange fraction. The insert in the upper right hand corner indicates the method used by G. Dissanaïke (Dissanaïke 1953) to determine this fraction. He scattered a beam of alpha particles at 90° from metal foils of beryllium, aluminum, and silver. The scattered particles were then separated by a magnetic field. The charged particles were counted by a zinc sulphide screen while the neutral particles were counted by a secondary-electron-multiplier. The beam was monitored using another secondary-electron-multiplier opposite the magnet and at 90° to the incident beam. The quoted accuracies are $\pm 2\%$ for $E_\alpha > 0.5 \text{ Mev}$ and $\pm 5\%$ for $E_\alpha < 0.5 \text{ Mev}$; and the charge-exchange fraction was asserted to be independent of the target material.

The circled points were determined from the present experiment by assuming that the solid angle of the magnetic spectrometer was constant over the field settings of interest, and that the neutrals (in the energy region where the neutral correction was important) were given accurately by the work of Dissanaïke. The charge-exchange fraction can then be computed by comparing the number of singly-charged alpha particles to the number of doubly-charged alpha particles at a given energy. The deviation of the circles from the curves indicates the magnitude of the discrepancy.

Figure 2

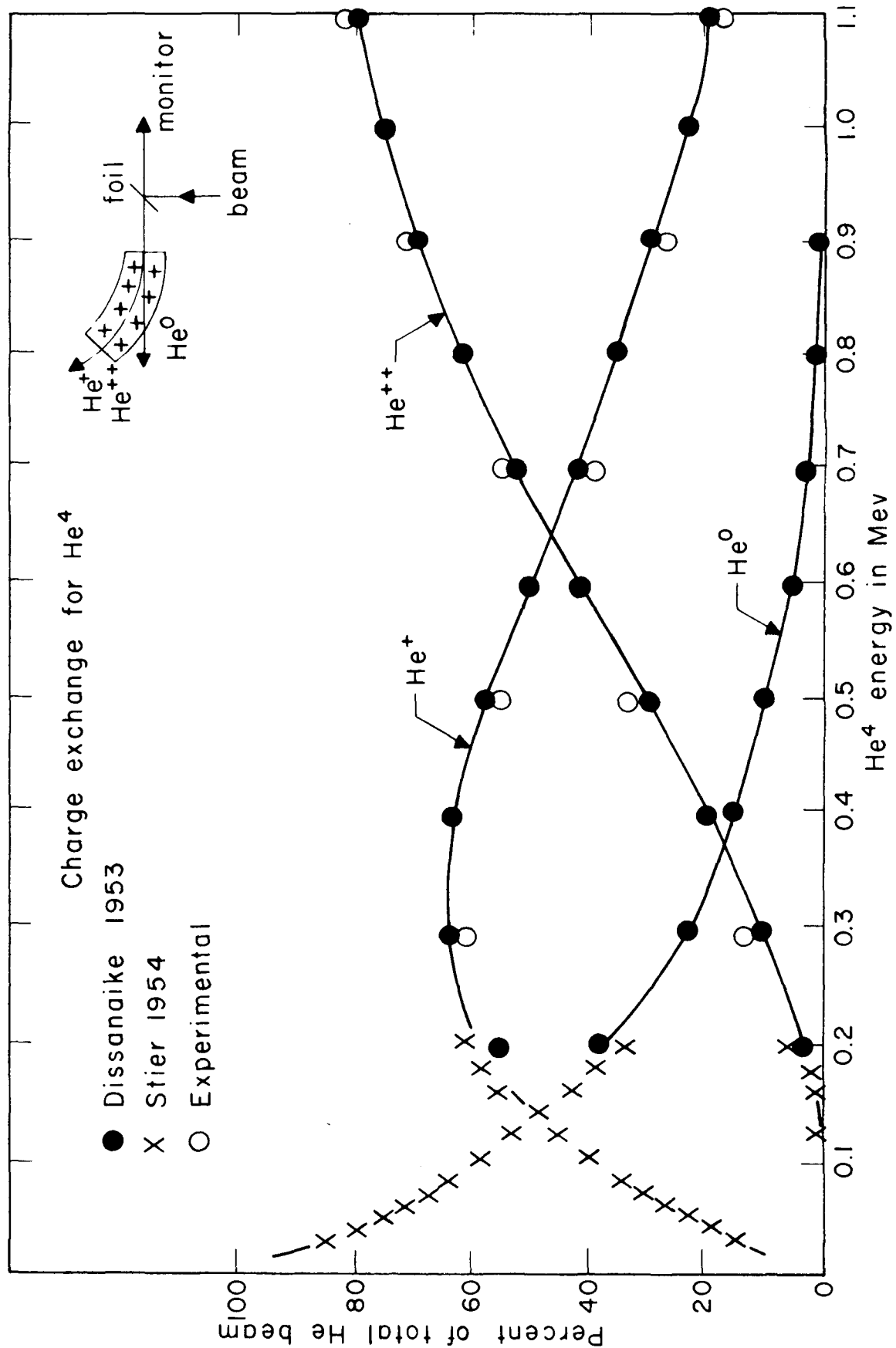


Figure 3. Alpha-particle spectrum from C^{12}

The reason for repeating the $B^{12}(\beta)C^{12} \rightarrow Be^8 + He^4$ experiment was to obtain qualitative agreement with the results of C. Cook et al. (Cook 1958). This agreement would indicate that the experimental arrangements were functioning properly. Figure 3 compares Cook's data points with those of the present experiment.

The apparent disagreement around 1.3 Mev is probably due to the method of normalization and the fact that poorer resolution, $\frac{\Delta P}{P} = 12\%$, was used in obtaining the recent experimental points than was used previously by Cook, $\frac{\Delta P}{P} = 5\%$, (Cook 1957a). The curves were normalized to the same height at a Bp setting of 300 kilogauss-cm. The area method of normalization was not used because of the difficulties involved in estimating the area under the solid-state counter curve. These difficulties arise from the uncertainty in the beta-particle background. The background can be seen clearly on the drawing. The agreement was considered adequate to justify not repeating the quantitative part of the B^{12} experiment and to indicate that the experimental arrangements were sufficiently sensitive to detect alpha-particle decay from the $N^{16}(\beta)O^{16}$ etc. and $F^{20}(\beta)Ne^{20}$ etc. reactions.

Figure 3

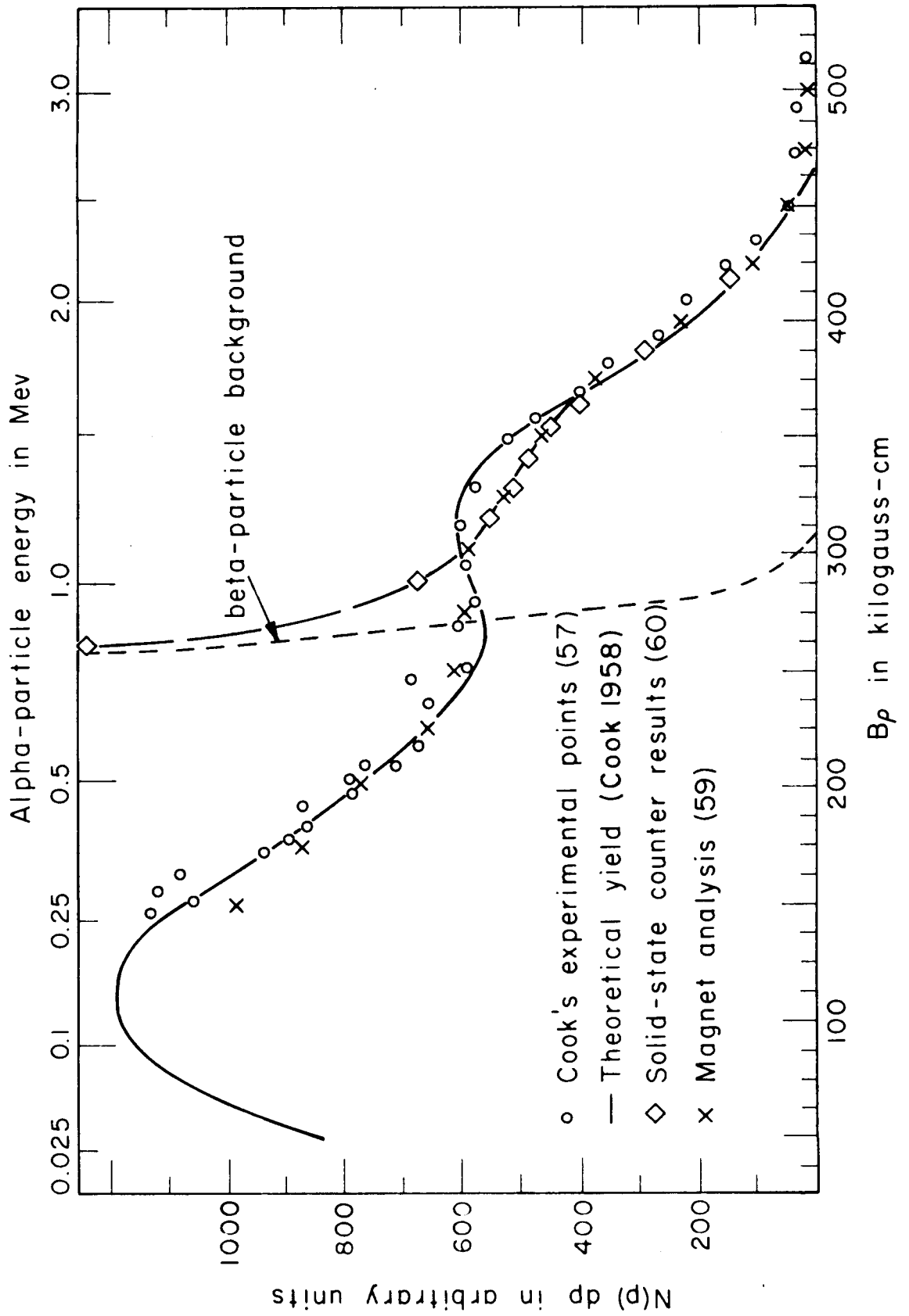


Figure 4. Energy levels of O^{16}

N^{16} beta-decays from its ground state to various levels in O^{16} with the branching ratios indicated in figure 4. The excited levels of interest are the 9.85-Mev (2^+) level, the 9.59-Mev (1^-) level and the 8.88-Mev (2^-) level. The first two are allowed to alpha-decay to C^{12} while the last is not. Heretofore the first two levels were not known to be populated by the beta-decay process. Alpha particles from the 9.59-Mev level were observed, figure 21, with a peak energy of 1.69 Mev in the laboratory system. The shift in energy of the spectrum's peak from the value obtained from the reaction dynamics was consistent with the theoretical shift induced by penetration factors, beta-decay phase-space, target geometry, and solid-state counter effects as discussed in sections III-I and IV-A, B. The 8.88-Mev level is forbidden by spin and parity to emit alpha particles. The absence of alpha particles from this level gives rise to a limit on the positive-parity admixture in the 8.88-Mev level, and thus a limit on the magnitude of the parity non-conserving term in the nuclear potential.

Figure 4

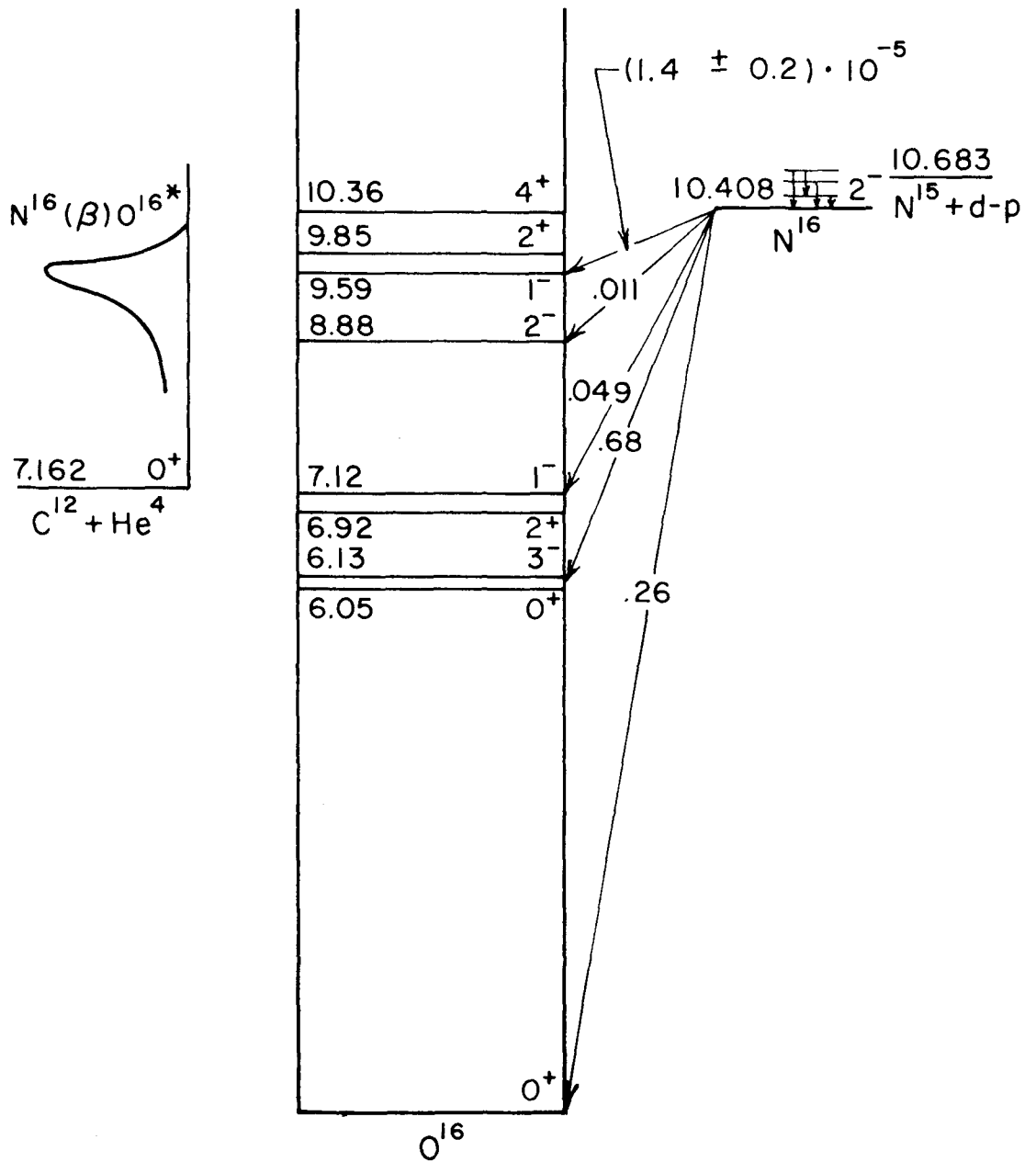


Figure 5. Experimental arrangement

A deuteron beam from the Kellogg 2-Mev electrostatic accelerator is incident on a mass separating system and then magnetically analyzed. A tantalum shutter above the analyzer interrupts the beam according to the timing schedule illustrated in figure 7. After magnetic analysis, the beam enters the target chamber and strikes the target at a target angle, $\omega = 15^\circ$, where ω is defined in figure 11. For a detailed discussion of the target chamber see figure 6. The reaction products are analyzed at a laboratory angle, $\psi = 90^\circ$, figure 12b, by either a solid-state counter or the alternating gradient magnetic spectrometer (Martin 1956, 1957). The gamma rays were monitored in a plastic scintillator (1.70 inches in diameter and 0.62 inches deep) or a NaI crystal (2.0 inches in diameter and 2.0 inches deep) oriented in the horizontal plane at 48° to the incident deuteron beam. In addition to the lucite target chamber walls, a 1.5-inch-thick carbon absorber was placed between the crystal and the target chamber to absorb the beta particles.

Figure 5

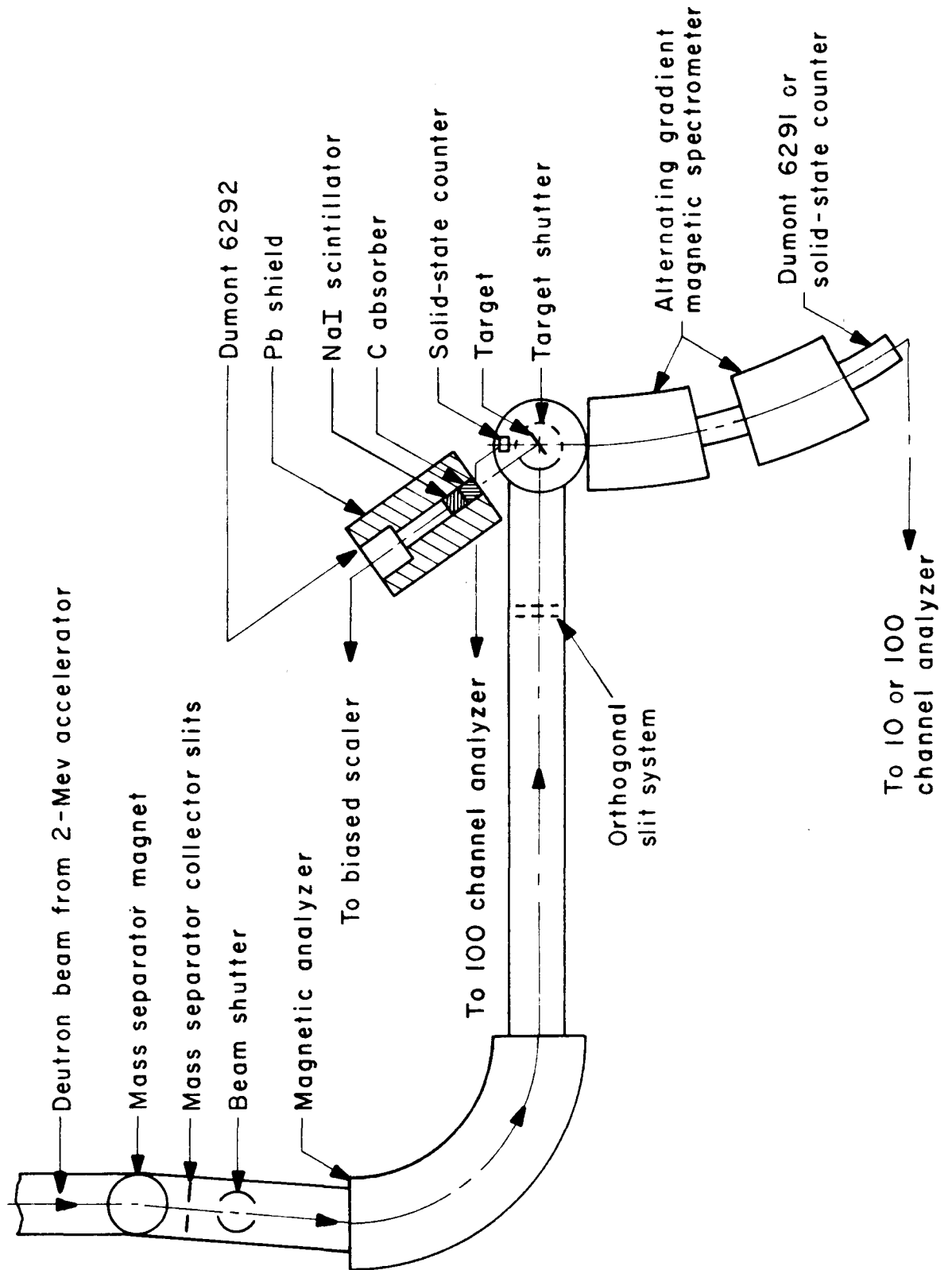


Figure 6. Target chamber

This figure illustrates the geometrical arrangement of the counters and the target chamber shielding system. The solid-state counter is mounted on the left and is sealed in the vacuum system. The counter solid angle can be adjusted by varying the two positioning screws shown above and below the counter. The counter is mounted behind a 0.010-inch-thick tantalum shield with a 3/16-inch-diameter hole in its center. The area of this hole and its distance from the target define the solid angle of the counter. A 0.0064-mm. aluminum foil mounted over a 3/8-inch-diameter hole in a tantalum blank is suspended from a single point such that it rotates under the force of gravity when the counter mount is rotated about its axis of symmetry. This foil was positioned over the solid-state counter in order to absorb the alpha particles while the background was being determined.

The target shield, a 0.020-inch-thick right circular cylinder of tantalum one inch in diameter with a 3/8-inch section removed for the beam, is shown in the "beam on" position. The beam strikes the target activating the N^{15} , and the recoiling N^{16} and scattered deuterons that escape from the target are collected on the tantalum shield. When the beam is turned off the shield drops and the flat tantalum plate covers the entrance aperture of the target chamber. This plate intercepts any residual beam that may pass down the beam tube during the counting part of the cycle.

Typical spectrometer parameters for these experiments were $\frac{\Delta P}{P} = 12\%$ and $\Omega = 0.01$ ster.

Figure 6

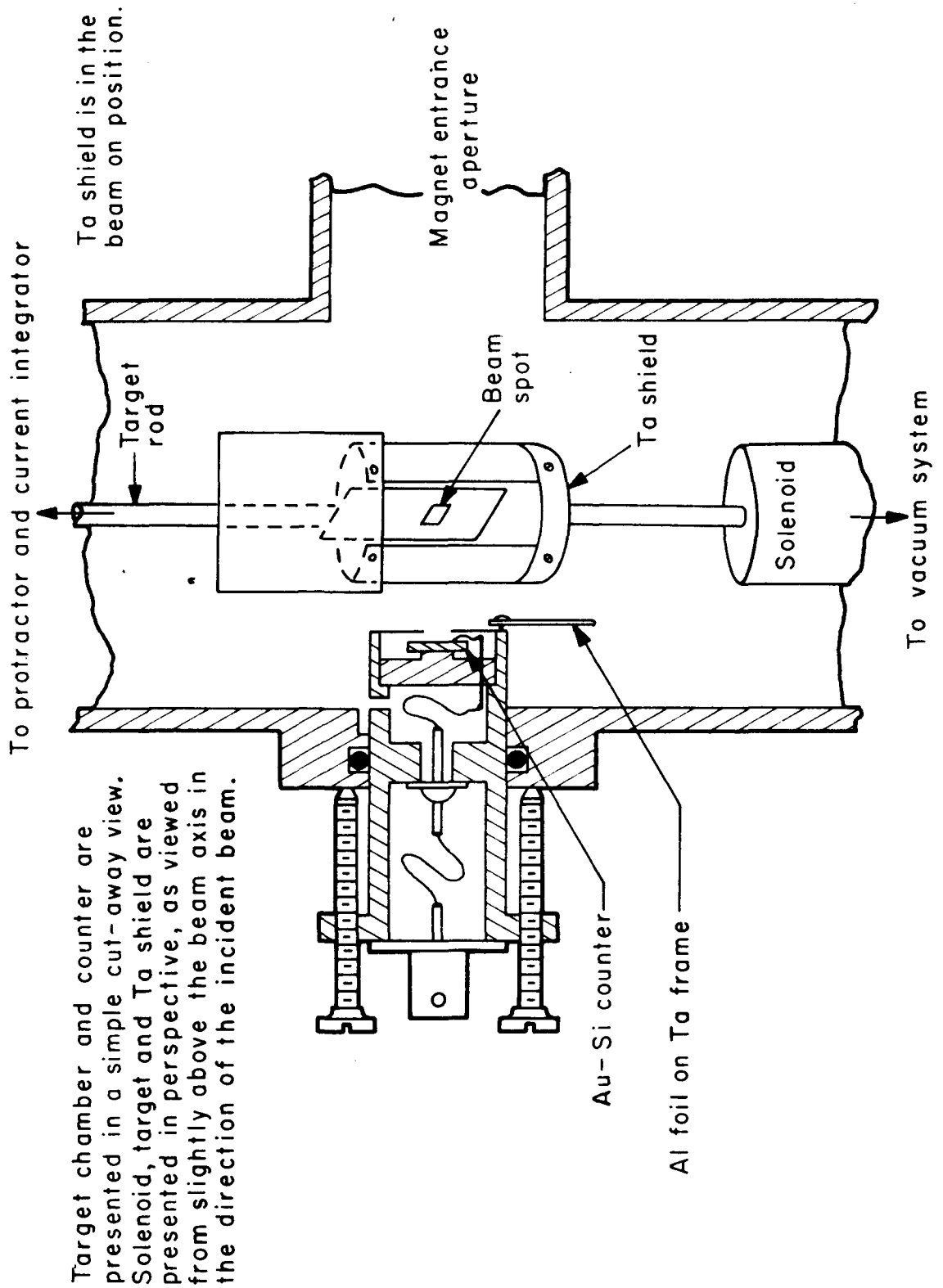


Figure 7. Timing

Before the start of a given cycle the scalars are gated off and the alpha-counter bias is turned off. The cycle is started by turning on the spray supply for the belt. The accelerating voltage increases gradually and the accelerator requires about three seconds to reach the final energy after which the beam strikes the target for about eight seconds before the spray supply is turned off. The voltage on the accelerator decays with a time constant of five seconds. In order to stop higher mass beams from striking the target as the accelerating voltage decreases, two shutters intercept the beam. One is above the magnetic analyzer (figure 5) and the other is in the target chamber (figure 6). The bias on the solid-state counter is applied immediately after the beam leaves the target so that accumulated charges can be swept out of the barrier region before the gates to the scalars are opened, 1.5 seconds later. Switching pulses do not affect the scalars because the scalars are gated off during the switching periods.

Figure 7

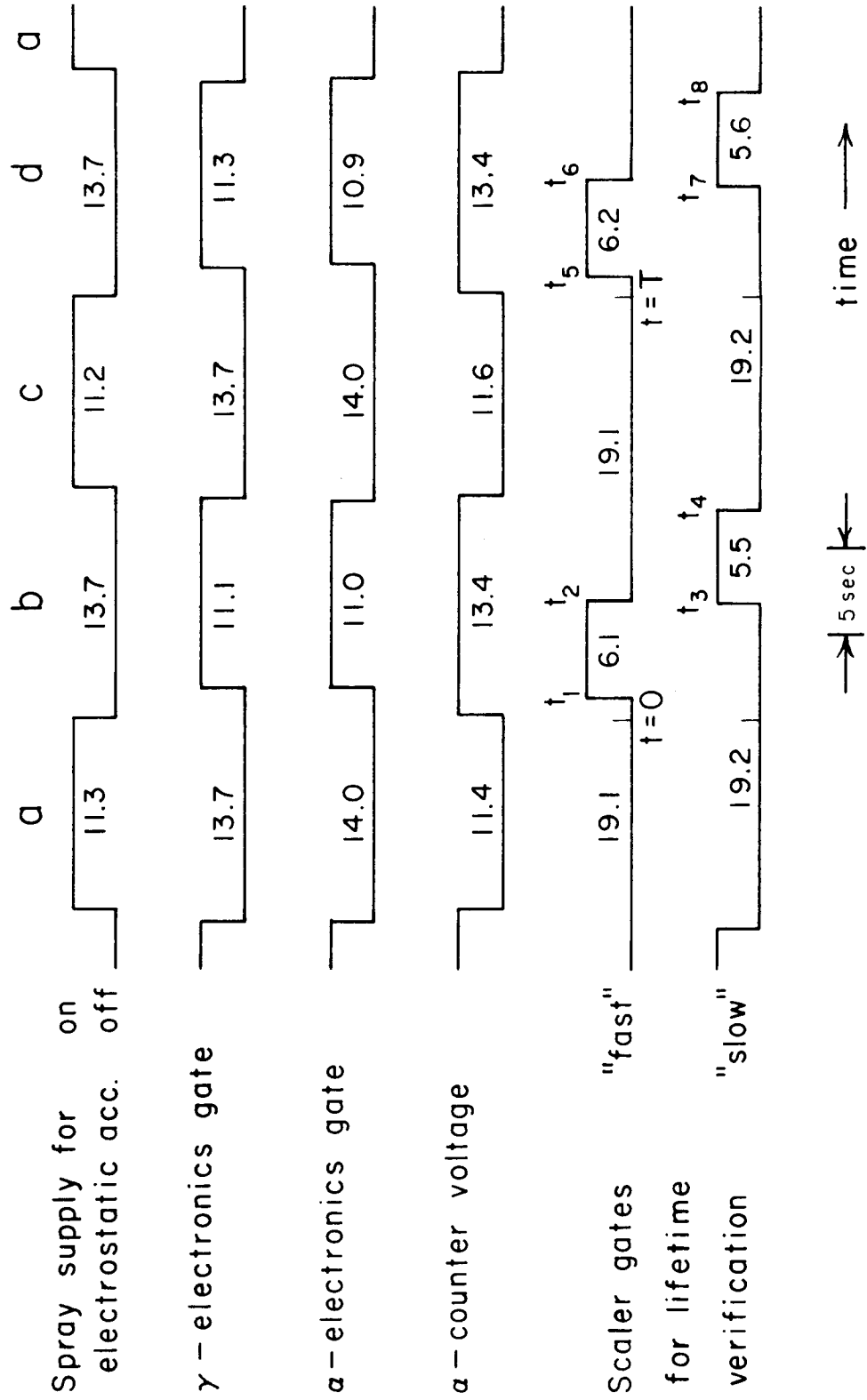


Figure 8. Target thickness

The target was made and its thickness was measured by D. Hebbard (Hebbard 1960).

By using the $N^{15}(p,\gamma)C^{12}$ reaction and studying the gamma-ray yield as a function of incident proton energy, one can obtain the distribution of N^{15} in the target. The resonance used occurs at a proton energy of 0.429 Mev and has a width, $\Gamma \approx 800$ ev. The target was 7 kev thick to 0.431-Mev protons which corresponds to 28 kev for 1.7-Mev alpha particles (Whaling 1958). This represents a surface density of $1.8 \cdot 10^{17}$ target nuclei $\cdot cm^{-2}$.

Figure 8

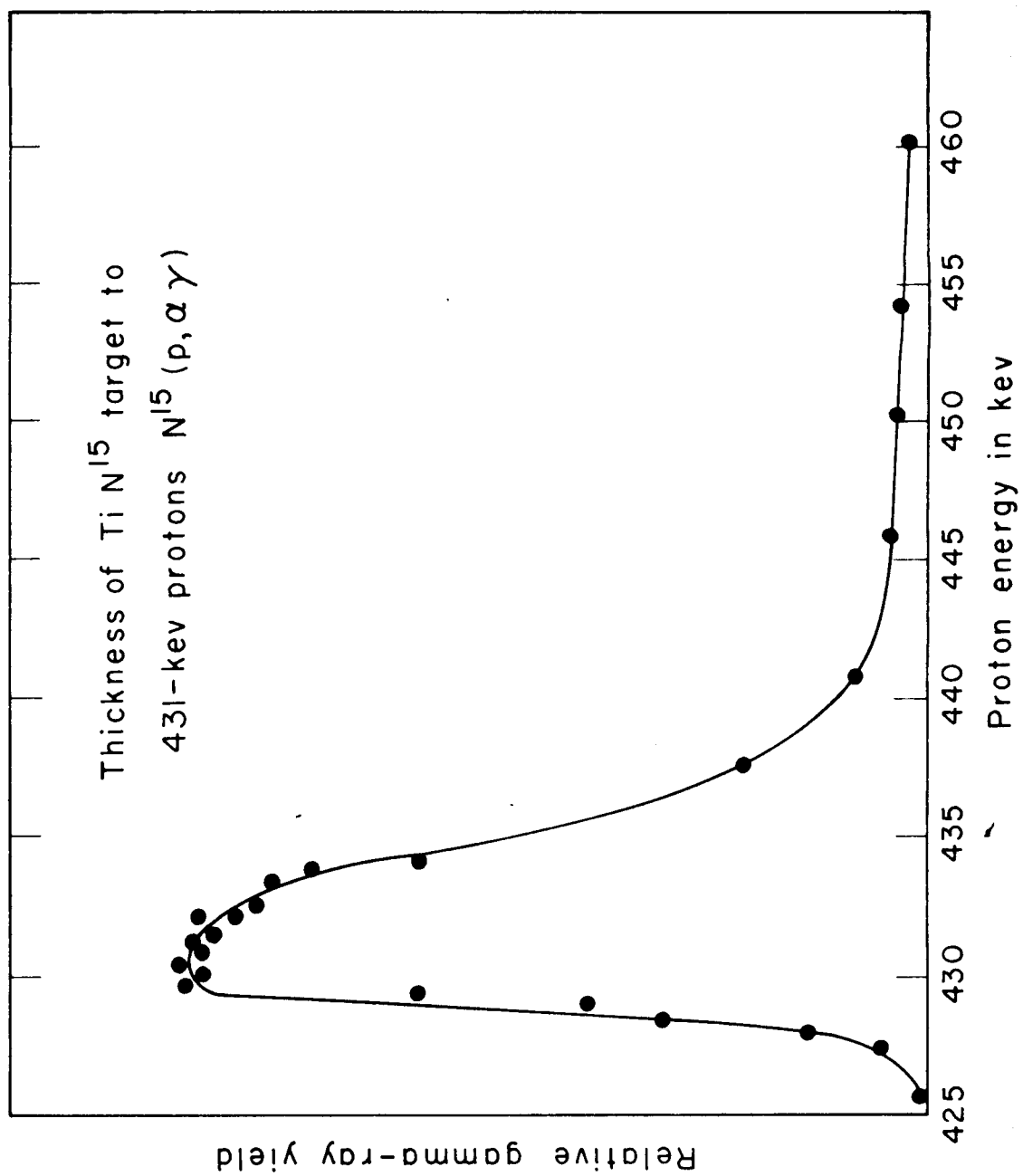


Figure 9. Solid-state counter calibration

A typical calibration curve for the solid-state counter is shown in figure 9. The data points were obtained by three different methods. The crosses were obtained by scattering alpha particles from a thick gold target through the alternating gradient spectrometer into the counter. The open circles at 1.75 Mev came from scattering the alpha particles through a thin gold foil directly into the solid-state counter. The solid points at 2.65 Mev came from a Po^{210} ($E_\alpha = 5.3 \text{ Mev}$) source after the amplifier gain had been decreased by a factor of two. The scatter in the last two groups was due to gain changes in the amplifier, and indicates the order of magnitude of the correction to the abscissa that was necessary in order to combine the spectra of different days.

Figure 9

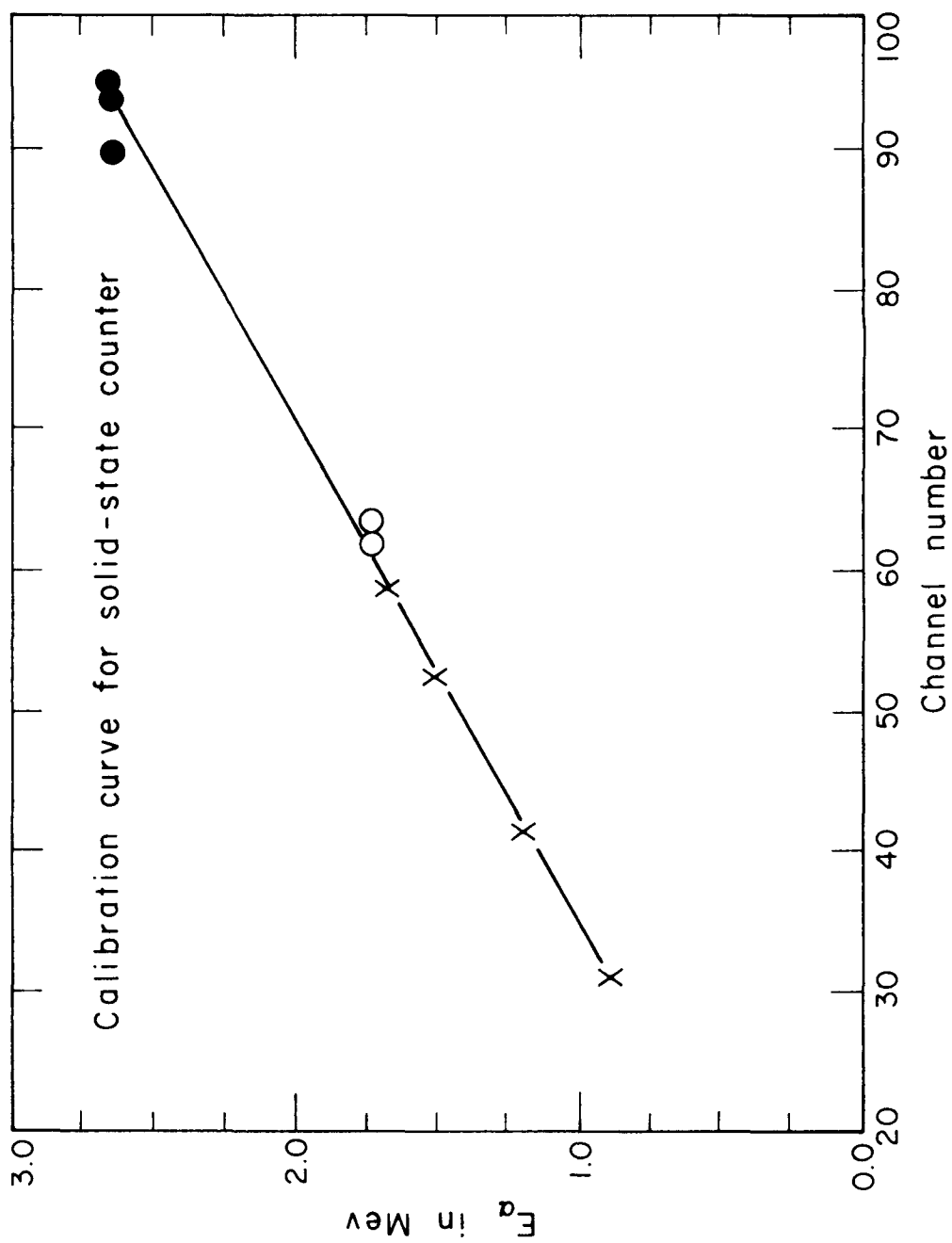


Figure 10. Monitor gamma-ray spectrum

This figure displays the gamma-ray spectrum which was used to determine the total number of beta-decays that occurred during the counting period. The branching ratio of the beta-decay to the 7.12-Mev and 6.13-Mev levels in O^{16} was given by Ajzenberg-Selove and Lauritsen (Ajzenberg-Selove 1959), and thus by working backwards one can obtain the N^{16} activity during the counting cycle. The bias of the monitor scaler is shown on the drawing. The gamma rays were counted in a cylindrical 2 x 2 inch NaI crystal that had a 1.5-inch-thick carbon absorber interposed between the source and the crystal in order to stop the beta particles. The efficiency of the monitor counter was determined using the $F^{19}(p, \alpha \gamma)O^{16}$ reaction with the same geometry that was used in the $N^{16}(\beta)O^{16} \rightarrow C^{12} + He^4$ experiment. The measured efficiency was 0.24%. See section III-H.

Figure 10

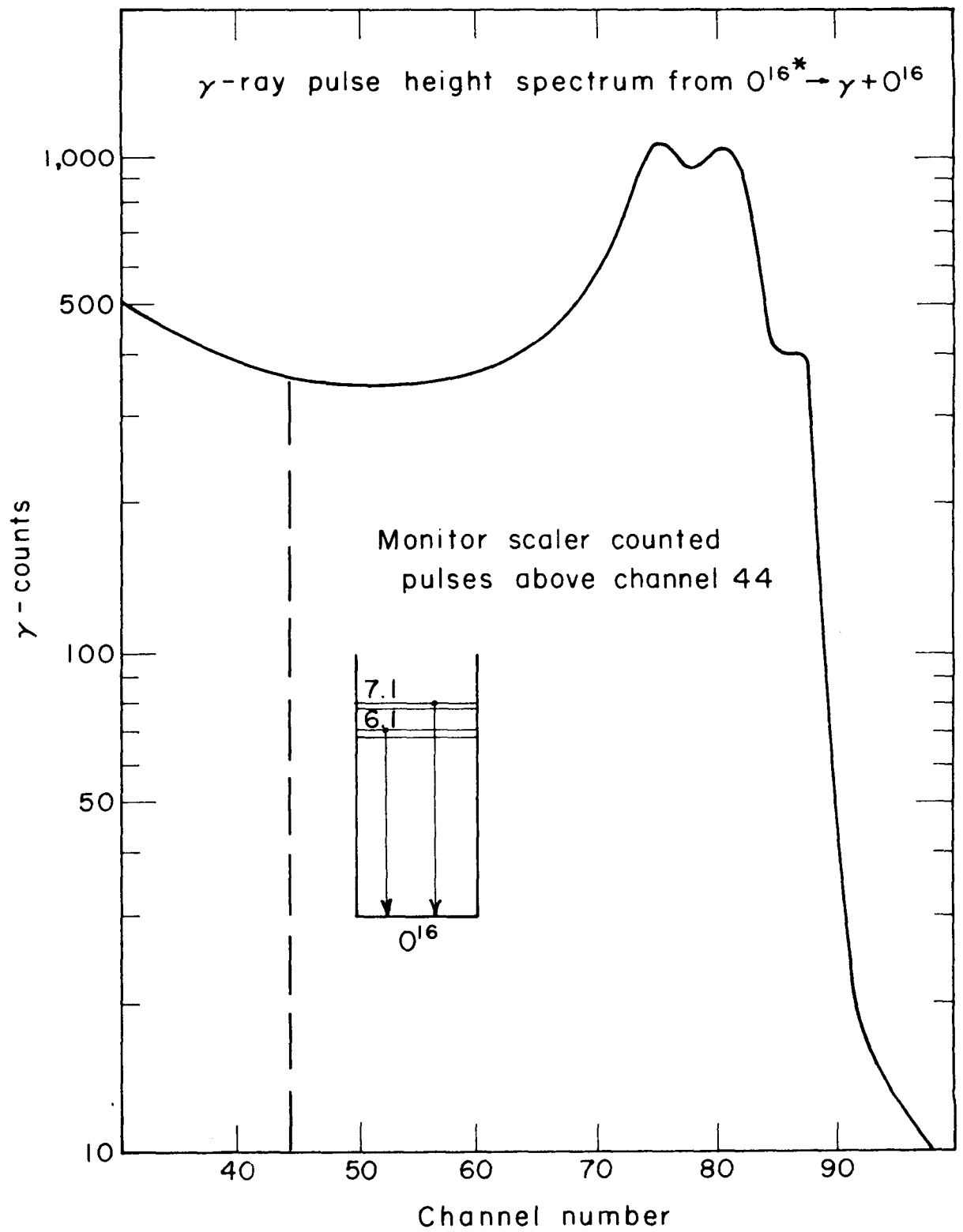


Figure 11. Geometric effects

As the target angle ω is decreased from $\omega = 48^\circ$ to $\omega = 0^\circ$, the number of recoil N^{16} nuclei that escape from the target surface increases from none to one half of the induced activity. See section III-1. The N^{16} nuclei that escape from the surface during bombardment are caught on the tantalum shield and are removed from the field of view of the solid-state counter when the shield drops. If the gamma rays following the N^{16} decays on the tantalum shield were observed in the monitor scaler, the α/γ ratio would decrease as the target angle is decreased, and the number of escaping N^{16} nuclei increases. Results of the measurements of the angular dependence of this ratio in figure 11a show that it is constant to within the experimental accuracy. The variation of the solid angle is 1% between $\omega = 15^\circ$ and $\omega = 45^\circ$ and has been neglected.

As the target angle is decreased the absolute number of N^{16} produced increases as $\text{cosec } \omega$ because the effective target thickness increases as the cosec ω . If this factor of the angular dependence of the number of N^{16} created is factored out of the observed gamma-ray yield, the resultant yield should decrease with target angle in proportion to the number of recoil N^{16} nuclei that escape from the target surface. This is illustrated in figure 11b, where the normalization is such that 100% of the N^{16} formed are counted at $\omega = 48^\circ$.

Figure 11

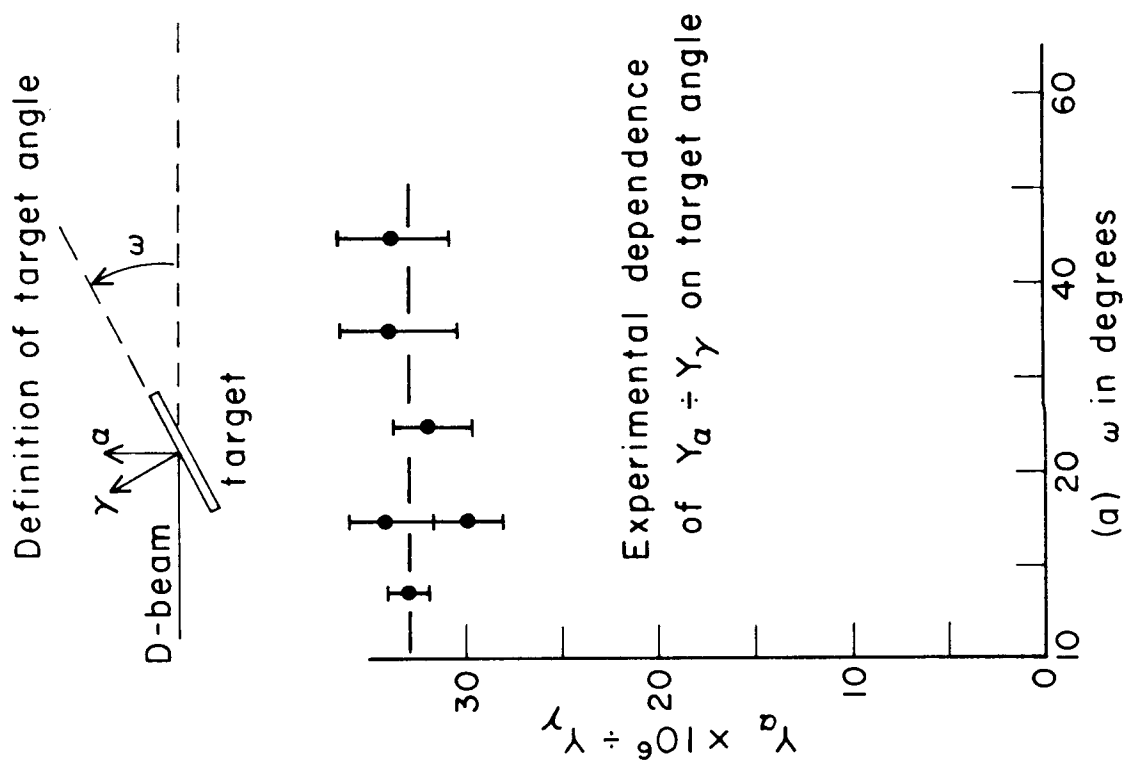
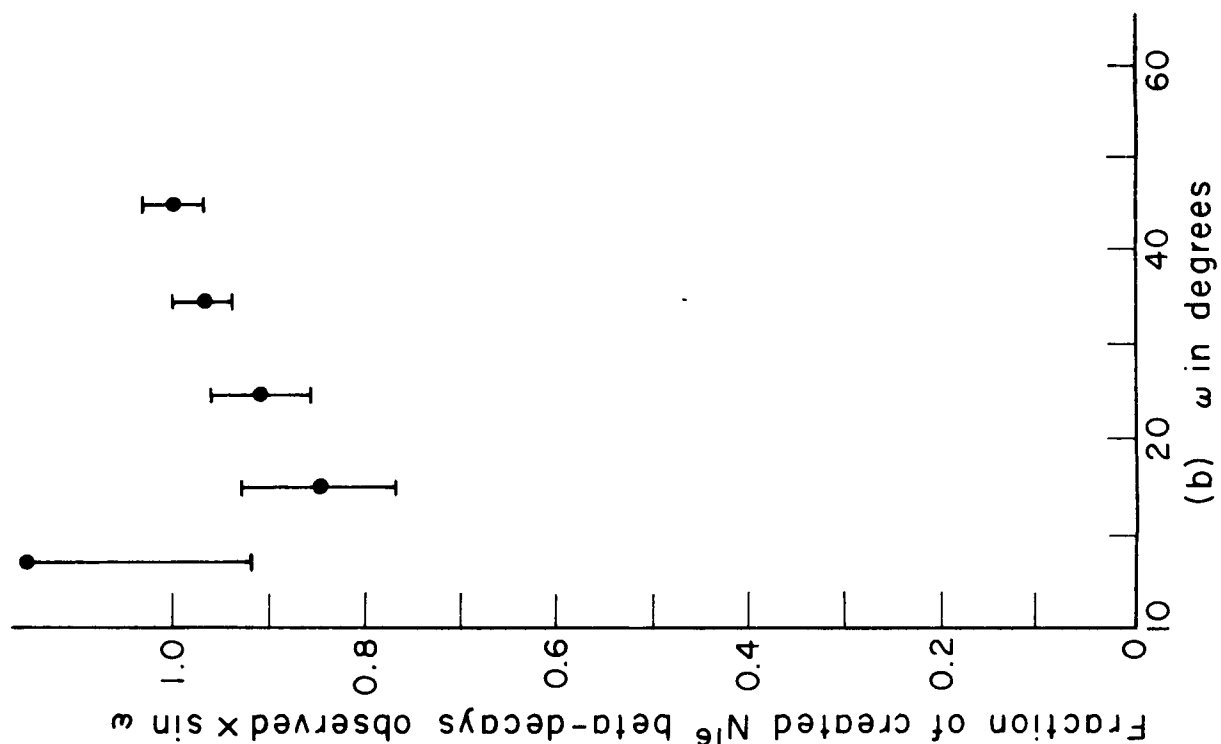


Figure 12. Response functions used in analyzing the data

The response function due to the energy loss of alpha particles escaping from the target for a delta-function alpha-particle source at 1.65 Mev is illustrated in figure 12a. This response function was calculated from the reaction dynamics of the $N^{15}(d,p)$ reaction. The differential cross-section, range, and straggling were all taken into account. The computation leads to a density of alpha particles originating from a given depth in the target which can be converted to an energy loss spectrum after the alpha particles escape from the target. This calculation is illustrated in Appendix II.

The effect on the target response function of the N^{15} distribution in the target has not been taken into account. This distribution would affect the total response function similarly to the artificial low energy plateau included in figure 12b, curve (2), and would result in a better value for the upper limit of F^2 .

In order to determine what effect the target chamber geometry had on the alpha-particle pulse-height spectrum, the solid-state counter was exposed to alpha particles of the same energy both inside and away from the target chamber. The pulse-height spectrum inside the target chamber was obtained by observing alpha particles scattered at $\psi = 90^\circ$, and $\omega = -45^\circ$ through a thin self-supporting piece of gold leaf. This gave rise to the curve illustrated by figure 12b, curve (1). The counter was then exposed to a group of particles at the image point of the alternating gradient spectrometer. This spectrum is illustrated by the circles in figure 12b. See section III-I.

Figure 12

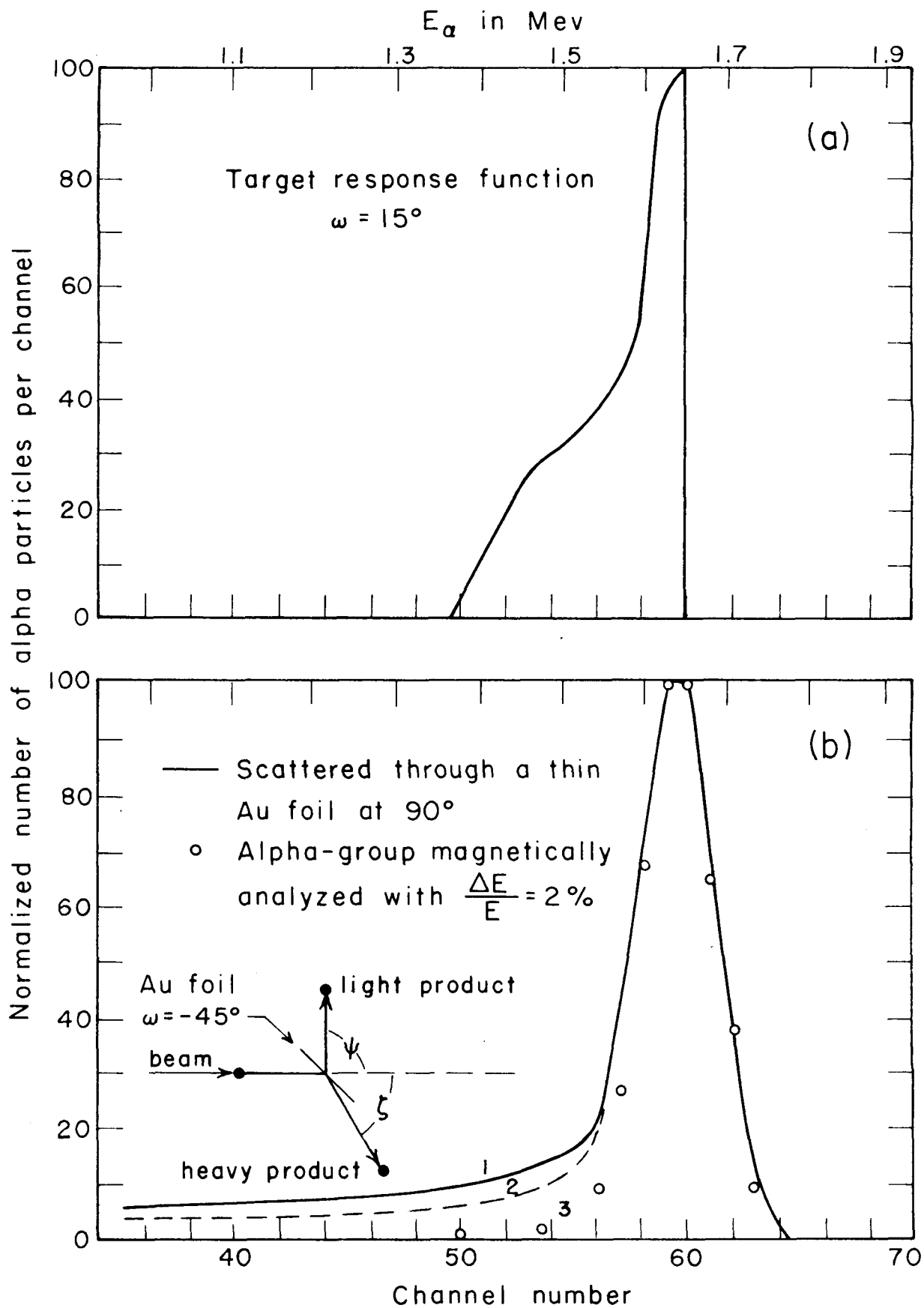


Figure 13. Experimental alpha-particle yield

The spectrum shown in this figure is the uncorrected data from one day's run. The spectrum was accumulated on a 100-channel pulse-height analyzer. No corrections have been made to either the abscissa or the ordinate. The background, indicated by the open circles, was determined by placing a 0.0064-mm aluminum foil over the entrance aperture of the solid-state counter and is due primarily to 10-Mev and 4-Mev beta-particle pile-up. The gamma-ray monitor (figure 10) recorded a corresponding total of $2.9 \cdot 10^7$ counts during this run, Table V, run 3.

Figure 13

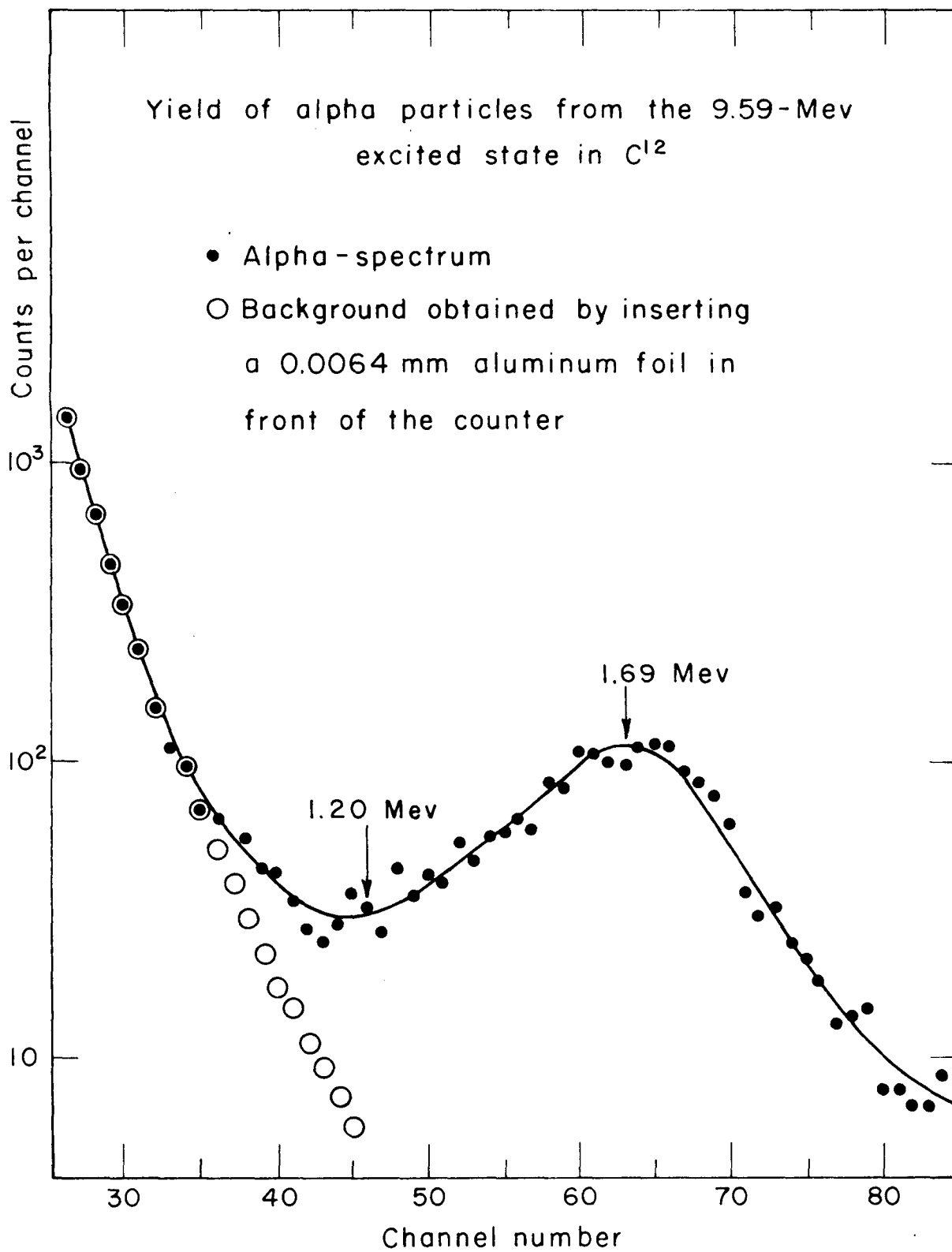


Figure 14. Corrected experimental data points

The curve consists of the semi-empirical values used in the computer program which evaluated the difference between the different theoretical curves and the semi-empirical values. By "semi-empirical values," the fact is emphasized that the values used were those of a curve that had been drawn through the observed data points. The ordinate of the data points has been corrected for the beta-particle background, and the abscissa has been corrected for amplifier gain changes between runs. These corrections were made before combining data accumulated on different days. The combined yield has been normalized to a peak height of 100 in arbitrary units. The integrated yield corresponds to 8465 actual counts, and a gamma-ray monitor total of $1.2 \cdot 10^8$ counts.

Figure 14

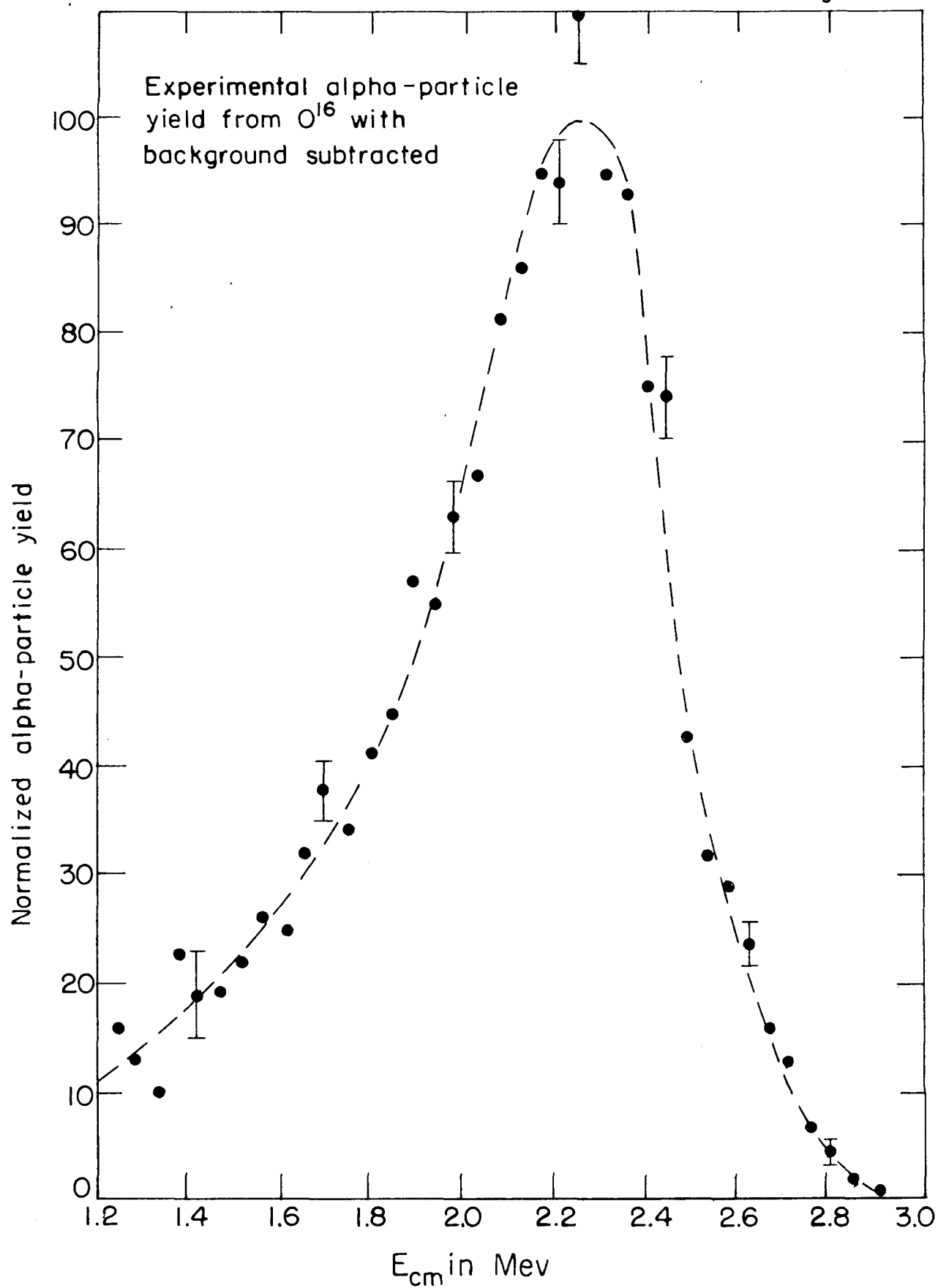


Figure 15. Beta-decay phase-space considerations

This graph illustrates the energy dependence of the beta-decay process. It can readily be deduced from the graph that the population of the high energy region of the broad 9.59-Mev level will be less than that of the low energy region. This effect tends to shift the maximum particle yield to lower energy values than would be expected from a simple analysis of the reaction dynamics.

The function plotted in figure 15 is the Fermi Integral Function, $\lambda(E)$, which is related to the beta-decay probability, λ_0 , by the following expression, $\lambda_0 = \frac{|P|^2}{\tau_0} \lambda(E)$ where τ_0 is a characteristic time, and P is the beta decay matrix element.

The matrix element has been assumed to equal unity over the broad level. The plotted values of $\lambda(E)$ were obtained by integrating the Fermi Function $f(Z, \eta)$ given in Fano's table (Fano 1952), as described in section IV-A.

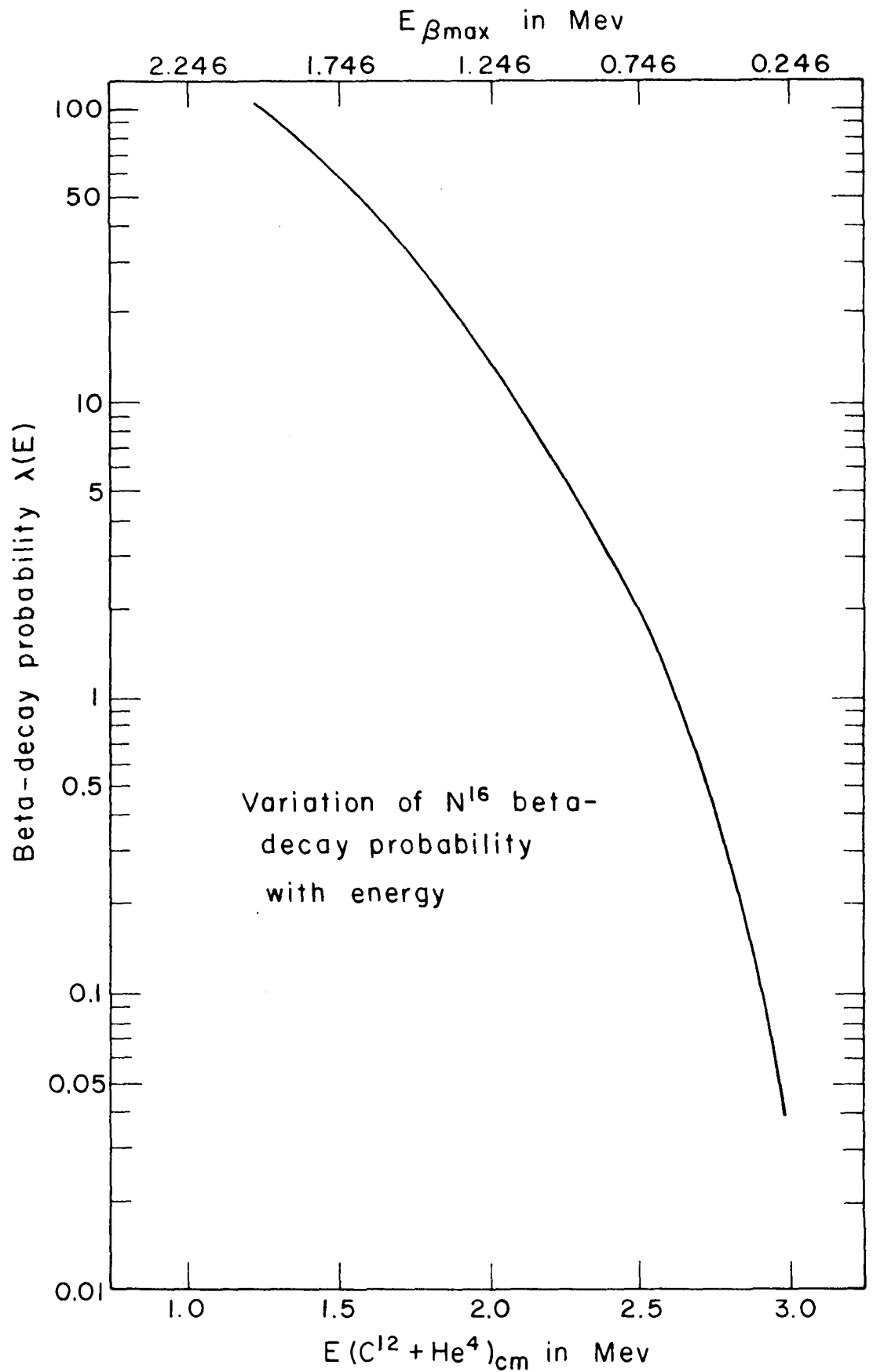


Figure 16. Variation of the theoretical alpha-particle spectrum shape with changing interaction radius a

The dependence of the spectrum shape on the interaction radius, a, is illustrated for the particular set of values $l = 1$, $\gamma_{\alpha 1}^2 = 0.6$ Mev, and $E_R = 2.43$ Mev. The theoretical expression used was the usual Breit-Wigner resonance formula with the beta-decay phase-space factor $\lambda(E)$ included:

$$\sigma(E) \approx \frac{\lambda(E) \Gamma_{\alpha f}(E)}{(E - \Delta_{\alpha f}(E) - E_{\alpha f})^2 + \frac{\Gamma_{\alpha f}^2(E)}{4}}$$

where $E_{\alpha f}$ is defined such that at resonance

$$E_R - \Delta_{\alpha f}(E_R) - E_{\alpha f} = 0$$

It can be seen from the illustration that changing the interaction radius varies the width of the resultant spectrum and shifts the energy at which the maximum yield occurs. The symmetry properties of the spectrum are also affected by the interaction radius. For further discussion of the mathematical relationships, see section IV-B.

Figure 16

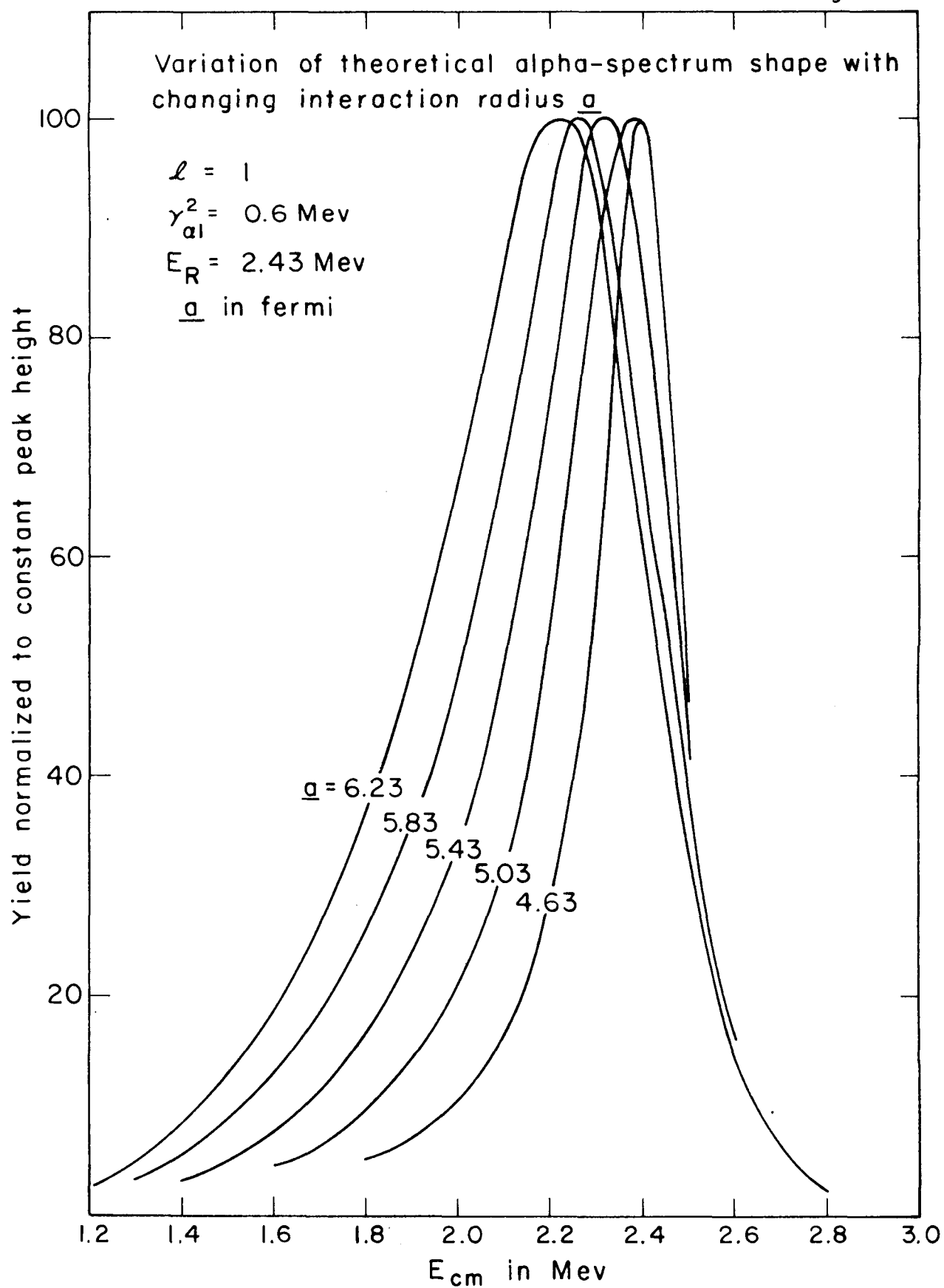


Figure 17. Variation of the theoretical alpha-particle spectrum shape with changes in the resonance energy

The dependence of the spectrum shape on choices of the resonance energy is illustrated in this graph for the following selection of parameters: $f = 1$, $a = 5.43$ fermi, and $\gamma_{a1}^2 = 0.6$ Mev. The theoretical expression used is given in the argument for figure 16.

Figure 17

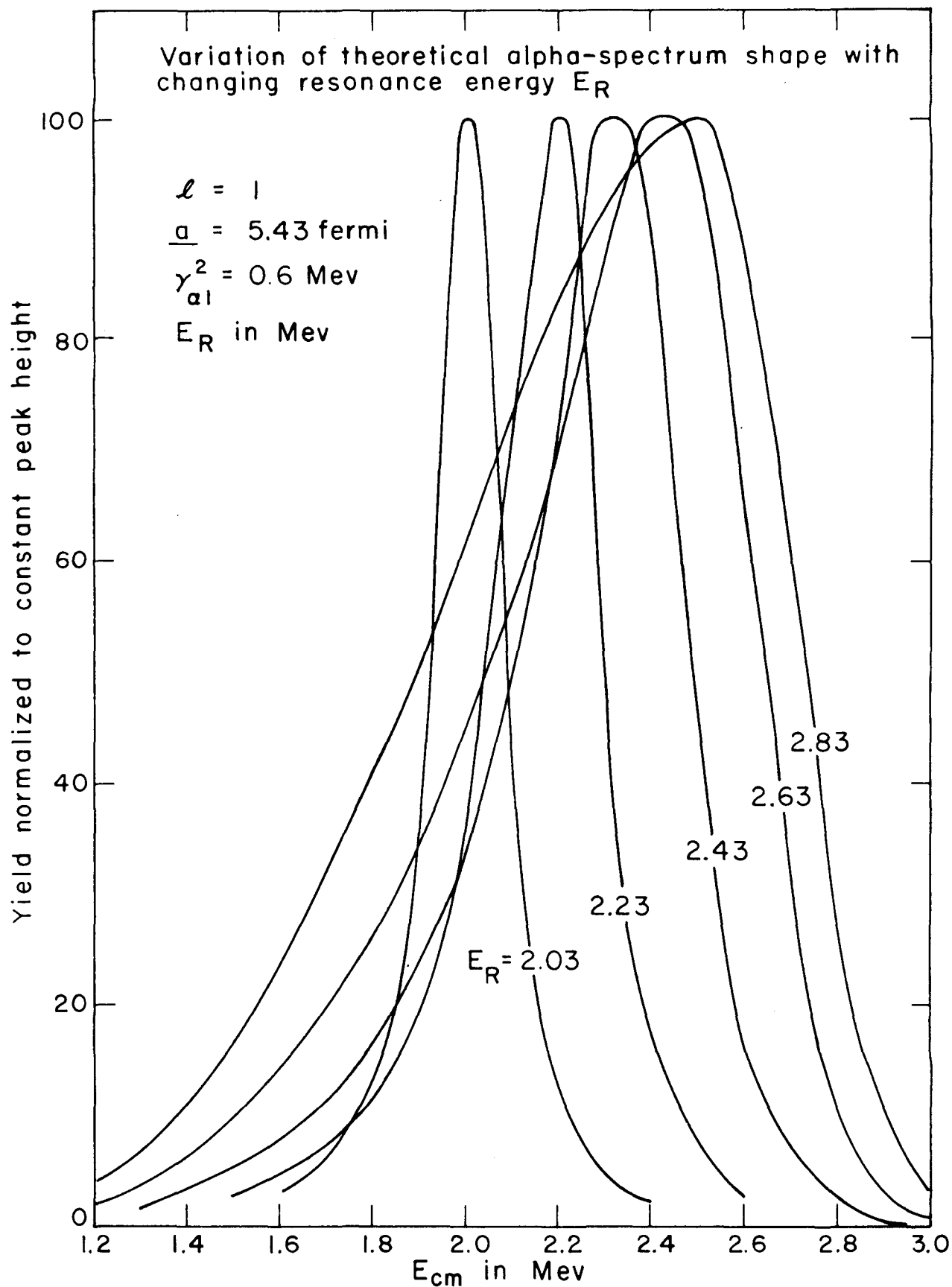


Figure 18. Variation of the theoretical alpha-particle spectrum shape with changes in the reduced width

The dependence of the theoretical spectrum shape on variations in the reduced width is illustrated in figure 18. The parameters chosen were: $l = 1$, $E_R = 2.43$ Mev, and $\underline{a} = 5.43$ fermi. The theoretical expression used is given in the discussion of figure 16.

Figure 18

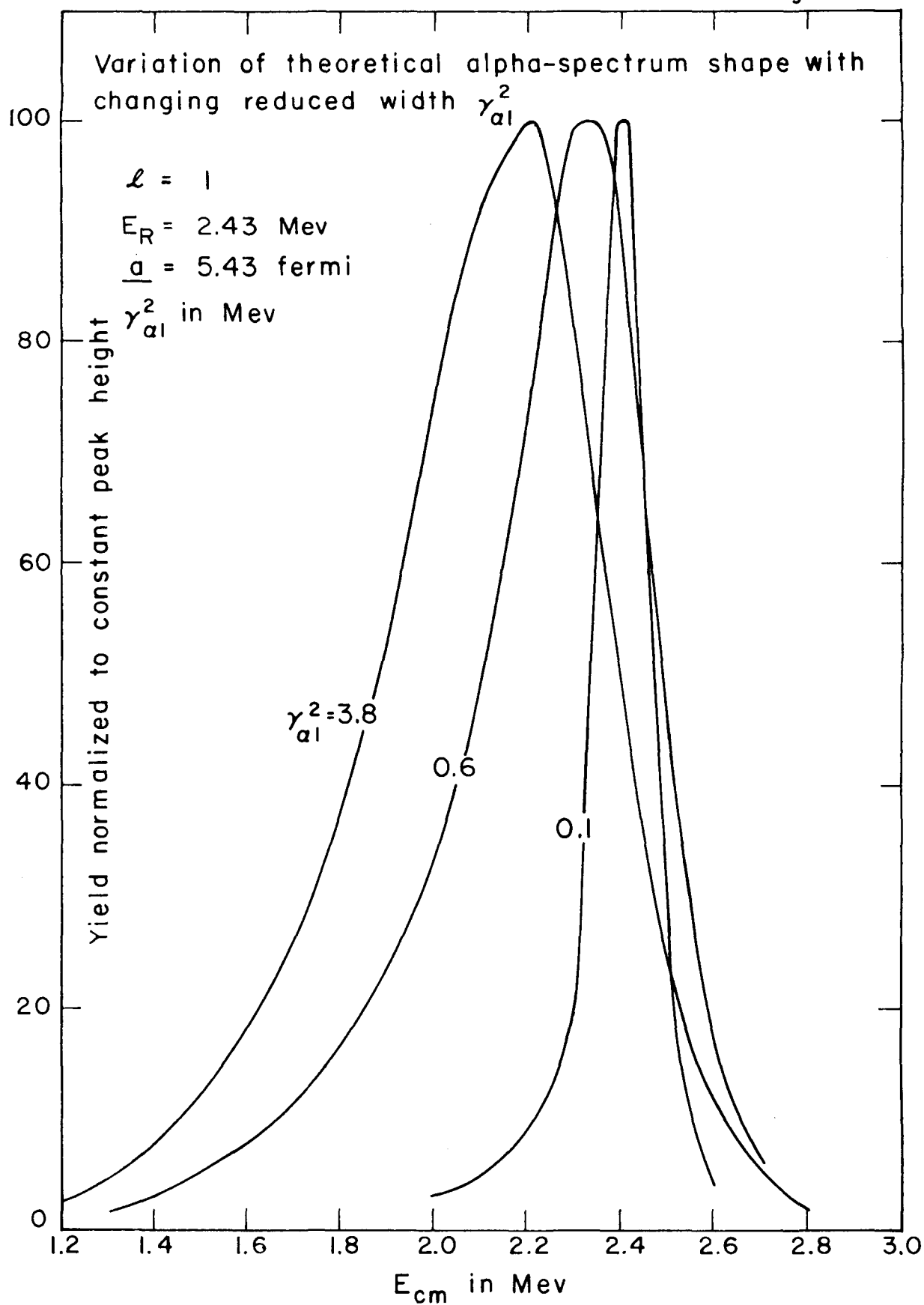


Figure 19. Effect of the counter response function on the
theoretical spectra

The upper graph illustrates the variation of the level parameters that is necessary to maintain a good fit between the semi-empirical points and the theoretical spectra when different counter response functions are used. Curves (a), (b), and (c) correspond to the response functions illustrated in figure 12b, curves (1), (2), and (3), respectively. This experiment excludes values of the level parameters that lie above curve (c). The most probable values for the level parameters are those which lie to the left of the Wigner Limit and between curves (a) and (c).

The lower family of curves shows the variation of the level shift Δ_{a1} as a function of the center of mass energy for various values of the interaction radius \underline{a} .

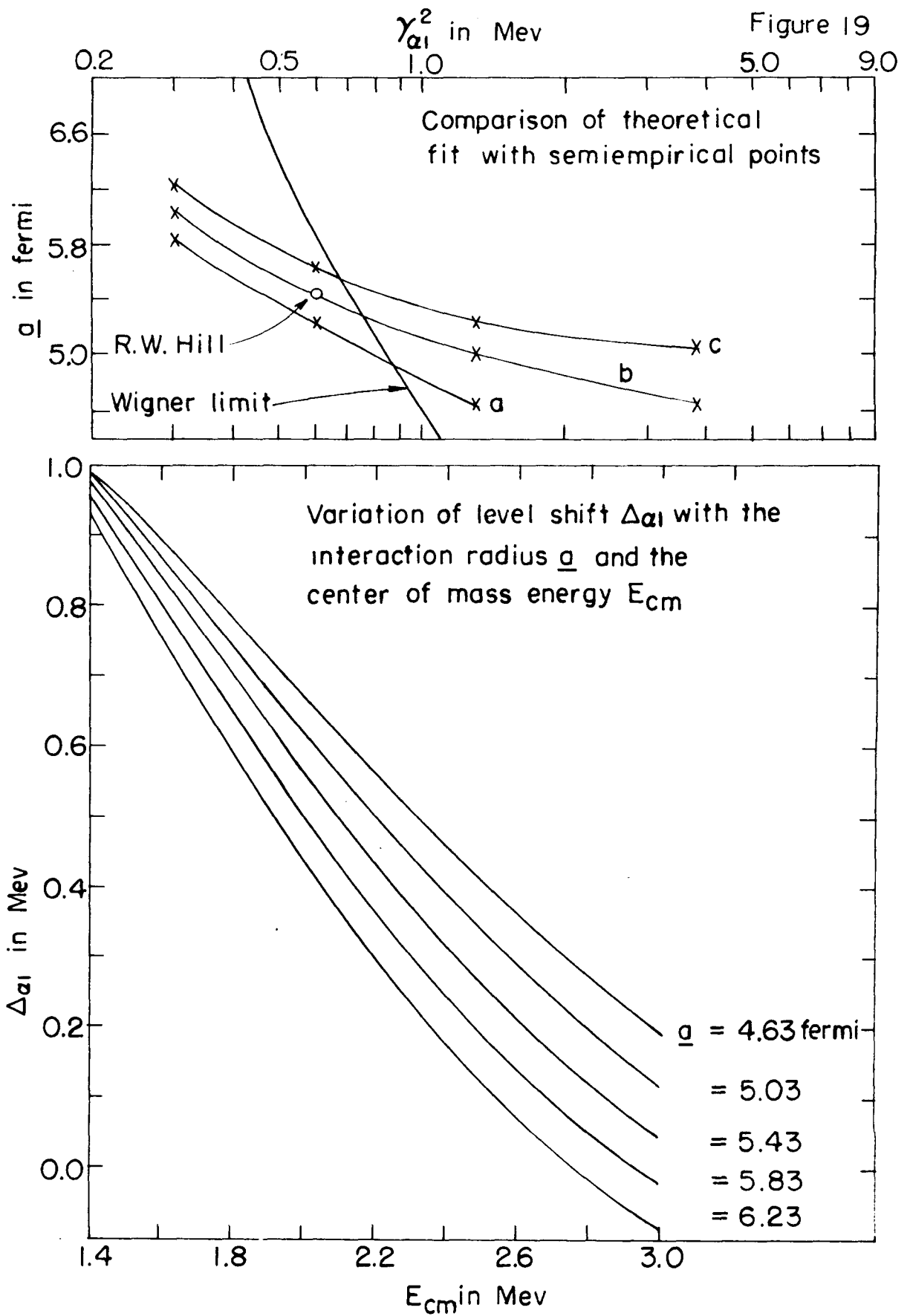


Figure 20. Comparison between theoretical and experimental spectra

The four illustrated spectra correspond to trial sets of parameters considered in the upper graph of figure 19. The data points in figure 20 represent the semi-empirical points with which the theoretical spectra were compared. The parameters for each theoretical curve and the root square deviation δ , equation 19, are indicated on each illustration.

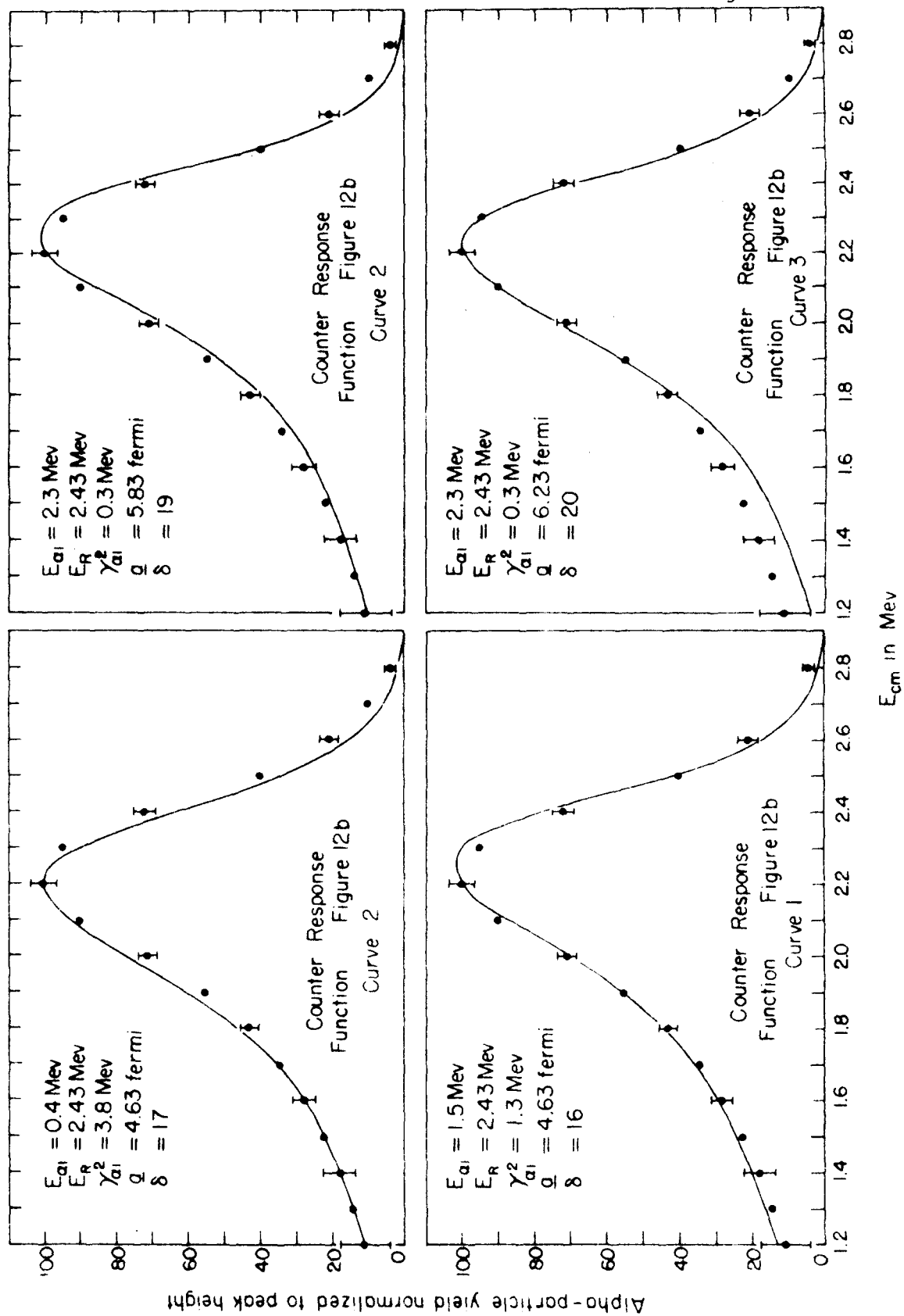


Figure 21. Fitting the experimental spectrum with the level parameters used by R. W. Hill

The semi-empirical spectrum with errors is illustrated by the circles and the error bars. The theoretical spectrum from a thin target, in a target chamber representing good geometry, and observed with high resolution, is illustrated by the dashed curve. If one now folds into the dashed curve the target response function and the counter response function obtained from the magnetically-analyzed group of alpha particles figure 12b, curve (3), one obtains curve (c). By using the counter response function obtained in the target chamber figure 12b, curve (1), one obtains curve (a). The response function figure 12b, curve (2) produces curve (b).

The dotted curve represents the theoretical alpha-particle spectrum from a 500 ev wide 2^+ ad- mixture in the 8.88-Mev level, and corresponds to a ratio of $\frac{Y_a(8.88)}{Y_{aT}} = 1.7 \cdot 10^{-2}$ for the level.

Figure 21

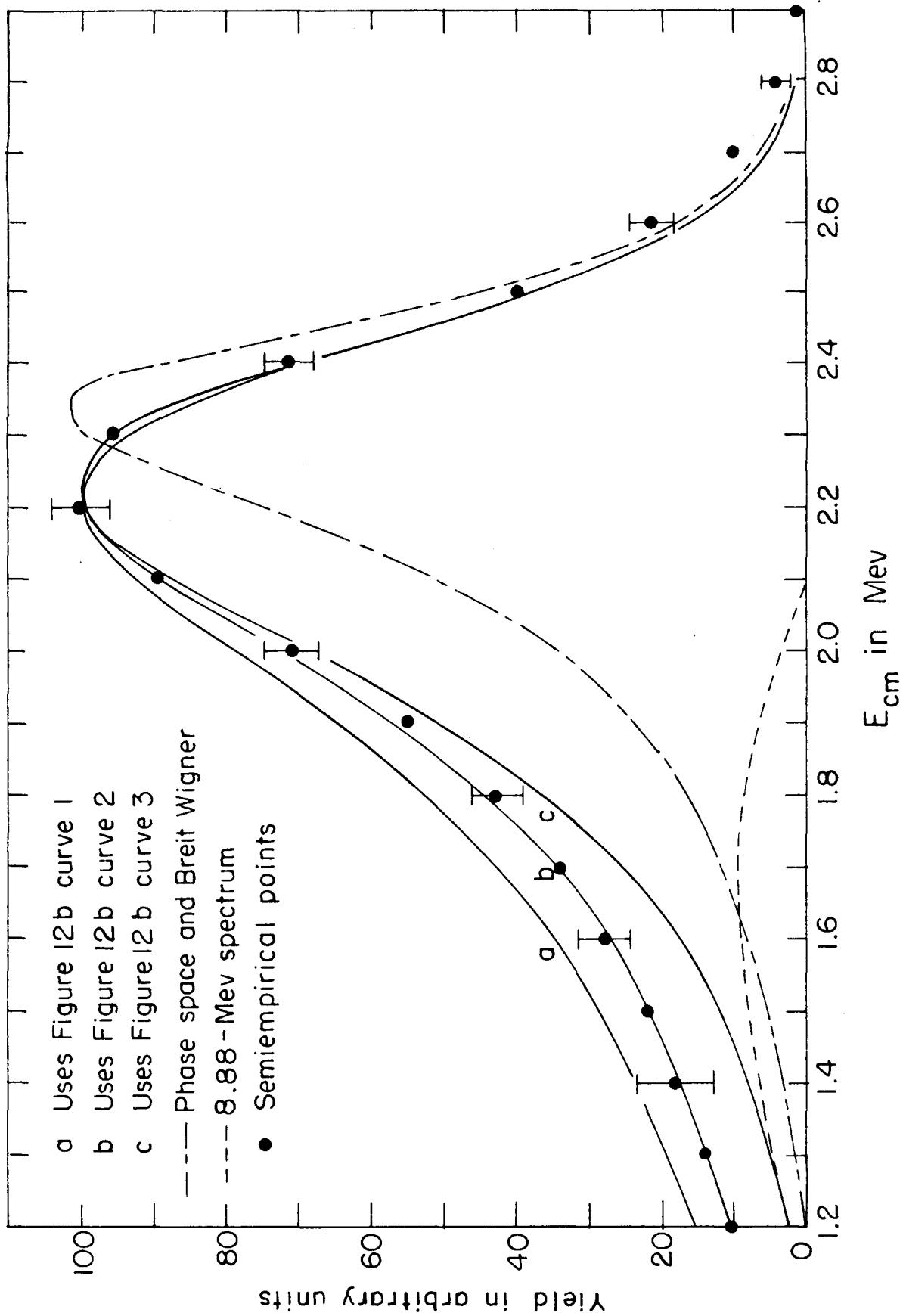


Figure 22. Energy levels of Ne^{20}

F^{20} was formed by the $\text{F}^{19}(\text{d}, \text{p})$ reaction using 1.8-Mev deuterons, where the cross-section is about 45 millibarns (Jarmie 1957). F^{20} is known to beta-decay almost entirely to the first excited state of Ne^{20} which deexcites by the emission of a 1.6-Mev gamma-ray to the ground state. The beta-particle branches of interest in this experiment are those to the 5.63-Mev and 5.8-Mev levels. The levels have spin and parity assignments of 3^- and 1^- respectively according to the results of the Chalk River Tandem Accelerator Group (Chalk River 1961). The results from this experiment and an experiment by R. W. Kavanagh (Kavanagh 1958) indicate that the beta-decay is at least first forbidden. This is consistent with a spin and parity assignment for either level of 1^- or 3^- which agrees well with the results of Chalk River.

Figure 22

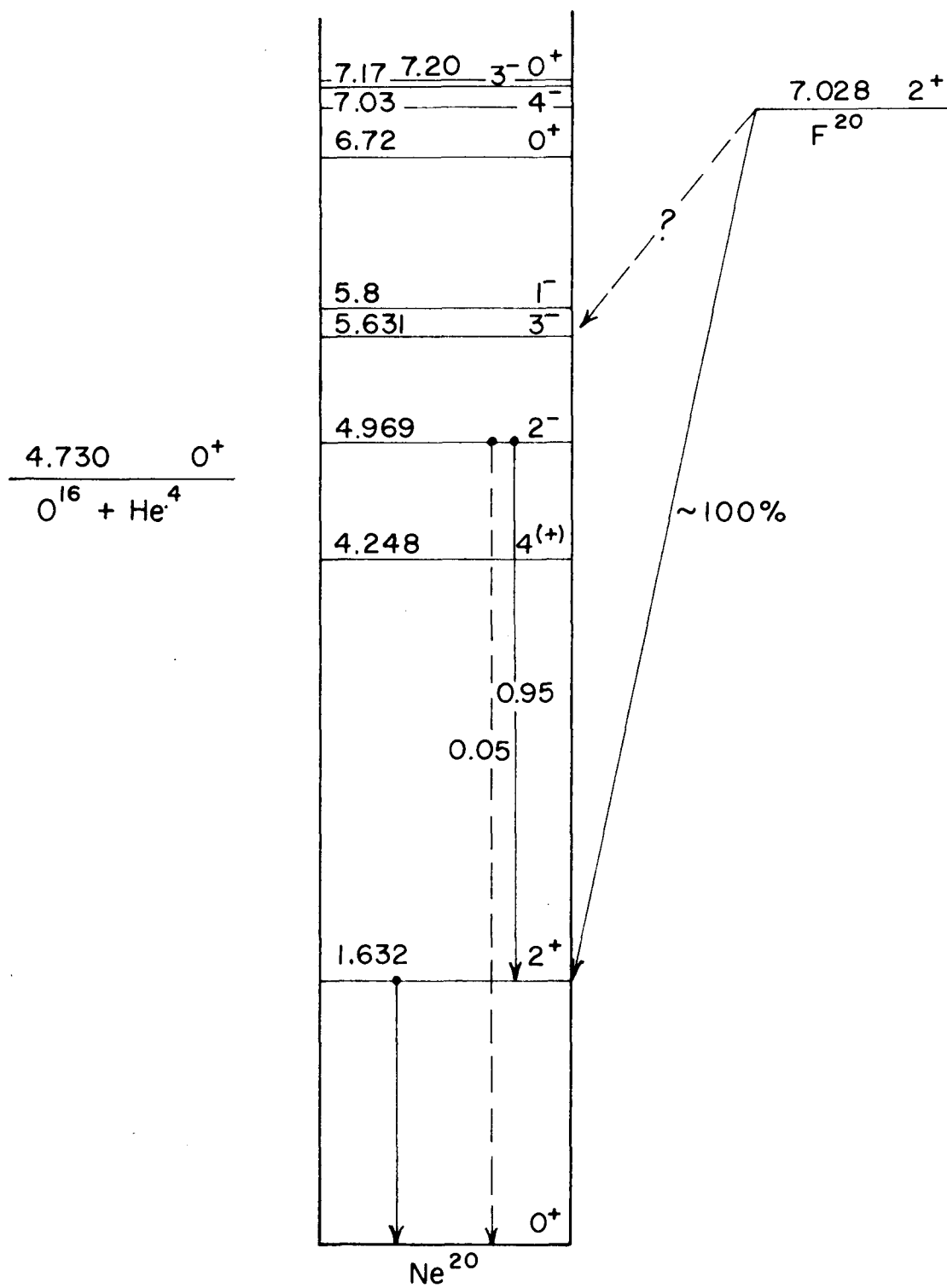


Figure 23. The object position for the alternating gradient spectrometer.

In order to obtain results that are reasonably insensitive to variation of the beam position, it is desirable to determine the position in space at which the maximum yield occurs and to arrange some method of returning the beam to this position. The method used to fix the beam position is identical to the method described by Cook (Cook 1957a) and consists of locating the beam spot by means of a telescope mounted on the spectrometer. The position of maximum yield was determined by varying the beam position and recording the dependence of the counting rate at the image point as a function of the object position. The position of maximum yield in the vertical direction was first obtained and then the curves illustrated in figure 24 for different positions in the horizontal plane were obtained. For target angles of $\omega = -80^\circ$, -45° , and -20° , the yield plotted corresponds to the observed yield less a constant value which is given by $Y_p(1-x)$, where Y_p is the peak yield and x is the fraction indicated on the graph, 0.22, 0.33, and 0.20. The yield is plotted perpendicularly to the target angle. The position of maximum yield can be seen to lie approximately $1/20$ of an inch to the right of the target axis, which is indicated by the intersection of the three target angles. The beam was located optically to coincide with this position of maximum yield each day before accumulating data.

Figure 23

Yield as a function of target position
in the horizontal plane

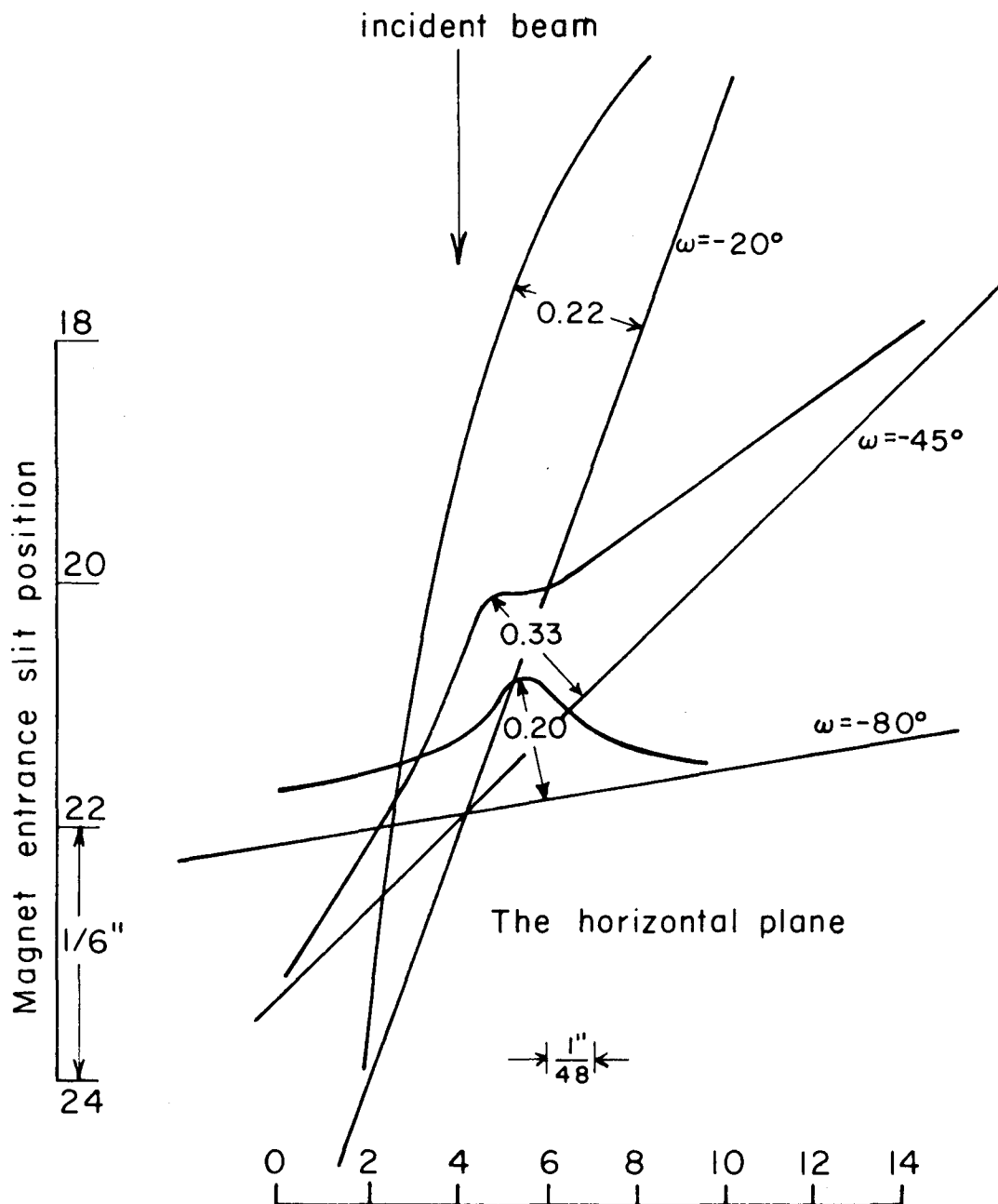


Figure 24. Pulse-height calibration for the alpha-particle counting system

In order to determine the gain and bias settings for the ten channel analyzer used to display the alpha-particle spectrum, alpha particles were scattered from a thick target and observed through the spectrometer. The magnet settings were converted to energy and the fine attenuator setting on the amplifier was adjusted to place the peak in the middle channel of the pulse height analyzer. The values of energy versus attenuator setting were plotted against one another for constant values of the photo-tube high voltage. The results are displayed in figure 24. The following typical example illustrates the use of these curves. If one wishes to observe a group of 700-kev alpha particles, one first estimates the shift in the spectrum due to energy loss in the target, penetration factors, and beta-decay phase-space arguments. Having done this for the usual target thickness, a value around 620 kev was obtained for the peak yield of alpha particles. In order to place this peak in the center of the pulse height analyzer one determines from figure 24 that the high voltage should be 1080 volts and the fine attenuator should be set at 40.

Figure 24

Pulse height calibration for He^4 in a 0.5 mil CsI crystal as a function of fine gain setting and photomultiplier voltage

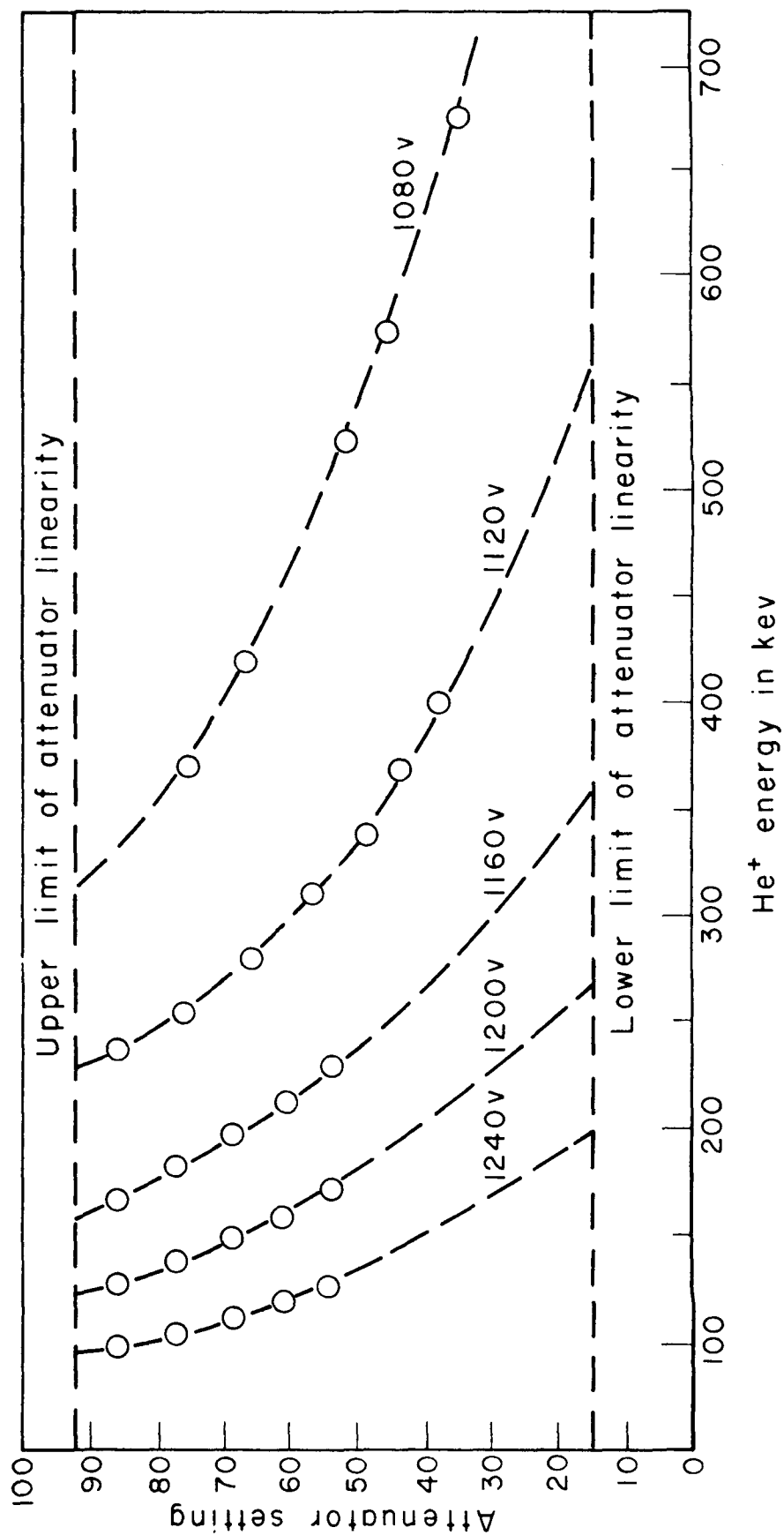


Figure 25. The target thickness

The target was a thin layer of CaF_2 evaporated on a thick, polished, copper backing. The thickness of the CaF_2 layer was determined by observing the shift of the elastically scattered proton step from the copper backing due to the evaporated CaF_2 layer. The proton step from a polished copper target at $\omega = -45^\circ$ and $\psi = 90^\circ$ is shown on the right side of figure 25. The proton yield from calcium and fluorine, and the shifted yield from the copper backing are illustrated on the left side of figure 25. From the displacement of the step, one obtains a thickness for the CaF_2 layer of about 50 kev for 0.9-Mev protons. The different targets that were used in the experiment varied in thickness between 15 kev and 25 kev to 1.0-Mev protons. The average thickness, 20 kev, corresponds to an approximate thickness of 120 kev for 0.7-Mev alpha particles.

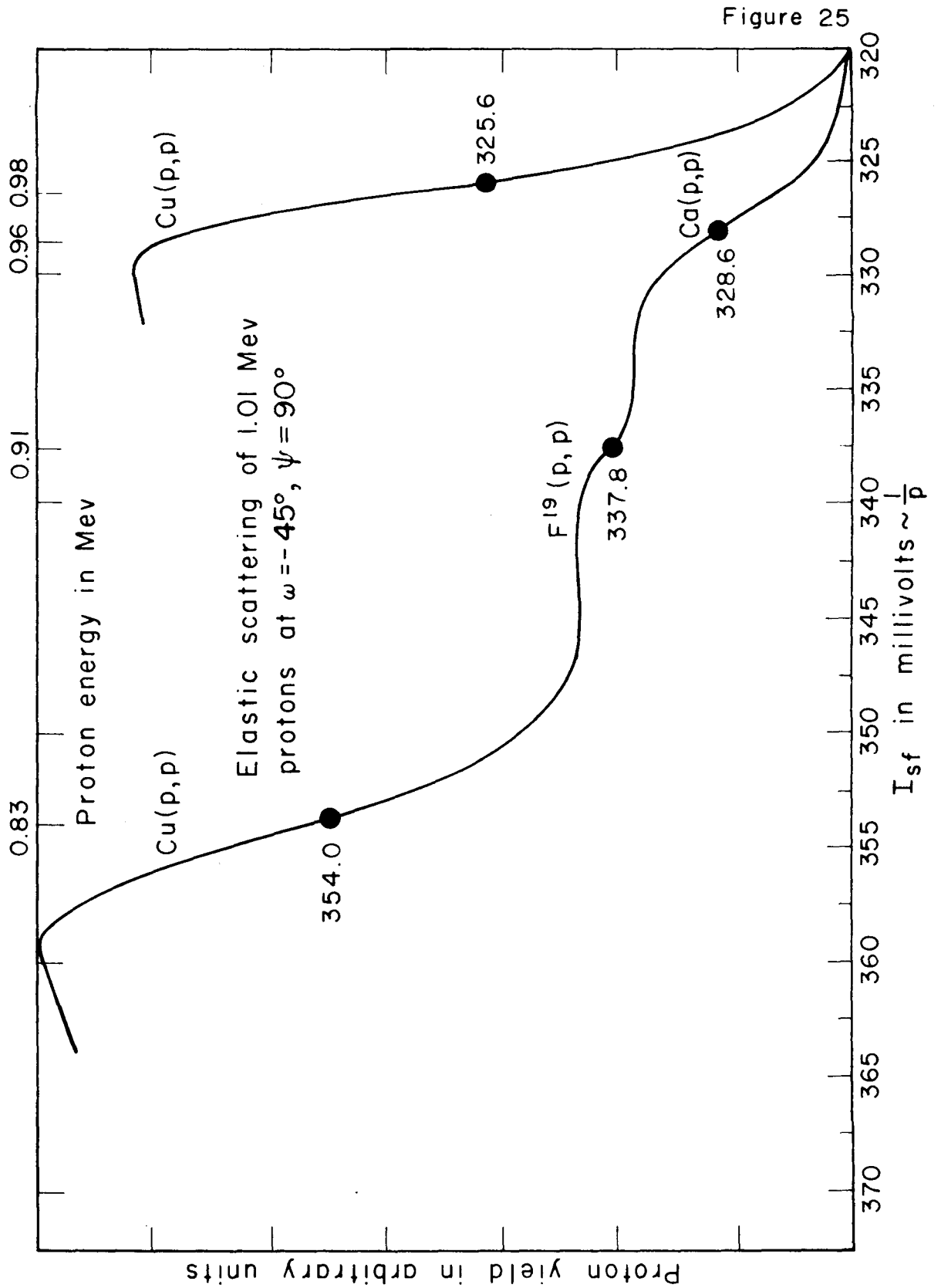


Figure 26. Pulse-height spectrum of alpha particles from the
5.63-Mev energy region of Ne^{20}

The upper curve was taken with the lower level bias set at twenty volts, and the peak of alpha-particle spectrum was expected to appear with a pulse height of thirty-two volts. The lower spectrum was obtained by decreasing the lower level by four channels or ten volts. This illustrates the background in the experiment most of which is due to either electronic noise, 5.4-Mev beta particles, or phosphorescence. Both histograms are plotted to the same abscissa. In order to determine the lower limit for the log ft, the difference between the background and the real counts was used. This difference was then multiplied by two in order to account for the fact that the momentum window of the spectrometer admits only half of the spectrum, and by two to account for the charge-exchange effect. The monitor counter recorded $9.4 \cdot 10^5$ counts during the $7 \cdot 10^{-3}$ coulomb run and $5.4 \cdot 10^5$ counts during the $3 \cdot 10^{-3}$ coulomb run.

Figure 26

Alpha-particle yield from the 5.63-Mev region in Ne^{20} when that level is supposedly populated by beta-decay from F^{20}

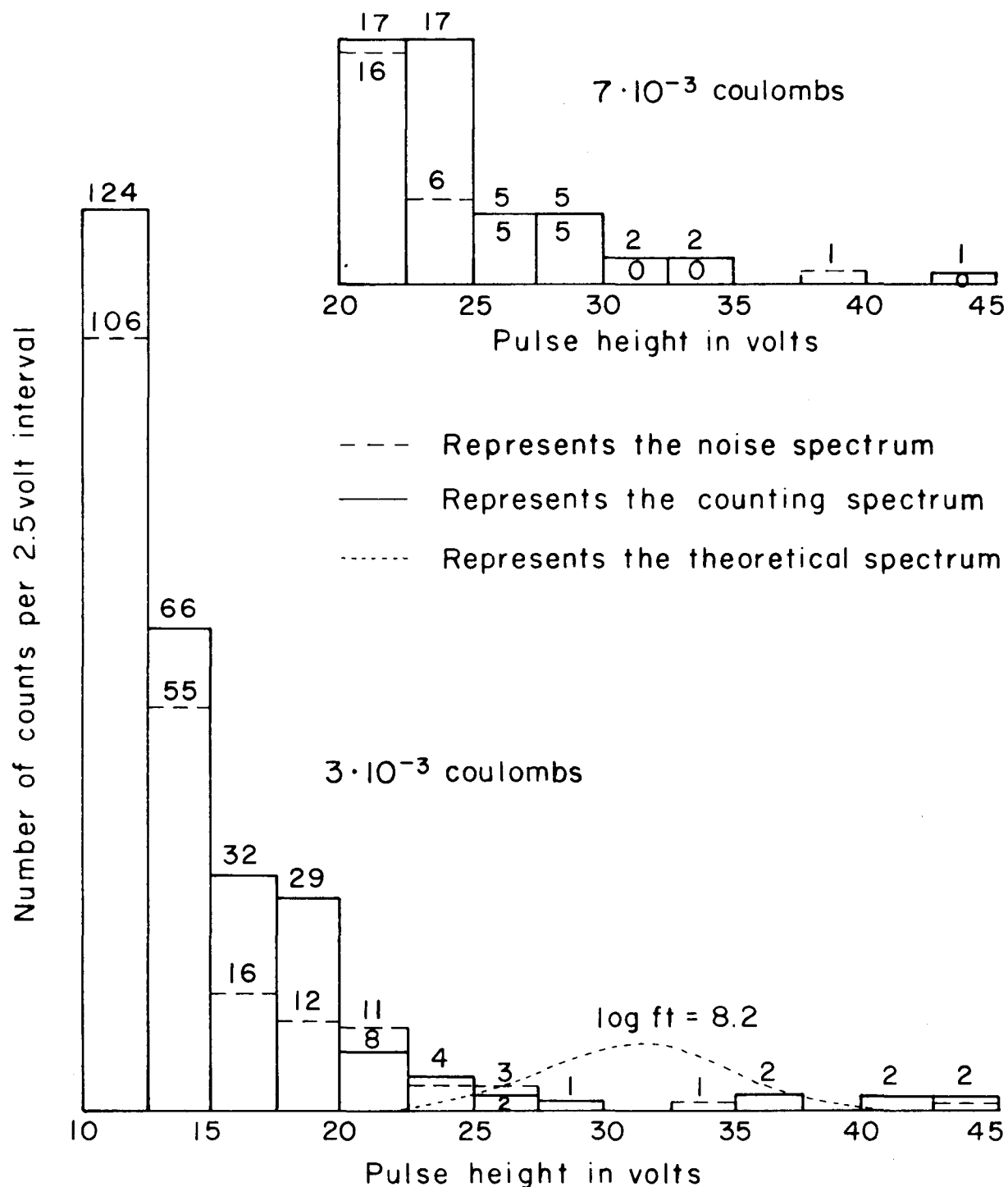


Figure 27. The gamma-ray spectrum from Ne^{20*}

In order to determine the log ft for beta-decay to the 5.63-Mev and 5.80-Mev levels, it is necessary to know how many F²⁰ nuclei decayed during the period of observation of the alpha particles. Since the beta-decay proceeds almost entirely to the first excited state of Ne²⁰, it is sufficient to observe the number of gamma decays from this state during the counting cycle, and then to determine the branching ratio and log ft from this number. The gamma-ray spectrum as observed in a 1.7-inch-diameter plastic scintillator is displayed in figure 27. The bias shown is the lower level for the scaler that monitored the gamma rays. The efficiency for this arrangement was calculated from the tables of G. R. White (White 1952) (Grodstein 1957) as 0.0036%, where the solid angle and counter bias have been included. The solid angle was 0.01 steradians, and the bias introduced a factor of two increase in the number of gamma rays. The factor of two was obtained by extrapolating the recorded spectrum to zero gamma-ray energy with a horizontal line passing through the intercept of the spectrum and the bias setting. This assumption may be in error by a factor of two and the error has been included in the error of the log ft values.

Figure 27

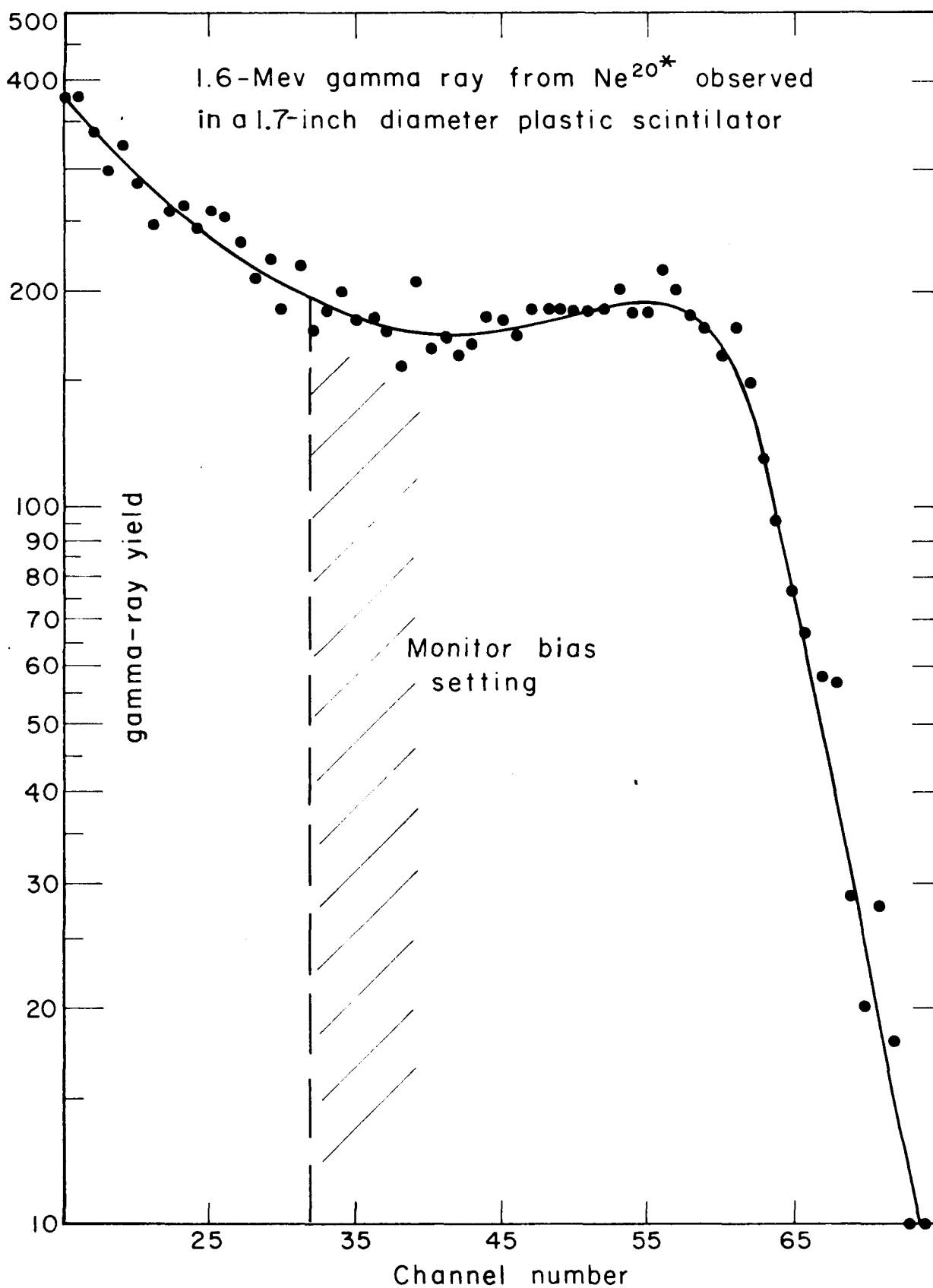
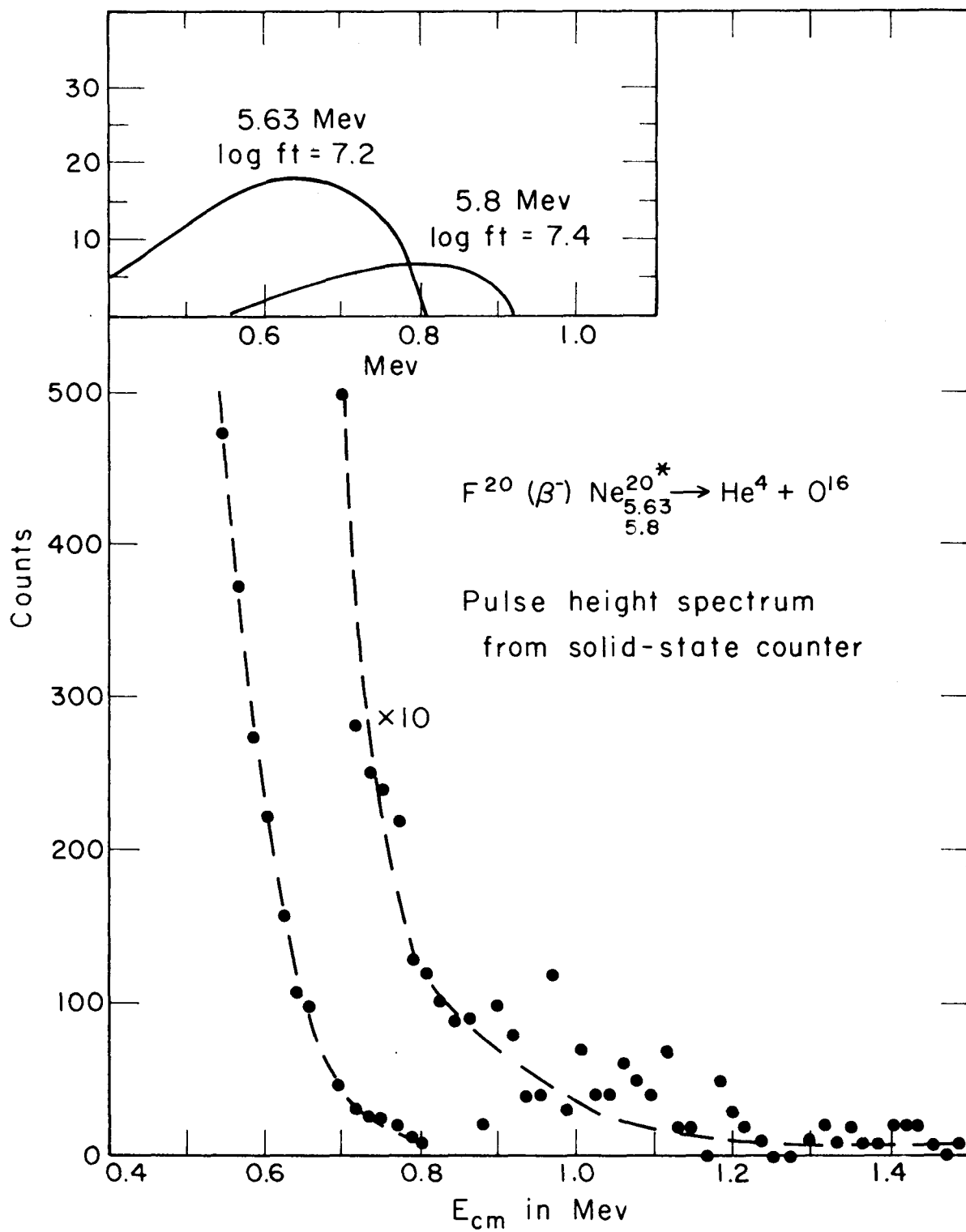


Figure 28. The pulse-height spectrum from the solid-state counter

The spectrum shown indicates the experimental data as points and the beta-particle spectrum and background as the dashed curve. The dashed curve was obtained by placing a 0.0064-mm aluminum foil in front of the solid-state counter and recording the spectrum for the same number of monitor counts as were recorded during the runs without the foil. The displayed spectrum was obtained with a solid angle of 0.039 steradians. While the spectrum was being accumulated, the monitor scaler recorded $4.5 \cdot 10^6$ counts, in a 2-inch-diameter NaI crystal with a solid angle of 0.127 steradians, a crystal efficiency of 36%, and a bias such that only the photo-peak was counted.

The predicted shape and position of the yield of alpha particles from the 5.63-Mev and 5.8-Mev levels (taken as the upper limit of detectability in the present experiment) is plotted to scale along the abscissa in the upper part of figure 28.

Figure 28



REFERENCES

- (Ajzenberg-Selove 1959) F. Ajzenberg-Selove, and T. Lauritsen, Energy Levels of Light Nuclei VI, (1959), Nuclear Phys. 11, 1-340.
- (Alburger 1961) D. E. Alburger, R. E. Pixley, D. H. Wilkinson, and P. Donovan, Beta-Decay of N^{16} ; Conservation of Spin and Parity in O^{16} , (1961), Phil. Mag. 6, 171-174.
- (Bittner 1954) J. W. Bittner and R. D. Moffat, Elastic Scattering of Alpha Particles by Carbon, (1954), Phys. Rev. 96, 374-377.
- (Bleuler 1947) E. Bleuler, P. Scherrer, M. Walter und Z. Zünti, β -Zerfall von N^{16} , (1947), Helv. Phys. Acta 20, 96-104.
- (Blin-Stoyle 1960) R. J. Blin-Stoyle, Parity Nonconserving Inter-nucleon Potentials, (1960), Phys. Rev. 118, 1605-1607.
- (Bloch 1951) I. Bloch, M. H. Hull, Jr., A. A. Broyles, W. G. Bouricius, B. E. Freeman, and G. Breit, Coulomb Functions for Reactions of Protons and Alpha-Particles with the Lighter Nuclei, (1951), Revs. Modern Phys. 23, 147-182.
- (Burbidge 1957) E. M. Burbidge, G. R. Burbidge, W. A. Fowler, and F. Hoyle, Synthesis of the Elements in Stars, (1957), Revs. Modern Phys. 29, 547-650.
- (Chalk River 1961) Chalk River Tandem Accelerator Group, Rotational Bands in Ne^{20} , (1961), PD-317, Ontario.

- (Cook 1957a) C. W. Cook, Alpha-Particles from B^{12} ; The Astrophysical Significance, (1957), Ph. D. Thesis, California Institute of Technology.
- (Cook 1957b) C. W. Cook, W. A. Fowler, C. C. Lauritsen, and T. Lauritsen, B^{12} , C^{12} , and Red Giants, (1957), Phys. Rev. 107, 508-515.
- (Cook 1958) C. W. Cook, W. A. Fowler, C. C. Lauritsen, and T. Lauritsen, High-Energy Alpha Particles from B^{12} , (1958), Phys. Rev. 111, 567-571.
- (Dissanaike 1953) G. A. Dissanaike, A Study of Charge Exchange by Helium Ions in Metals, (1953), Phil. Mag. 44, 1051-1063.
- (Evans 1955) R. D. Evans, The Atomic Nucleus, (1955), McGraw-Hill Book Co.
- (Fano 1952) U. Fano, Tables for the Analysis of Beta Spectra, (1952), National Bureau of Standards, Applied Mathematics Series 13.
- (Feenberg 1950) E. Feenberg, and G. Trigg, The Interpretation of Comparative Half-Lives in the Fermi Theory of Beta-Decay, (1950), Revs. Modern Phys. 22, 399-406.
- (Feynman 1959) R. P. Feynman, Series of Lectures on the Theory of Fundamental Processes, (1959), California Institute of Technology.
- (Fowler 1961) W. A. Fowler, "The Origin of Nuclear Species by Means of Nuclear Reactions in Stars," Modern Physics for the Engineer Ch. 9, (1961), McGraw-Hill Book Co.

- (Freeman 1957) J. Freeman and R. C. Hanna, Excited States of N^{16} , (1957), Nuclear Physics 4, 599-614.
- (Griffy 1960) T. A. Griffy and L. C. Biedenharn, Beta Decay Involving the $Be^{8*}(2+)$ State, (1960), Nuclear Physics 15, 636-645.
- (Grodstein 1957) G. W. Grodstein, X-ray Attenuation Coefficients from 10 kev to 100 Mev, (1957), N.B.S. Circular 583, U. S. Government Printing Office.
- (Hebbard 1960) D. F. Hebbard, Proton Capture by N^{15} , (1960), Nuclear Physics 15, 289-315.
- (Hildebrand 1956) F. B. Hildebrand, Introduction to Numerical Analysis, (1956), McGraw-Hill Book Co., 82.
- (Hill 1953) R. W. Hill, Elastic Scattering of Alpha-Particles by Carbon, (1953), Phys. Rev. 90, 845-848.
- (Jarmie 1957) N. Jarmie, and J. D. Seagrave, Charged Particle Cross Sections, (1957), Los Alamos Scientific Laboratory, LA-2014.
- (Kaufmann 1961) W. Kaufmann and H. Waffler, A Search for Parity-Forbidden Alpha-Decay from the 8.88 Mev (2^-) State in O^{16} , (1961), Nuclear Physics 24, 62-68.
- (Kavanagh 1958) R. W. Kavanagh, Coincidence Studies of B^{12} and F^{20} , (1958), Bull. Amer. Phys. Soc. 3, 316.
- (Kuehner 1959) J. A. Kuehner, A. E. Litherland, E. Almquist, D. A. Bromley, and H. E. Gove, Unnatural Parity States in O^{16} II, (1959), Phys. Rev. 114, 775-785.

- (Lane 1958) A. M. Lane, and R. G. Thomas, R-Matrix Theory of Nuclear Reactions, (1958), Revs. Modern Phys. 30, 257-353.
- (Lane 1960) A. M. Lane, Reduced Widths of Individual Nuclear Energy Levels, (1960), Revs. Modern Phys. 32, 519-566.
- (Marion 1960) J. B. Marion, 1960, Nuclear Data Tables Part 3, (1960), U. S. Government Printing Office.
- (Martin 1954) H. C. Martin, Cross-Sections for the $O^{16}(n,p)N^{16}$ Reaction from 12 to 18 Mev, (1954), Phys. Rev. 93, 498-499.
- (Martin 1956) H. J. Martin, Jr., Angular Correlation Experiments with the $F^{19}(p,\alpha\gamma)O^{16}$ Reaction, (1956), Ph. D. Thesis, California Institute of Technology.
- (Martin 1957) H. J. Martin, and A. A. Kraus, Alternating-Gradient Magnetic Spectrometer, (1957), Rev. Sci. Instr. 28, 175-177.
- (Nordberg 1961) M. E. Nordberg, Jr., Comparison of the β - α Angular Correlations in the Beta Decays of Li^8 and B^8 , (1961), Ph. D. Thesis California Institute of Technology.
- (Powers 1962) D. R. Powers, The Range of Heavy Ions in Solid Materials, (1962), Ph. D. Thesis, California Institute of Technology.
- (Salpeter 1957a) E. E. Salpeter, Nuclear Reactions in Stars. Buildup from Helium, (1957), Phys. Rev. 107, 516-525.
- (Salpeter 1957b) E. E. Salpeter, Stellar Energy Sources, (1957), Revs. Modern Phys. 29, 244-254.

- (Segel 1961) R. E. Segel, J. W. Olness, and E. L. Sprenkel, Parity Conservation in Nuclear Reactions: Search for α -Decay of the 8.88-Mev State in O^{16} , (1961), Phys. Rev. 123, 1382-1385.
- (Sharp 1955) W. T. Sharp, H. E. Gove, and E. B. Paul, Graphs of Coulomb Functions, (1955), Atomic Energy of Canada Limited, Chalk River Project TPI-70.
- (Stier 1954) P. M. Stier, C. F. Barnett, and G. E. Evans, Charge States of Heavy-Ion Beams Passing through Gases, (1954), Phys. Rev. 96, 973-982.
- (Tanner 1957) N. W. Tanner, Parity in Nuclear Reactions, (1957), Phys. Rev. 107 1203-1204.
- (Van Allen 1941) J. A. Van Allen and N. M. Smith, Jr., The Absolute Number of Quanta from the Bombardment of Fluorine with Protons, (1941), Phys. Rev. 59, 501-508.
- (Whaling 1958) W. Whaling, The Energy Loss of Charged Particles in Matter, (1958), Handbuch der Physik 34, Springer-Verlag.
- (White 1952) G. R. White X-Ray Attenuation Coefficients, (1952), National Bureau of Standards, Report 1003.
- (Wigner 1947) E. P. Wigner and L. Eisenbud, Higher Angular Momenta and Long Range Interaction in Resonance Reactions, (1947), Phys. Rev. 72, 29-41.
- (Wilkinson 1956) D. H. Wilkinson, B. J. Toppel, and D. E. Alburger, 2^- State at 8.87 Mev in O^{16} , (1956), Phys. Rev. 101, 673-684.

(Wilkinson 1957) D. H. Wilkinson, Low-Lying States of N^{16} , (1957),
Phys. Rev. 105, 686-691.

(Wilkinson 1958) D. H. Wilkinson, Parity Conservation in Strong
Interactions, (1958), Phys. Rev. 109, 1603-1619.

(Wolicki 1956) E. A. Wolicki, R. Jastrow, and F. Brooks, Calculated
Efficiencies of NaI Crystals, (1956), N.R.L. Report 4833.

(Wong 1954) C. Wong, Beta Decay of F^{20} , (1954), Phys. Rev. 95,
761-764.

(Zimmermann 1958) W. Zimmermann Jr., Experiments Concerning
the Low-Energy States of N^{16} and O^{19} , (1958), Ph. D. Thesis,
California Institute of Technology.